The fetal electrocardiogram

determination of the fetal heart rate and electrocardiogram from abdominal recordings

Vullings, R.

Award date:
2005

Eindhoven University of Technology
Faculty of Applied Physics

The fetal electrocardiogram

Determination of the fetal heart rate and electrocardiogram from abdominal recordings

Master's thesis

R. Vullings

August, 2005
MRL/KFM 2005-02

máxima medisch centrum

TU/e technische universiteit eindhoven

Supervisors:
Ir. C.H.L. Peters
Prof. Dr. Ir. P.F.F. Wijn

Abstract

A major problem in modern obstetrics with respect to fetal monitoring is the lack of possibilities to extract information from the fetus to assess its condition. The fetal heart rate is one of very few useful fetal signals that can be measured non-invasively and in many cases in clinical practice the only source of information available. A possible additional source of information is the fetal electrocardiogram (ECG). The ECG provides information about the depolarization and repolarization properties of the heart, expressed in the shape of the waveform. Since fetal distress is reflected in the ECG as changes in the morphology, determination of the fetal ECG in addition to the fetal heart rate can improve the prediction of fetal distress.

The fetal ECG can be measured non-invasively on the maternal abdomen, but when recording the ECG the signal is contaminated by maternal components and other sources of noise. To reconstruct the fetal cardiac traces, these maternal components and noise have to be eliminated. Several techniques of retrieving the fetal ECG from a noisy signal are proposed in literature but due to insufficient elimination of the maternal components or relatively large computation times, none of these techniques complies with the goals of this study: the development of an algorithm that is capable of online calculating the beat-to-beat fetal heart rate and fetal ECG from abdominal recordings. Since the relationship between maternal uterine contractions and changes in the fetal heart rate is used by physicians to interpret the fetal condition, the developed algorithm also has to be capable of calculating maternal uterine activity.

The calculation of the fetal heart rate is realized by an algorithm that operates in two steps. In the first step the maternal ECG is estimated using segmentational adaptive averaging (SAA). SAA divides each maternal ECG complex into several segments, depending on the shape of the complex, and estimates these segments by adaptive averaging of the corresponding segments of 20 preceding ECG complexes. After the subtraction of the estimated maternal ECG signals from the abdominal recordings, four abdominal signals – the recordings are performed using 12 of 13 electrodes positioned on the maternal abdomen – are linearly combined to increase the signal-to-noise ratio (SNR) of the fetal signal. The fetal R-peaks are detected in this linear combination using a peak detection algorithm and based on the positions of these R-peaks the instantaneous fetal heart rate is calculated.

The fetal ECG complexes are calculated by subtracting the maternal ECG by means of applying SAA, detecting the fetal R-peaks and increasing the SNR of the resultant signals by averaging and filtering. Averaging is performed by aligning ten successive fetal ECG complexes by their R-peaks and calculating the average complex, excluding complexes that have a relatively small correlation with the other complexes. To further increase the SNR of the resultant fetal ECG complexes an adaptive filter, working with a moving window, is applied. To evaluate the condition of the fetus, physicians have to interpret ECG leads that are commonly determined for humans. For this reason, the measured ECG complexes have to be transformed to these commonly determined ECG leads. This transformation is performed by reconstructing the fetal vectorcardiogram (VCG) from the recorded ECG leads and by calculating the standard and extremity ECG leads from this VCG.

Maternal uterine activity is calculated by two different methods, based on two different phenomena. First the uterine activity is calculated from the electromyogram (EMG) signals originating from the uterus. Furthermore, uterine activity can be calculated from motion artifacts, caused by deformations of the abdominal surface. Uterine activity is calculated from motion artifacts by applying a high-pass filter on the data signals and summing the activities in all signals. The uterine EMG signal is obtained by applying FastICA, an algorithm based on independent component analysis, on the recorded data and uterine activity is determined from this EMG signal by calculating the contributions of the EMG signal to the recorded signals in the spectral band between 0.6 Hz and 3 Hz.

The fetal heart rates calculated from the abdominal recordings are compared to the heart rates calculated from a simultaneously measured direct fetal ECG, obtained by using a scalp electrode. The correlation coefficient between the abdominally determined heart rates and the directly measured heart rate is 0.998 and the mean value of the differences between them is 0.0 ± 0.7 BPM. Furthermore, the algorithm is capable of calculating 90 percent of the fetal heart rates from all performed measurements, except for gestational ages between 28 and 32 weeks. For these ages the fetus is electrically shielded from its environment by the vernix caseosa, a waxy substance coating the skin of the fetus. As a result of this shielding less than 60 percent of the fetal heart rates can be determined.

The fetal ECG complexes calculated from the fetal VCG show similar waveforms as for the same leads recorded on a healthy human being outside the uterus. Furthermore, the mean P-R/R-R interval length ratio from the abdominally determined fetal ECG complexes agree well with the mean P-R/R-R interval length ratio calculated from the directly measured fetal ECG; the mean value of the differences between instantaneous values is -0.01 ± 0.01. As a result of noise, the agreement between instantaneous values is worse; the correlation

coefficient is 0.583. The mean QRS-interval length calculated from the abdominal recordings also agrees well with the mean QRS-interval length determined from the directly measured ECG; the mean value of the differences between instantaneous values is -0.001 ± 0.002 s.

Uterine activity determined from both motion artifacts and uterine EMG signals is consistent with an intra-uterine pressure measurement conducted simultaneously with the abdominal recordings, i.e. bursts in uterine activity calculated from both methods coincide with bursts in the intra-uterine pressure. Difference between both methods is that for the uterine activity calculated from the uterine EMG the SNR is relatively high, but the amplitude of a particular burst with respect to other bursts cannot be determined. In contrast, the uterine activity calculated from abdominal deformations has a relatively low SNR but the amplitude of a particular burst with respect to other bursts can be determined.

Based on these results, it can be concluded that the developed algorithm provides a valuable tool for determining the fetal heart rate, the fetal ECG complex and maternal uterine activity from measurements performed on the maternal abdomen. However, at the moment the computation times are too long and therefore have to be reduced to determine the beat-to-beat fetal heart rate online. Furthermore, the calculation of the fetal VCG is inaccurate and has to be improved.

Acknowledgements

I would like to take this opportunity to thank the people without who the fulfillment of my graduation project would have been impossible. First of all special thanks goes to Ir. Chris Peters for being my supervisor, dealing with all my questions and for creating a nice – and occasionally loud – environment to work in. Furthermore I would like to thank Prof. Dr. Ir. Pieter Wijn for his useful comments and for teaching me how to look more critically at my own work. Also thanks to Rian for arranging everything that needed arranging and for the coffee breaks in your office. I'll really miss your daily attempts to make fun of me!

Furthermore thanks to Prof. Dr. Guid Oei for showing the clinical aspects of the project and for creating the weekly TOP meetings. It is very interesting and inspiring to hear what other people are working on and to have them give comments on my work. Thanks to all who participated in these meetings.

I also would like to thank the medical physicists in training, Dr. Ir. Carola van Pul and Ir. Jannie van den Tillaart, for their comments and advises and thanks to all the students that I have worked with. Gijs, Taco and Natasha for giving advise whenever I had problems with my computer. Gijs, I hope your memory has improved since you've left. Cindy for always knowing what was on the menu for lunch and Joyce and (Hend)Rik for improving my programming skills with Matlab. I really enjoyed working with you!

I would like to thank my parents for all their financial support during my education. To put it in your own words, I'll express my gratitude by giving you the biggest salary raise you'll ever have; you can stop paying for my education. Finally, thanks to Petra for the moral support during the last half-year of my graduation project; you have been (and are) a really great friend.

Contents

Abbreviations

ADC	Analog Digital Converter
AV	Atrioventricular
aVF	Augmented Voltage lead Foot
aVL	Augmented Voltage lead Left
aVR	Augmented Voltage lead Right
BPM	Beats Per Minute
CAA	Common Adaptive Averaging
CTG	Cardiotocograph
ECG	Electrocardiogram
EEG	Electroencephalogram
EMG	Electromyogram
FFT	Fast Fourier Transform
FHR	Fetal Heart Rate
HR	Heart Rate
ICA	Independent Component Analysis
SA	Sinoatrial
SAA	Segmentational Adaptive Averaging
SNR	Signal-to-noise ratio
STFT	Short Time Fourier Transform
VCG	Vectorcardiogram

1 Introduction

Birth is probably the biggest challenge a human being has to encounter in life. Not only does a newborn have to adjust to completely new surroundings, moreover the transition from life inside the maternal uterus to life outside it is associated with hypoxia, a decrease of the oxygen level in peripheral tissues. In order to come through labor well, the fetus is equipped with protective mechanisms which enable it to cope with significant oxygen deficiency. A healthy fetus which encounters hypoxia during labor but handles this adequately, is likely to develop normally after birth.

The fetal protection mechanism against oxygen deficiency consists of several reactions that enable the fetus to maintain sufficient oxygen supply to central organs, such as the fetal heart and brain. A first reaction to oxygen deficiency is a reduction of fetal activity, i.e. the reduction of fetal movement and fetal respiration. As the lack of oxygen continues, the fetus reacts by redistributing the blood circulation to central organs at the expense of the oxygen supply to peripheral organs. Furthermore, activity of the autonomic nervous system is increased, stimulating anaerobe metabolism in the peripheral organs. When the fetal protection is fully intact, the fetus reacts optimally to hypoxemia (a decrease of the arterial blood oxygen level) and acute hypoxia during labor, minimizing the risk of damage. When fetal protection is missing, minimal reaction to hypoxia is observed since most of the defensive mechanisms have been used already or did not have had the opportunity to develop. In this case the risk of damage as a result of asphyxia (global oxygen deficiency including the central organs) is significant and several non-characteristic signs of fetal distress can be expected.

Consequently, fetal monitoring during labor has become very important and has enabled physicians to take action when fetal protection is activated but when an increased risk of long-term consequences exists.

As mentioned, one of the main defensive mechanisms of the fetus against hypoxia consists of blood flow regulation and distribution. Both effects are directly related to blood pressure and therefore maintaining a stable blood pressure guarantees a sufficient perfusion of blood to vital organs. The driving force behind the control of variations in blood pressure is the cardiovascular control system, which operates under influence of the autonomic nervous system. This autonomic nervous system exists of two parts, the sympathetic nervous system and the parasympathetic nervous system, between which an essential difference exists. The sympathetic system uses a network for the transfer of action potentials whereas innervation by the parasympathetic system takes place directly. As a result, the sympathetic system is significantly slower than the parasympathetic system.

The controlling of blood pressure by the autonomic nervous system occurs by means of so-called baroreceptors. These baroreceptors are located in the wall of blood vessels and are sensitive to strain. A decreasing blood pressure results in a decrease in the stimulation of baroreceptors, which in turn leads to increased sympathetic activity and lowered parasympathetic activity. This change in sympathetic and parasympathetic activity causes an increase in heart rate and cardiac contraction power and the occurrence of vasoconstriction (the narrowing of blood vessels), which results in an increase in blood pressure. Thus, regulation of blood flow by the cardiovascular control system is achieved in two different ways: the primary way is regulation of the arterial blood pressure by altering the degree of vasoconstriction in blood vessels and the secondary way is the regulation of the heart rate.

It is impossible to determine the blood pressure of a fetus inside the maternal uterus. The fetal heart rate however can be determined non-invasively during pregnancy. For this reason, the fetal heart rate is currently the main source of information from which the physiological condition of the fetus can be obtained.

The fetal heart rate can be determined in several ways, based on two different physical principles. Electrical activity of the fetal heart can be determined by positioning electrodes either directly on the fetus or by positioning electrodes on the maternal abdomen. Positioning the electrodes directly on the fetus is an invasive technique and can only be performed when the fetal membranes have ruptured. Positioning the electrodes on the maternal abdomen is preferable since it is a non-invasive technique, which therefore can be applied in all stages of pregnancy. However, due to the low signal-to-noise ratio, determination of the fetal heart rate from abdominal recordings with existing techniques is inaccurate and not reliable.

A second physical principle from which the fetal heart rate can be determined is used in Doppler ultrasound measurements. Ultrasonic waves experience a shift in frequency when they reflect and scatter at a moving interface. The magnitude and direction of this shift contains information about the motion of that interface. This effect is known as the Doppler principle. Since the fetal heart moves during contraction, Doppler ultrasound can be used as a non-invasive technique to determine the fetal heart rate. The use of Doppler ultrasound is therefore incorporated in the most widely used device to monitor the fetal heart rate non-invasively, the fetal cardiotocograph monitor.

Next to fetal heart rates, this cardiotocograph (CTG) also monitors uterine activity. As uterine contractions can impose stress on the fetus, the relationship between uterine activity and fetal heart rates can

provide information on the fetal condition. This relationship has therefore been investigated extensively through the years. Many guidelines and scoring systems have been proposed for the interpretation of CTG recordings and several of these guidelines are used in clinical practice. However, the information provided by the CTG has turned out to be only sufficient when the condition of the fetus is clearly good or clearly bad. Very often, it is not possible to draw conclusions from CTG recordings and additional tests, such as microblood examination, are required to evaluate the condition of the fetus. Besides the lack of information for accurately evaluating the fetal condition, the use of the CTG is also associated with the drawback that, since it is based on ultrasound, the CTG is very sensitive to motion and noise.

From this it is clear that any additional source of information from which the fetal condition can be assessed or any reliable and accurate alternative to determine the fetal heart rate is highly appreciated. Additional sources of information could be provided by spectral analysis of the fetal heart rate and by the fetal electrocardiogram (ECG). The spectrum of the heart rate contains information about the activity of the central nervous system and in particular about the sympathetic and parasympathetic parts. As the activity of these systems is affected by changes in the physiological circumstances, spectral analysis provides indirect information on the physiological circumstances of the fetus and therefore also on the fetal condition. However, for the frequency spectrum to contain significant information the fetal heart rate is required to be available on a beat-to-beat basis. The fetal ECG provides information on the depolarization and repolarization properties of the heart, which are expressed in the shape of the waveform. Indications have been found that fetal distress is reflected in the ECG signal as changes in the morphology of the waveform [Rosén, 1976].

The main purposes of this project are the development of an algorithm, that is capable of determining the fetal heart rate on a beat-to-beat basis from recordings performed by electrodes positioned on the maternal abdomen. Furthermore, the algorithm has to be able to determine the fetal ECG and maternal uterine activity in order to provide additional information on the condition of the fetus. The last goal of the project is to reduce computation times to such extents that the algorithm is capable of monitoring the fetal heart rate online.

The information, obtained this way, is superior to Doppler ultrasound recordings in several aspects. Not only are the abdominal recordings more reliable in the sense that they are much less sensitive to motion, but as a result the obtained fetal heart rate signal is almost a continuous signal without blank periods requiring interpolation, as is often the case with ultrasound recordings. Spectral analysis, performed on abdominal recordings, is therefore more accurately. Finally, the abdominal recordings provide additional information with respect to ultrasound recordings by means of the fetal ECG. Besides the more reliable and additional information, electrical recordings on the maternal abdomen have one more advantage over ultrasound recordings: electrical recordings do not feed energy to the fetal and maternal body.

This thesis starts with providing some background information on the physiology of the fetal heart and maternal uterus in chapter 2. In this chapter the relationship between activity of these organs and electrical activity detected at the skin surface is discussed. Furthermore, the relationship between fetal heart rate variability and maternal uterine activity is described briefly. Next, chapter 3 discusses the data-acquisition system that is used to record electrical activities at the maternal abdomen. Chapter 4 and 5 handle the developed algorithm. Distinction is made between electrical signals originating from the fetus (chapter 4) and signals originating from the mother (chapter 5). For the fetus both the heart rate and electrocardiogram are determined. The determination of the fetal heart rate is performed in two very similar, but slightly different ways. The first way is used to monitor the fetal heart rate online while the second way is used to determine the heart rate on a beat-to-beat basis. For the mother the uterine activity and maternal heart rate are determined. Determination of the uterine activity is performed in two different ways based on two different phenomena. Finally, chapter 6 presents and discusses the results from each separate algorithm and compares these results to measurements performed with a scalp electrode, an electrode positioned directly on the fetus, and intra-uterine pressure catheter.

2 Physiology

2.1 The heart

2.1.1 Physiology of the heart

The heart is a muscular organ that actually consists of two separate pumps. The right heart pumps blood through the lungs and the left heart pumps the blood through the peripheral organs. Each of these hearts is a pulsatile two-chamber pump composed of an atrium and a ventricle. The atrium functions principally as a weak primer pump for the ventricle, helping to move the blood into the ventricle. The ventricle in turn supplies the main force that pushes the blood through either the pulmonary or peripheral circulation.

The heart has a specialized system for generating rhythmical impulses to cause rhythmical contraction of the heart muscle and conducting these impulses rapidly throughout the heart. When this system functions normally, the atria contract about one sixth of a second ahead of ventricular contraction, allowing the extra filling of the ventricles before they pump the blood through the lungs and peripheral circulation [Guyton, 1996]. Another special feature of the system is that it allows all parts of the ventricles to contract almost simultaneously, which is essential for effective pressure generation in the ventricular chambers.

The fibers of the specialized conducting system have the capability of self-excitation, a process that can cause automatic rhythmical discharge and contraction. The fibers of the sinoatrial (SA) node display this capability to the greatest extent and for this reason the SA node ordinarily controls the rate of beat of the entire heart. The nodal fibers of the SA node discharge spontaneously causing an action potential to travel rapidly through both atria and from there through the atrioventricular (AV) bundle into the ventricles. It is primarily this AV bundle that delays the transmission of action potentials from the atria into the ventricles, allowing time for the atria to empty their contents into the ventricles before ventricular contraction begins. Figure 2.1 shows an illustration of the conduction path of the action potential.

RA = right atrium
LA = left atrium
RV= right ventricle
LV = left ventricle

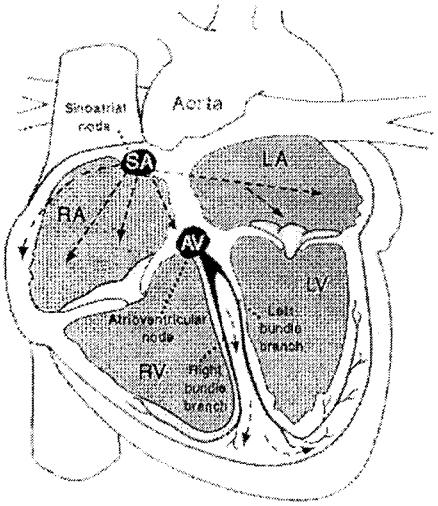

Figure 2.1: Illustration of the conduction path of the action potential throughout the heart. The action potential is generated in the SA node and travels rapidly through both atria. Conduction into the ventricles is achieved through the AV node and the AV bundles.

After penetrating the fibrous tissue between the atrial and ventricular muscle, the distal part of the AV bundle passes downward in the ventricular septum and divides into left and right bundle branches. Each branch spreads downward to the apex of the ventricle, progressively dividing into smaller branches that course around each ventricular chamber and back towards the base of the heart. The terminal Purkinje fibers penetrate about one third of the way into the muscle mass and then become continuous with the cardiac muscle fibers.

The Purkinje fibers lead from the AV node through the AV bundle branches into the ventricles and have characteristics quite opposite of those of the AV node. In order to allow all ventricular muscle fibers to contract almost simultaneously, the cardiac impulse has to appear at each muscle fiber at approximately the same time. For this reason, the Purkinje fibers are relatively large fibers that transmit the action potential at velocities about 6 times larger than transmission velocities in cardiac muscle fibers.

As the cardiac impulse passes through the heart, electrical currents spread into the tissues surrounding the heart. A small part of these currents spreads all the way to the surface of the body, where the electrical potentials,

generated by these currents, can be recorded by electrodes positioned on the skin. This recording is known as the electrocardiogram.

2.1.2 The electrocardiogram

At rest, the potential of the intracellular fluid is negative with respect to the potential of the extracellular fluid. The main reason for this are different concentrations of Na^+, K^+ and Ca^{2+} across the cell membrane. When an action potential propagates along the cell, the action potential causes the Na^+ permeability of the membrane to increase. As a result, tremendous numbers of Na^+ ions flow into the interior of the cell, causing the potential of the intracellular fluid to become positive with respect to the potential of the extracellular fluid: the cell is depolarized. Another result of the propagation of the action potential is the increase in membrane permeability to K^+ ions. As a result, K^+ ions flow from the interior of the cell to the extracellular fluid. Since the increase in K^+ permeability is slower than the increase in Na^+ permeability, the potential of the intracellular fluid first increases rapidly to positive values due to the inflow of Na^+ ions, before it returns relatively slowly to the rest potential due to the outflow of K^+ ions: the repolarization of the cell.

The contraction of muscles is initiated by a chemical process. When an action potential propagates along a muscle fiber it causes the sarcoplasmic recticulum to release large quantities of Ca^{2+} ions into the myofibrils. These Ca^{2+} ions initiate attractive forces between the actin and myosin filaments, causing them to slide together which is the actual contraction of the muscle. For this reason, contraction of the atrial and ventricular muscles can be described by means of de- and repolarization of the muscle fiber cells.

Figure 2.2 shows the propagation of a depolarization wave and a repolarization wave through a cylindrical tissue fiber. The de- and repolarization front act as electrical dipole layers causing small circular currents to flow through the surrounding tissue.

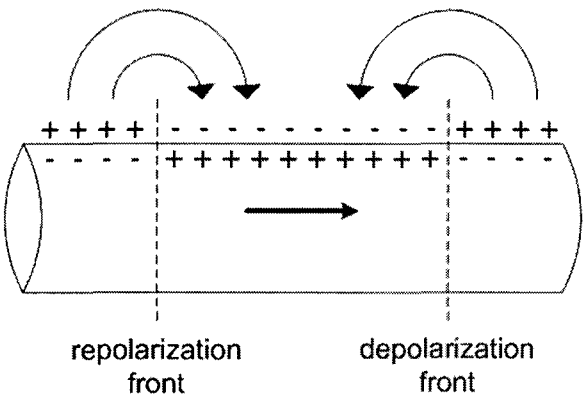

Figure 2.2: The propagation of a de- and repolarization wave through a cylindrical tissue fiber. The waves propagate in the direction of the arrow.

From the generation of these circular currents by the de- and repolarization fronts, it is possible to examine the actual generation of the electrocardiogram (ECG) by taking into account the progression of the wavefronts through the heart. Figure 2.3 shows a typical example of a normal ECG.

After the electrical activation of the heart has started at the SA node, the depolarization wave propagates along the atrial walls to the AV node. This process is represented in the ECG by the P-wave. After the depolarization wave has passed the AV node it spreads through the ventricular walls, which is represented by the QRS-complex. The ventricular repolarization wave starts on the outside of the heart and travels inward. The direction of this wave is therefore opposite from the direction in which the ventricular depolarization wave propagates. As a result, the deflection of the repolarization wave in the ECG, the T-wave, has the same sign as the deflection of the QRS-complex. The repolarization of the atrial walls occurs simultaneously with the depolarization of the ventricles and has small amplitude. For these reasons, the atrial repolarization wave is not visible in the ECG.

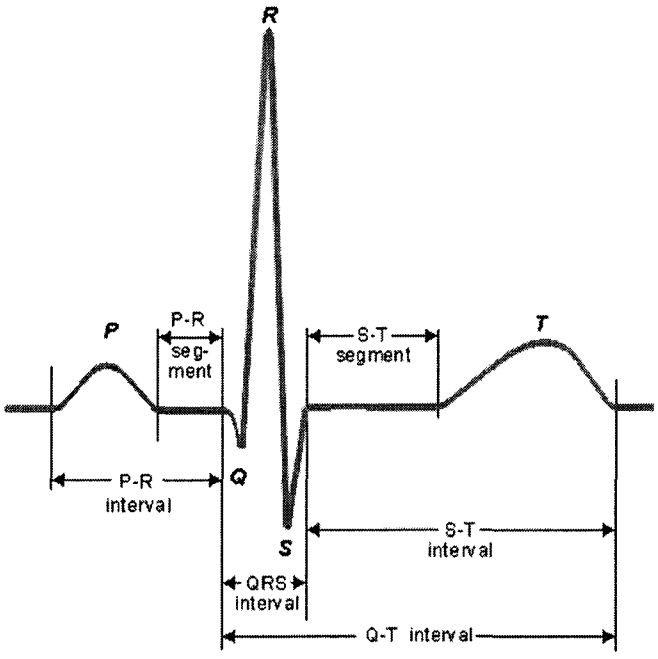

Figure 2.3: Illustration of the normal ECG with corresponding nomenclature. Note that segments are isoelectrical periods, whereas the intervals contain de- or repolarization waves.

The nature of the repolarization wave is in principle very different from the nature of the depolarization wave. The depolarization of a cell produces an electric field which triggers the depolarization of adjoining cells. This way, the depolarization proceeds as a propagating wave within the cardiac tissue. The repolarization of the cell occurs due to the finite duration of the action potential and is therefore not triggered externally. If the action potentials of all cells have equal durations, the repolarization wave would follow the same sequence as the depolarization wave. In ventricular muscle tissue, however, this is not the case. Action potentials in the epicardial cells have smaller duration than action potentials in the endocardial cells. As a result the repolarization appears to be propagating from the epicardial tissue to the endocardial tissue.

2.1.3 Variability in the electrocardiogram

Variability in the electrocardiogram mainly originates from respiratory effects. Changes in the autonomous nervous system, induced by respiration, affect the ECG time intervals. Respiratory movements of the chest and heart affect the ECG wave amplitudes.

During inspiration and expiration the neural activity in the sympathetic and parasympathetic fibers increases [Guyton, 1996]. Stimulation of the right parasympathetic fibers slows down the spontaneous discharging of the sinoatrial nodal fibers. On the other hand, stimulation of the left parasympathetic fibers inhibits the conduction in the AV node. As a result, there is a certain degree of overlap between these effects. Slowing down the discharging of the nodal fibers in the SA node results in longer T-P segments. Inhibition of the conduction in the AV node results in longer P-R segments. Since the next beat is not delayed, this implies that the T-P segment becomes shorter. For this reason both the P-R and T-P segments are affected by respiration.

Stimulation of the sympathetic fibers has essentially the opposite effect on the heart as those caused by parasympathetic stimulation. Stimulation of the sympathetic fibers increases the rate of sinus nodal discharge and increases the rate of conduction in all portions of the heart. As a result, both the P-R and QRS interval become shorter due to sympathetic stimulation.

Respiration is accompanied by changes in the body geometry. During inspiration the cavity of the thorax is enlarged due to the contraction of the diaphragm and the movement of the ribs and sternum. At the same time the heart is forced to assume a different position. Consequence of these movements is a change in the area and shape of the contact surfaces between the heart, the diaphragm and the lungs. During inspiration the contact area of the heart with the diaphragm, which is a good conductor, decreases while the contact area with the less conductive, inflated lungs increases. Therefore the magnitudes of the P-wave, the QRS-complex and the T-wave decrease with inspiration.

2.1.4 Clinical significance of the fetal heart rate and fetal electrocardiogram

At present, the fetal heart rate is virtually the only fetal signal that can easily be monitored before labor. For this reason the use of fetal cardiotocograph monitors during pregnancy is probably the most important method by which fetal distress can be diagnosed. Cardiotocographs simultaneously record fetal heart rate, using Doppler ultrasound, and uterine activity. This situation, in which the fetal condition is evaluated based on only one source of information, is far from ideal – actually the fetal condition is evaluated based on the response of the fetal heart rate to changes in uterine activity. Two possibly additional sources of information on the fetal condition are provided by spectral analysis of the fetal heart rate and by the fetal electrocardiogram.

The variability in the fetal heart rate is influenced by the central nervous system, in particular by the sympathetic and parasympathetic parts of this system. The activity of these systems is influenced by changes in the physiological circumstances and therefore spectral analysis of the fetal heart rate provides indirect information on the fetal condition. However, for the information in the frequency spectrum to be significant, the fetal heart rate has to be determined on a beat-to-beat basis.

The fetal ECG complex holds several features associated with fetal growth and well-being. The durations of the fetal P-wave and QRS-complex are strongly related to gestational age and birth weight [Stinstra, 2002] while hypoxia during labor alters the shape of the ECG complex. In particular the ratio between the P-R and R-R intervals is altered and the ST-segment is depressed or elevated [Sundström, 2000]. The durations of the P-wave and QRS-complex reflect the conduction times of action potentials through the atrial and ventricular tissues, respectively. Increase in cardiac mass and dimensions with gestational age and weight results in longer conduction times and is therefore represented in the ECG complex by an increase in P-wave and QRS-complex durations.

During hypoxia, the available amount of oxygen decreases while the workload of the cardiac muscle is maintained. This causes a negative energy balance, which is represented in the ECG by a biphasic ST-segment. As the heart adapts to the hypoxic situation glycogenolysis and anaerobic metabolism are initiated, regaining equilibrium in the energy balance. However, as a result of the glycogenolysis, K^+ ions are released causing an increase in the T-wave magnitude. In addition, the release of K^+ ions causes the conductive properties of the AV node to change, decreasing the duration of the P-R interval.

2.2 The uterus

2.2.1 Physiology of the uterus

The uterus is a hollow, thick-walled, muscular organ situated deeply in the pelvic cavity between the bladder and the rectum. An illustration of the anatomy of the uterus is to be seen in figure 2.4. Extending from the top of the uterus on either side are the fallopian tubes. These tubes are continuous with the uterine cavity and allow the passage of ova from the ovaries to the uterus. If the ovum is fertilized it imbeds itself in the uterine wall and is normally retained in the uterus until prenatal development is completed.

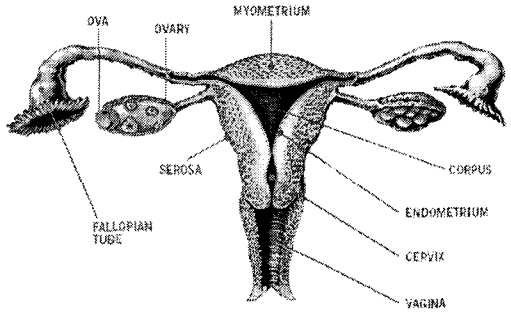

Figure 2.4: Anatomy of the human uterus.

The uterus is composed of two distinct anatomic regions, the cervix and the corpus. The cervix is a narrow cylindrical passage which connects with the vagina at its lower end. At its upper end the cervix widens to form the corpus, the main part of the uterus, which grows during pregnancy to carry the fetus.

The thick wall of the uterus consists of three layers: endometrium, myometrium and serosa. The endometrium is the innermost layer that lines the cavity of the uterus. Throughout the menstrual cycle, the endometrium grows progressively thicker with a rich blood supply to prepare the uterus for potential embryo implantation. In the absence of implantation, a portion of this layer is shed during menstruation. The

myometrium is the middle and thickest layer of the uterus and is composed of smooth, involuntary muscle. The myometrium contracts during menstruation to help expel the sloughed endometrial lining and during childbirth to propel the fetus out of the uterus. The outermost layer, or serosa, is a thin fibrous layer contiguous with extrauterine connective tissue structures, such as ligaments, that give mechanical support to the uterus within the pelvic cavity.

During pregnancy, the uterus becomes enormously enlarged due to growth of preexisting muscle and development of additional connective tissues. The growth of the uterine muscle occurs by means of hypertrophy of the myometrium, i.e. an increase in the size of individual cells characterizing the tissue, without their division. At the same time, the number of gap junctions increases greatly, allowing the fast propagation of action potentials and increasing the coordination of contractility.

As the muscle tissue of the uterus transforms throughout pregnancy, the characteristics of uterine contractions are expected to change as well. During the first 30 weeks of pregnancy, the uterus exhibits very low-amplitude contractions at a frequency of approximately one per minute, the Alvarez waves. From the twentieth week of gestation, the so-called Braxton-Hicks contractions appear. These contractions have higher amplitude and occur every 3 to 4 hours. As pregnancy progresses, these contractions become more and more frequent and increase in strength [Devedeux, 1993].

Like the heart, contraction of the uterus is initiated by the propagation of an action potential. In normal labor, this action potential starts from a pacemaker located at the junction of the fallopian tube and the uterus on one side. From this location, the contractile wave propagates in descending direction along the uterus. The recording on the maternal abdomen of this propagating action potential is called the uterine electromyogram.

2.2.2 The uterine electromyogram

The abdominally recorded uterine electromyogram (EMG) is a noninvasive tool which can be used for the detection and characterization of contractions in obstetric monitoring. Uterine contractions are represented as bursts in the recorded signals and therefore the number of bursts in a given time represents the frequency of uterine contractions whereas the duration of the bursts is associated with the duration of the contractions. The amplitude of the bursts can not be used to characterize contractions due to the fact that this amplitude is affected significantly by external sources, such as electrode properties and filtering by the skin. Since the strength of contractions increases with the rate of action potential firing and conduction, spectral analysis can be applied on the bursts in the EMG signal to obtain information on the strength of the contractions. However, when tetanization of the uterine muscles occurs, this correlation between frequency of action potential firing and contractile strength is lost.

In contrast with skeletal muscles, the conduction speed of action potentials through the myometrial muscle is relatively small. For this reason, the main frequency in the uterine EMG bursts ranges from 0.1 Hz to 3 Hz, whereas for skeletal muscle this frequency can range between 0 Hz and 200 Hz. However, as pregnancy progresses the conduction speed of action potentials increases due to the increasing number of gap junctions, causing the frequency spectrum to shift to higher frequencies.

2.3 Relationship between uterine activity and fetal heart rate

Labor can be regarded as a stress test in which the performance of the cardiovascular system is continuously tested. Compression of the umbilical cord, caused by contraction of the uterus, reduces the blood flow to the fetus. As a result, several pressure sensitive receptors in the heart and main vessels respond, enabling the fetus to adapt immediately to these changes.

At the start of a contraction, compression of the umbilical cord causes blood to be shifted across to the fetus through the large cord vein. Since the heart needs to pump this extra volume, the fetal heart rate increases, causing an increase in blood pressure. As a result, pressure sensitive baroreceptors are activated, causing a drop in fetal heart rate. The persisting compression of the umbilical cord causes the blood flow from the placenta to the fetus to decrease, reducing the blood volume returning to the heart. With less blood to be pumped, the heart needs to adapt rapidly with a sharp drop in heart rate. As the uterine contraction is prolonged, the placenta becomes incapable of handling the blood pushed from the fetus to the placenta causing the flow in the umbilical cord artery to stop. To restore the blood pressure to normal, baroreceptors are activated, causing a vagally-mediated wide variable deceleration. With the decrease in uterine activity, at the end of contraction, blood flow and fetal heart rate return rapidly to normal.

When the fetus is suffering from acute hypoxia, receptors sensitive to a decrease in partial oxygen pressure are activated. These so-called chemoreceptors stimulate both sympathetic and parasympathetic activity,

which results in an initial reduction in fetal heart rate. As the placental blood flow decreases during contraction, the fetal oxygen supply might reduce. As a result, chemoreceptors are activated and repeated decelerations, which start after the contraction has reached its peak, can be seen. A pattern of this kind may also be induced by the increase in blood pressure as part of the cardiovascular adaptation to hypoxia. These decelerations are called late decelerations. With the return of blood flow and oxygenation, the sympathetic activation is maintained, causing tachycardia [Sundström, 2000].

Monitoring the response of the fetal heart rate to uterine activity therefore supplies additional information on the condition of the fetus. In addition to normal decelerations and late decelerations due to hypoxia, there are several other stimuli that affect the fetal heart rate, but discussing all of them is beyond the scope of this thesis; the provided information is merely a simplification of the interpretation of the cardiotocograph recording by a gynecologist.

3 Data acquisition

3.1 Electrodes

Measurements are performed using several Ag/AgCl electrodes positioned on the shoulders and abdomen of the mother. Two different configurations have been used to position the electrodes on the maternal abdomen. The reason for using different electrode configurations is the fact that at first, measurements were performed to determine whether it was possible to develop a technique to obtain the fetal electrocardiogram (ECG) and fetal heart rate from the abdominal recordings. Since the amplitude of the fetal signal is not equal across the maternal abdomen, two transversal lines of six electrodes each were positioned on the abdomen to ensure having at least one electrode in the vicinity of an optimal measuring position. However, to minimize patient discomfort it is desired to measure with as few electrodes as possible. For this purpose a second electrode configuration has been defined. In this configuration electrodes are positioned on the abdomen in such a way as to cover as much uterine surface area as possible. This way, it is possible to analyze which positions provide the highest fetal ECG amplitude. Figure 3.1 shows an illustration of both electrode configurations.

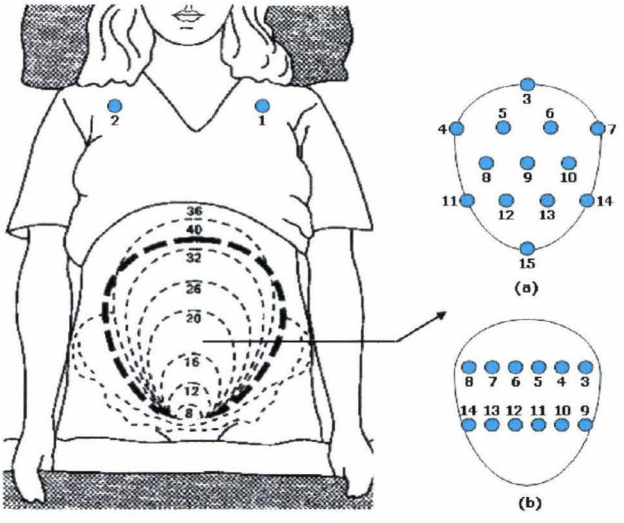

Figure 3.1: Illustration of electrode configurations. Configuration (a) is used to cover as much uterine surface area as possible in order to determine which electrode positions provide the highest fetal ECG amplitude. Configuration (b) is used to make sure that at least one electrode is positioned in the vicinity of a location that provides a high amplitude fetal ECG. For both configurations one electrode is positioned on each shoulder in order to obtain a high amplitude maternal ECG and for configuration (a) one electrode has been positioned on the left ankle for reasons that are made clear in section 3.2. The distance between electrode positions increases as pregnancy progresses and uterine surface area increases.

In order to validate the fetal heart rate calculated from abdominal recordings, an electrode is positioned directly on the fetal head. This scalp electrode is connected to a HP 8040A (Agilent, Palo Alto, California) second-generation fetal CTG monitor. The analog output of this monitor is connected to a computer, which samples the data at a frequency of 1024 Hz using a NI 6034E acquisition board. Naturally, direct measurements of the fetal ECG with the scalp electrode are only performed during labor when fetal membranes have ruptured.

To validate the EMG, calculated from abdominal recordings, uterine activity can be measured using two different methods. The first method to measure uterine activity is by measuring the pressure inside the uterus using an intra-uterine pressure catheter. This method is very reliable but can only be applied during labor and is accompanied with the risk of damaging some tissue structures in the uterus. The second method to measure uterine activity is less reliable but can be applied in stages of pregnancy earlier than labor. It implies the use of a so-called toco transducer, a device that converts abdominal deformations into electrical potentials.

3.2 Amplifier

Measurements are performed using a Porti-16/ASD amplifier from TMS International B.V. [TMS International BV, 2001]. The Porti-16/ASD is a 16-channel ambulatory system for physiological research and can have both unipolar and bipolar electrophysiological inputs. The unipolar inputs are configured as a reference amplifier, i.e. all channels are amplified against the average of all connected inputs. Main advantage of this configuration is that any mutual disturbances or artifacts in the measurements are present in the average as well, resulting in partial cancellation when referencing to this average. However, this feature is only useful whenever the electrodes are positioned in close vicinity to each other, for instance with EEG measurements when all electrodes are positioned on the head of the patient.

For electrode positions mentioned in section 3.1 this configuration is far from ideal. Since the distance between electrodes is relatively large, artifacts detected at a particular position are not necessarily present in other electrode positions. The average signal, however, is affected by such artifacts and as result of referencing so are all other electrode signals.

To determine which positions on the maternal abdomen provide the highest amplitude fetal ECG, it is desired to use bipolar leads instead of unipolar leads. By subtracting signals from electrodes positioned on either side of the fetal heart, it is possible to increase the signal-to-noise ratio of the fetal ECG, while reducing the amplitude of the maternal ECG. As a result of this subtraction, the negative effect of referencing the signals to the average is eliminated. Because the signals are partly reflected and attenuated as they propagate through several tissue interfaces, it is desired for the electrodes not only to be positioned on either side of the fetal heart, but also as close to the heart as possible. Reducing the length of the propagation path reduces the amount of tissue between the electrode and the heart and therefore also reduces signal attenuation.

Since the position and orientation of the fetal heart inside the uterus are unknown, the challenge is to define as few as possible electrode positions meanwhile maintaining a large enough SNR of the bipolar leads to determine the fetal ECG and fetal heart rate. As mentioned in the comments on figure 3.1, an additional electrode is positioned on the left ankle of the mother. The purpose of this electrode is grounding the mother to the amplifier. The human body has nonzero potential and by equalizing the potential of the amplifier and the potential of the mother, the possibility of signals exceeding the input range of the ADC is reduced.

After amplifying the referenced signals at a gain of 20, the signals are digitized by the ADC. This ADC has a 22 bit resolution and an input range between -3 V and +3 V. For analog input this means that the stepsize of the digital output represents a voltage of 71.5 nV.

The frequencies of the electrical signals of interest, the fetal ECG and the maternal uterine EMG, are in the range between 0.1 Hz and 80 Hz. In order to obtain reliable information in this frequency range, the output sample frequency of the ADC has to be set to about 5 times the highest frequency in this range. For this reason, the output sample frequency of the ADC is set to 400 Hz.

Figure 3.2 shows an illustration of the measurement system, including a photograph of electrodes positioned on the maternal abdomen and a photograph of the amplifier. The shown amplifier is however not the Porti-16/ASD amplifier, but a newly purchased programmable acquisition system M-PAQ (IDEE, Maastricht, The Netherlands). The Porti-16/ASD was lent to test whether it was possible to measure fetal ECG signals from the maternal abdomen. After these tests proved successful, the M-PAQ was purchased to serve as a permanent measurement system.

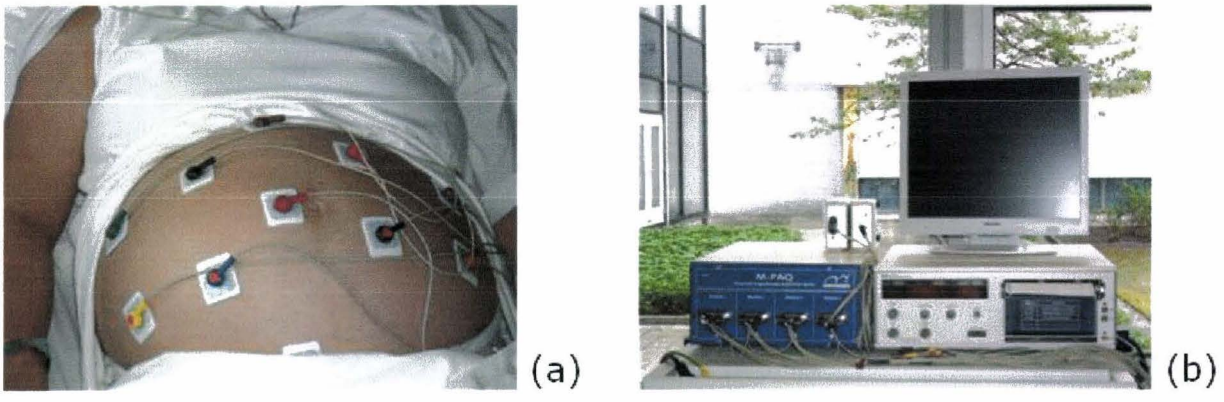

Figure 3.2: Illustration of the measurement system. In (a) a photograph of the electrodes positioned on the maternal abdomen (the electrode configuration of figure 3.1a) can be seen. (b) shows the M-PAQ programmable acquisition system (on the left) and the HP 8040A second-generation fetal CTG monitor (on the right).

3.3 Artifacts

Electrodes usually consist of a metal plate covered with a thin layer of solid salt. When positioned on the skin, the salt dissociates into ions that dissolve in the aqueous environment. This solution, the so-called electrolyte, has the ability to conduct electricity. Due to thermal excitation metallic ions leave the metallic lattice and spread through the electrolyte, causing the electrolyte to obtain a positive potential with respect to the electrode. As a result, a dynamic equilibrium is set between the thermal excitation of metallic ions and the electrostatic field forcing the ions to return to the lattice. This potential difference between electrolyte and metal is called the

electrode-bias and is in the order of magnitude of 1 V. In contrast, biological signals are in the orders of magnitude between 10 μV and 1 mV. This means that the D.C. component of the measured signals should be excluded from amplification.

The ions, attracted by the electrostatic field, are assumed to approach the electrode surface and form a layer balancing the electrode charge. The distance of approach is assumed to be limited to the radius of the ion. The overall result is two layers of charge, the so-called double layer, which is analogous to an electrical capacitor of two plates of charge separated by a certain distance. The existence of this double layer is accompanied by two specific problems: motion artifacts and polarization.

Ions in the double layer can move freely through the electrolyte, however at limited speeds. When the electrode is moved with respect to the electrolyte, the double layer remains behind, resulting in a momentary fluctuation in the electrode-bias. This fluctuation is represented as a source of noise in the signal. The magnitude of this noise depends strongly on the electrode material.

As a current passes through the electrode-electrolyte transition, the double layer is disturbed, again causing a momentary fluctuation in the electrode-bias. This fluctuation is called polarization and its magnitude depends on the frequency of the current, the current density in the transition, the electrode material and the concentration of ions in the electrolyte. In order to minimize the effect of polarization it is therefore desired to keep the current density through the electrode and the concentration of ions in the electrolyte small. One way to achieve this goal is by using an amplifier with large input impedance – the input impedance of the Porti-16/ASD is 10^{12} Ω.

The electrodes, used for performing the measurements, are Ag/AgCl electrodes which have beneficial characteristics with respect to electrode motion and polarization. The AgCl in the Ag/AgCl electrode dissolves very badly in water causing the electrolyte to be saturated quickly. As a result, the Ag^+ concentration near the electrode surface is almost constant since any fluctuation is compensated directly by the dissolving or precipitation of AgCl. This makes the Ag/AgCl electrode very insensitive to polarization and rather insensitive to electrode motion.

Noise caused by the motion of electrodes and by polarization is expressed as a variation in the offset of the signals, the baseline drift. Next to this particular kind of noise, signals are disturbed by noise due to powerline interference and myographic noise. In this context, myographic noise is the collective name of all electrophysiological signals associated with the conduction of action potentials to muscular tissues, with exception of conduction to the heart and uterus.

Myographic noise is closely related to motion artifacts. As action potentials propagate through the muscular tissue, the tissue contracts and, in some cases, motion at the body surface is perceived. This motion can result in the occurrence of motion artifacts. However, significant difference can be found in the characteristics of myographic noise and motion artifacts. While the frequencies of myographic signals range between 0 Hz and 200 Hz, motion artifacts are associated with low frequencies (« 1 Hz) only. The amplitude of both myographic signals and motion artifacts varies up to the same order of magnitude as the ECG amplitude, which is approximately 0.1 mV at the abdomen.

In contrast, fetal movements are almost completely represented by motion artifacts in the measured signals. Motion of the fetus causes the maternal abdomen to move, resulting in the occurrence of motion artifacts in the signals. Fetal myographic signals have amplitudes smaller than or equal to the amplitude of the fetal ECG and as a result the relative amplitudes in the abdominal signal are very small.

4 Signal processing: fetal signals

4.1 The fetal heart rate and electrocardiogram

The main objective of the project is to develop an algorithm to monitor the fetal heart rate. This chapter gives a description of the developed algorithms for calculating the fetal electrophysiological signals from abdominal recordings. Basically, the algorithm operates in two steps. First step is the subtraction of the maternal electrocardiogram (ECG), filtering of the 50 Hz powerline interference and elimination of the baseline drift. The second step consists of the detection of fetal R-peaks. Measurements are performed using twelve electrodes positioned on the maternal abdomen. The reason for using so many electrodes is that the signal-to-noise ratio of particular electrodes is high with respect to the other electrodes, depending on the position of the fetal heart. However, due to relatively large computation times, the number of signals processed by the algorithm has to be reduced. In order to achieve this goal, at first the algorithm performs a so-called initialization in which the signals containing the largest fetal component are determined. Flowcharts of the main components of the algorithm are shown in figure 4.5 at the end of this chapter.

4.1.1 The initialization process

The data obtained from the abdominal recordings are a mixture of electrophysiological signals and noisy interferences. One of the main noisy components is the 50 Hz powerline signal, which is cancelled out by the application of a fourth order Butterworth bandstop filter, filtering between frequencies of 48 Hz and 52 Hz. Since the signals of interest are in the range between 2 Hz and 80 Hz, harmonics of the powerline signal are cancelled out using a fourth order Butterworth low-pass filter with cut-off frequency of 90 Hz. The baseline wander of the signals is cancelled out by the application of a fourth order Butterworth high-pass filter with cut-off frequency of 1.5 Hz. All filters are applied in both forward and backward directions to compensate for phase shifts and are discussed in appendix A. Figure 4.1 provides a schematic view on how an abdominal recording is composed by the mixing of a simulated maternal ECG, a simulated 50 Hz powerline signal and a simulated fetal ECG.

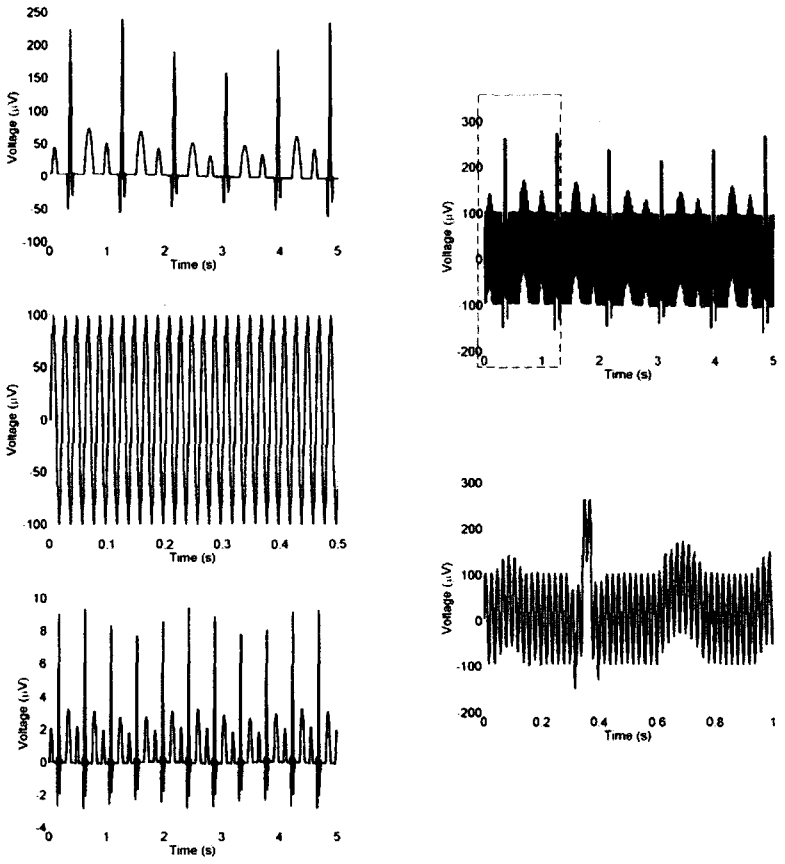

Figure 4.1: Schematic view of the composition of an abdominal recording. The upper left figure shows a simulated maternal ECG signal for a time period of 5 seconds. The center left figure shows a simulated 50 Hz powerline signal for a time period of 0.5 seconds. This signal is continued to a period of 5 seconds, but in order to increase the clarity of the figure, only 0.5 seconds is shown here. The bottom left figure shows a simulated fetal ECG signal. The composite signal, obtained by summing the maternal ECG, the 50 Hz powerline interference and the fetal ECG, is shown in the upper right figure. The bottom right figure shows the same composite signal for a time period of only 1 second, as indicated by the red square box in the upper right figure. Note that, due to its low amplitude, the fetal ECG signal cannot be seen in the composite signals. The vertical axes of the figures are set differently to increase clarity.

After filtering the data, the next step is the removal of the maternal ECG. For this purpose a new technique, segmentational adaptive averaging (SAA), has been developed. This algorithm is discussed in chapter 4.3. SAA estimates the morphology of the maternal ECG complex by averaging $N = 20$ preceding ECG complexes. In order to identify individual ECG complexes, first, the maternal R-peaks are detected using a peak detection algorithm, which is discussed in chapter 4.2. After the maternal R-peaks have been detected, the mean R-R interval duration T is calculated and used to define the alignment of the ECG complexes. The trigger of each ECG complex is defined as the point in time $0.40T$ before the detected R-peak; a maternal ECG complex is defined as the interval between two successive triggers. The reason for defining the trigger of the ECG complexes dependent on the mean R-R interval duration is discussed in chapter 4.3.1. As estimating the maternal ECG complex is more accurate when all complexes have equal amplitudes, each ECG complex is normalized against its maximum amplitude. After estimating the complex with SAA, both the originally recorded ECG complex and the estimated complex are scaled by the normalization factor to obtain the original amplitude.

Since the estimating of the maternal ECG is performed by averaging $N = 20$ preceding complexes and since these complexes are aligned by their R-peaks, fetal components are randomly mixed in the averaging and therefore suppressed in the estimated maternal ECG complex. For this reason, subtraction of the estimated maternal ECG from the filtered recordings does not affect the fetal ECG. In practice, the estimated and original maternal ECG are not completely identical. This means that subtraction of the estimated maternal ECG from the original recording cancels most of the maternal ECG, but residual maternal waveforms may still be present.

The amplitude and morphology of the fetal ECG depend on the position of the electrode with respect to the position of the fetal heart. Therefore, the fetal ECG is not detected with equal amplitudes by all electrodes. In order to determine which electrodes detect the largest fetal signal, the location of the fetal R-peaks has to be known. The processed data from the electrodes are combined and linearly transformed into independent components by the FastICA algorithm [Hyvärinen, 1999]. The FastICA algorithm is a blind source separation technique based on the principle of Independent Component Analysis (ICA) and is briefly discussed in chapter 4.4. Since the fetal ECG is uncorrelated and statistically independent of the maternal ECG and other noisy interferences, one of the independent components, as determined by FastICA, represents the fetal ECG signal. However, application of the FastICA algorithm is accompanied by a few drawbacks. For the purpose of detecting the locations of fetal R-peaks, main drawback is that the order and sign of the independent components can not be determined.

To distinguish between independent components representing the fetal ECG and independent components representing noise, such as residual waveforms of the maternal ECG, peak detection is performed on all independent components. In order to detect the peaks accurately, the polarity of the peaks has to be known. This polarity is determined by summing ten local extrema in the signal to increase the signal-to-noise ratio (SNR) and determining the sign of this summed extremum. The independent component representing the fetal ECG is the component with a mean heart rate in the physiological range (i.e. between 100 BPM and 200 BPM) and with minimal standard deviation from this mean. This last criterion is set to exclude the possibility of noise with random peak locations, but with an averaged peak rate in the physiological range, to be taken for a fetal ECG signal. Since it is possible for the mother to have a heart rate between 100 BPM and 200 BPM, an additional criterion has to be formulated. Distinction between a fetal and a (residual) maternal ECG signal, both with mean heart rate between 100 BPM and 200 BPM and small standard deviation from this mean, is made based on the prior knowledge of maternal peak positions.

Based on the locations of the peaks in the fetal independent component, the signal-to-noise ratio and polarity of each signal can be determined. The SNR is hereby defined as the ratio between the average of the squared amplitudes of the fetal peaks and the root mean square of the signal:

$$SNR = \frac{\frac{1}{M}\sum_{m=1}^{M} V^2\left(R_{peak}(m)\right)}{\sqrt{\frac{1}{N}\sum_{i=1}^{N} V^2(i)}}. \tag{4.1}$$

V is the amplitude of the signal, $R_{peak}(m)$ is the position of the m^{th} fetal R-peak, M is the number of fetal R-peaks and N is the number of samples in the signal. The polarity of the fetal ECG in each signal is determined by the sign of the signal at fetal peak positions. The SNR of equation (4.1) is not a true signal-to-noise ratio, as dimensions of the numerator and denominator do not agree. It however serves as a sufficient criterion to determine the amplitude of the fetal ECG signal with respect to the noise and is hence used as signal-to-noise ratio.

To monitor the fetal heart rate online, computation times have to be reduced significantly. For this reason, only the four signals with the largest signal-to-noise ratios will be processed by the online monitoring algorithm. The final step in the initialization process is generating a small database of ECG complexes. Since the segmentational adaptive averaging algorithm uses 20 preceding complexes to estimate the maternal ECG, this database has to contain the last 20 ECG complexes for each of the four signals that will be processed.

4.1.2 Online monitoring of the fetal heart rate

The most ideal way to determine the heart rate from an ECG signal is by measuring the time between the start of the depolarization at the SA-node of two successive heartbeats. In a standard ECG, this is expressed by the start of the P-wave. Due to noise in fetal ECG signals, it is not always possible to detect the start of this wave accurately. For this reason, the time between two successive R-peaks is used to determine the instantaneous heart rate. The use of the R-wave simplifies the determination of the heart rate but, due to variations in P-R interval length, additional jitter may occur.

The algorithm, used for online monitoring of the fetal heart rate, processes the data collected by the four electrodes with the largest fetal component in the signal. First step of the algorithm is the subtraction of the maternal ECG using segmentational adaptive averaging. The signals obtained after subtraction are averaged, regarding the SNR and polarity of the fetal ECG in the signal:

$$\overline{fecg(n)} = \frac{\sum_{i=1}^{4} pol_i \cdot SNR_i \cdot fecg_i(n)}{\sum_{i=1}^{4} SNR_i}. \tag{4.2}$$

$fecg_i(n)$ is the fetal ECG as determined by subtraction of the maternal ECG, pol_i is the polarity of the fetal R-peaks and is equal to ± 1. SNR_i is the signal-to-noise ratio of the fetal ECG.

Under some circumstances, the estimated maternal ECG complex can incorporate part of the fetal ECG complex. These situations occur when the amplitudes of the peaks in the maternal ECG are affected by the fetal ECG. In these situations subtraction of the estimated maternal ECG results in the partial or complete subtraction of the fetal ECG. To guarantee a sufficient signal-to-noise ratio for all peaks in the averaged fetal ECG, the maternal ECG is estimated again using common adaptive averaging. Common adaptive averaging (CAA) is a technique analogously to segmentational adaptive averaging. Main difference between CAA and SAA is the fact that in CAA the ECG complex is not segmentated but averaged as a whole. For this reason, the fetal ECG complex does not affect the maternal ECG estimate. Drawback of CAA, however, is the fact that CAA cannot estimate the maternal ECG complex accurately due to its incapability of considering the variability between individual ECG complexes.

In short, the averaged fetal ECG from SAA contains a very small number of residual maternal peaks and has a small number of fetal peaks that are affected by the subtraction of the maternal ECG. The averaged fetal ECG from CAA contains a relatively large number of residual maternal peaks and has practically no fetal peaks that are affected by the subtraction of the maternal ECG. Adding the averaged fetal ECG signals from both SAA and CAA therefore results in a signal containing all fetal peaks and a relatively large number of residual maternal peaks. However, the amplitude of these maternal peaks is relatively low with respect to the amplitude of the fetal peaks, with exception of those fetal peaks that are affected significantly by the subtraction of the maternal ECG as estimated by SAA.

After summing the results from SAA and CAA, the fetal R-peaks are detected using the peak detection algorithm described in chapter 4.2. The instantaneous fetal heart rate is calculated from the time between two successive R-peaks.

As mentioned before, both the segmentational adaptive averaging as the common adaptive averaging algorithm use N =20 preceding ECG complexes to estimate the morphology of a particular complex. These preceding complexes are stored in a small database containing 20 complexes for each of the four signals used by the online monitoring algorithm. In order to deal with significant changes in the morphology of the measured maternal ECG complex over time, the database is updated continuously replacing the oldest complex with the newest one.

In some situations the order of magnitude of the averaged fetal R-peak amplitudes is about the same as the order of magnitude of the noise. In these situations, it is possible that noise is detected as fetal R-peak. To reduce this possibility, the detected peak locations are verified by checking whether the interval between two successive

peaks is within a certain deviation, i.e. 20 percent, from the mean interval length. To guarantee a reliable mean interval length, at least ten fetal R-peaks have to be present in the processed data set. Therefore, the online monitoring algorithm processes 6 seconds of data for each of the four selected signals and returns a fetal heart rate that is averaged over these 6 seconds.

4.1.3 The fetal heart rate on a beat-to-beat basis

For research on heart rate variability it is necessary that the fetal heart rate is obtained on a beat-to-beat basis over a relatively long period of time. For this reason data are processed offline. The detection of fetal R-peaks is analogously to the detection of the fetal peaks by the online monitoring algorithm. Verification of the detected peak locations, however, is performed differently.

Since it is likely for the fetal heart rate to accelerate or decelerate in the analyzed time period, verifying the detected peak locations against the mean interval length is inaccurate. The instantaneous interval length for a deceleration or acceleration can differ significantly from the mean interval length and therefore result in rejecting the detected peak location. For this reason, instantaneous interval lengths are compared to a running average of the interval lengths.

4.1.4 The fetal ECG complex

The fetal ECG complex is determined from the signals resulting from the subtraction of the maternal ECG complex, as estimated by segmentational adaptive averaging, and defined analogously to the definition of the maternal ECG complex. That is, after the abdominal recordings have been filtered to remove the powerline interference and baseline drift and after the maternal ECG has been subtracted by using SAA, the fetal R-peaks are detected and each fetal ECG complex is defined as the interval between two successive triggers. These triggers are defined as the point in time $0.40T$, with T the mean R-R interval length, before a fetal R-peak. Due to the relatively low signal-to-noise ratio of the fetal ECG, it is not possible to extract particular features, such as intervals lengths, from the complex. Improvement of the SNR is therefore necessary and obtained in a few post processing steps.

First, the individual fetal ECG signals are subtracted from each other to obtain specific ECG leads. Next, for a specific lead, each normalized ECG complex is cross-correlated with N-1 preceding complexes. N is hereby set equal to $N = 10$, which is discussed in chapter 6.3. Since the maximal amplitude of the correlation supplies information about the similarity of the complexes, averaging the complexes while excluding complexes with a relatively low correlation, results in a higher SNR. The final step in improving the SNR of the fetal ECG complex is the application of an adaptive filter. This filter is described in chapter 4.5.

4.2 Peak detection

4.2.1 Length transformation

The R-wave of the ECG is characterized by the amplitude and the width of the wave. The amplitude of the peak depends on the position of the measurement with respect to the position of the heart. The width of the wave, however, is independent of the position. Since, for particular measuring positions, the amplitude of the P- or T-wave can almost exceed the amplitude of the R-wave, detection on amplitude basis is not recommended.

The so-called length transformation exploits the fact that the gradient of the R-wave is large with respect to the gradient of the P- and T-wave. The length transformation $L(n)$ represents the degree of variability in the amplitude of a digitally sampled signal $x(n)$:

$$L(n) = \sum_{i=0}^{N-1} \left| x(n+i+1) - x(n+i) \right| . \tag{4.3}$$

The number of samples N for which the variability in the amplitude is summed depends on the character of the signal. The fetal ECG with respect to the maternal ECG has smaller amplitude and smaller width of the R-wave. Therefore, the number of samples N is chosen smaller for the fetal ECG than for the maternal ECG. For a fetal signal, N has empirically been determined to equal 20 [Toonen, 1998]. For a maternal signal, N is set equal to 40.

Figure 4.2 shows a characteristic maternal ECG complex with the corresponding length transformation.

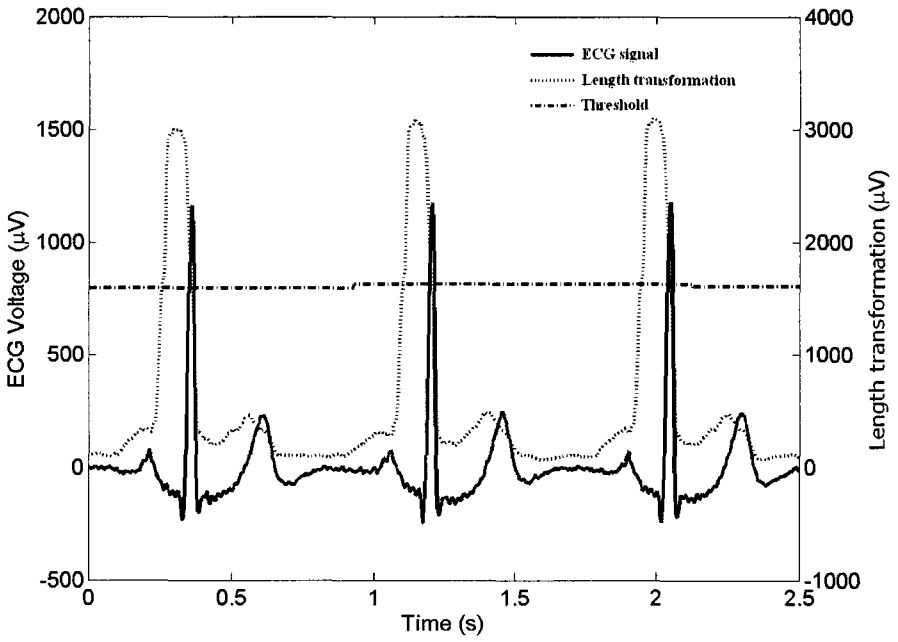

Figure 4.2: Maternal ECG signal (solid line) with the corresponding length transformation (dashed line). The number of samples N for which the variability in the amplitude of the ECG is summed is 40. This corresponds to a time interval of 0.1 s (f_{sample} = 400 Hz). The threshold line represents the threshold value which a peak in the length transformation has to exceed in order to be detected.

As can be seen in figure 4.2, the difference in amplitude between the peak representing the R-wave and the peak representing the T-wave in the length transformation is large with respect to the difference between corresponding amplitudes in the ECG signal. As a result, detection of R-peaks in the length transformation is more reliable than the detection of R-peaks in the ECG signal.

In order to differentiate between peaks in the length transformation that are caused by the P- or T-wave and peaks caused by the R-wave, a threshold is defined. When the length transformation exceeds this threshold, the peak is detected.

4.2.2 Threshold for peaks in the length transformation

The signal-to-noise ratio (SNR) of peaks in the length transformation depends on the SNR of the corresponding ECG signal. In particular for fetal ECG signals, the SNR can be relatively low. In order to differentiate between noise and actual peaks, the threshold for peak detection has to be high enough. However, when the amplitude of the ECG signal decreases, for instance due to respiration effects, this high threshold value can exceed the actual peak and therefore result in not detecting the peak. This problem can be overcome by defining a variable threshold, as shown in figure 4.2.

The determination of the variable threshold is performed in two steps. First, a running average of the length transformation is determined. The window size for this running average is equal to the number of samples N included in the length transformation. The second step is the resampling of the running average with a sampling frequency f_s of 0.83 Hz for the maternal signal and f_s = 1.67 Hz for the fetal signal. These values correspond to heart rates of 50 BPM and 100 BPM, respectively. The amplitude assigned to each (resampled) sample is an empirically determined percentage of the maximum amplitude of the running average in the interval surrounding that sample, i.e. in the interval $[t - 1/(2f_s), t + 1/(2f_s)]$, with t the point in time on which the running average is resampled. In other words, the threshold is defined proportional to the maximum amplitude of the smoothened signal in an interval centered around the peak in the length transformation representing the R-peak in the ECG signal.

Main advantage of defining the threshold this way is the fact that the threshold increases when the amplitude of the ECG signal increases, excluding the possibility of noise exceeding the threshold. Furthermore, the threshold decreases when the amplitude of the ECG signal decreases, excluding the possibility of peaks in the length transformation, caused by R-waves, not exceeding the threshold.

4.2.3 Detection of R-peaks in the ECG

The start of a peak in the length transformation is defined as the point in time on which the length transformation exceeds the threshold. The absolute maximum of the peak is detected in the interval between this start and the point in time on which the length transformation drops below this threshold. This peak in the length transformation indicates the approximate position of the peak in the ECG signal. Therefore the next step in the detection process is the detection of the peak in the ECG signal corresponding to the peak in the length transformation.

As can be seen in figure 4.2, the absolute maximum of a peak in the length transformation is often located near the start of the peak, as the rise of the R-peak is faster than its descent. Detecting a local maximum in the ECG signal, starting from this point in time could therefore lead to detection of the P-peak instead of the R-peak. For this reason, the detection of the R-peak starts from the point in time on which the amplitude of the length transformation drops below 95 percent of the absolute maximum. Naturally, this point in time depends on the number of samples N used in the length transformation.

This way, the position of the R-peak is determined with an accuracy of ± ½ sample. To improve this accuracy, parabolic interpolation is applied:

$$\tau = \frac{1}{2}\frac{y_{n-1} - y_{n+1}}{y_{n-1} - 2y_n + y_{n+1}}. \tag{4.4}$$

y_n is here the amplitude of the ECG signal on sample n and n is the position of the maximum in the ECG complex. The point in time $t_{R\text{-}peak}$ on which the R-peak is located is now defined by

$$t_{R\text{-}peak} = \frac{n + \tau}{f_{sample}} \tag{4.5}$$

with f_{sample} the sampling frequency of the measurement.

4.3 Segmentational Adaptive Averaging

The morphology of the maternal electrocardiogram is not constant in time. This variability of the ECG is caused by extrinsic sources, such as respiration, and intrinsic sources, such as changes in the conductive properties of the AV-node. Result of this variability is the incapability of common averaging techniques to estimate the maternal ECG accurately. This problem can be overcome by using segmentational adaptive averaging.

Segmentational adaptive averaging is a deterministic technique used to recover selected signals from a noisy registration. Basically, the algorithm operates in two steps. The first step contains the identification of individual maternal ECG complexes and dividing these complexes into independent segments. The second step of the algorithm consists of the adaptive averaging and scaling of each segment in order to recover the maternal ECG complex.

4.3.1 Definition of the segments

The variability of the ECG caused by intrinsic sources is characterized mainly by variations in the P-R and R-R interval length. Respiration, as an extrinsic source of ECG variability, can affect the amplitude of all waveforms in the ECG. Common averaging techniques are incapable of accurately estimating the morphology of the ECG, since these techniques estimate the shape of the ECG as a whole and do not consider variations in the waveform. In contrast, segmentation of the ECG complex into independent waves does consider the variability and as a result, is able to estimate the ECG complex more accurately.

The number of independent segments present in the ECG complex depends on the morphology of the complex and, since this morphology depends on the position of the electrodes with respect to the position of the heart, is not constant. Figure 4.3 shows possible independent segments of an ECG complex.

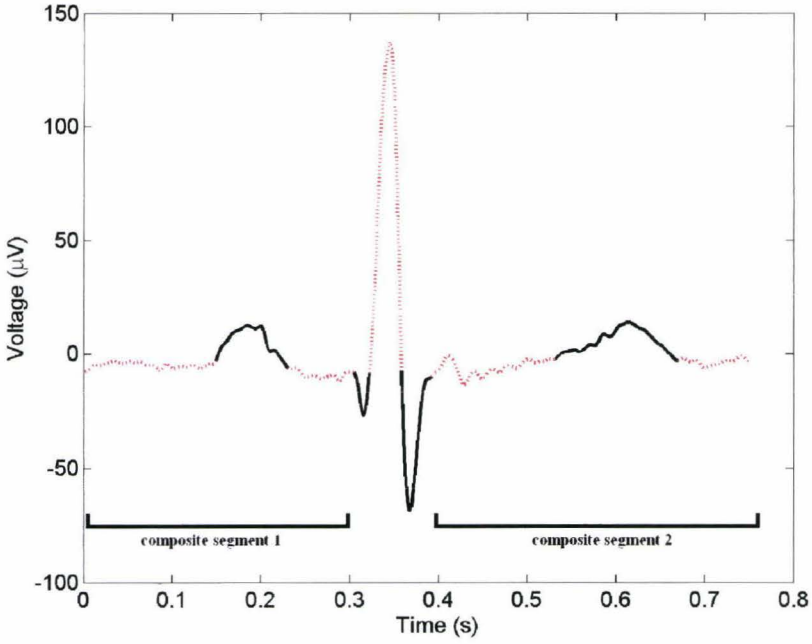

Figure 4.3: Illustration of independent segments that can be present in the maternal ECG complex.

Since the alignment of the ECG complex is triggered with respect to the R-peak, the location of this peak is constant in time. The Q- and S-peak are defined as the local minima before and after the R-peak, respectively.

The start of the Q-wave is determined as the location of the first local maximum before the Q-peak. The end of the Q-wave is determined as the time where the amplitude of the ECG equals the amplitude of the ECG at the start of the Q-wave. When the width of the Q-wave exceeds five samples (12.5 ms) the Q-wave is defined as an individual segment, otherwise it is included in the preceding segment. Reason for this is that a small width increases the possibility of inaccurately estimating the maternal ECG complex. The definition of the S-wave is analogous to the definition of the Q-wave.

The R-wave is defined as the segment between the end of the Q-wave and the start of the S-wave. However, since the amplitude of the segment is scaled in a later stadium, it is necessary for the start and end of the segment to have approximately equal amplitudes. Therefore, the location of the start or end of the R-wave is shifted in order to equalize these amplitudes. Since the P- and T-wave have relatively low amplitudes and large width, these waves are estimated using a different approach. The adaptive averaging technique is performed on the segment between the start of the complex and the start of the Q-wave, i.e. composite segment 1 in figure 4.3, and the segment between the end of the S-wave and the end of the complex, i.e. composite segment 2 in figure 4.3, as a whole. The scaling technique, however, is performed on the separate P- and T-wave. Advantage of this approach is that the influence of possibly present fetal components is minimized while the benefits of the scaling are maintained. Reasons for using a different approach for the averaging and scaling of the P-wave and T-wave are discussed in more detail in chapter 6.1.

As mentioned in chapter 4.1.1, the point in time on which each ECG complex is triggered is defined dependent on the mean R-R interval length, i.e. each ECG complex starts $0.40T$, with T the mean R-R interval length, before its R-peak. Reason for this is that this way the lengths of the composite segments in figure 4.3 with respect to each other are rather constant. Defining the trigger of the ECG complexes independent of the mean R-R interval length results in a relatively short composite segment 1 and a relatively long composite segment 2 when the R-R interval length is long. Likewise, a short R-R interval length results in a relatively long composite segment 1 and a relatively short composite segment 2 when the trigger of the ECG complex is defined independent of the R-R interval length. Since estimation of a short composite segment is less accurate than estimation of a long composite segment, defining the trigger of the ECG complexes dependent on the mean R-R interval length increases the accuracy of the maternal ECG estimate.

4.3.2 *Adaptive averaging of the segments*

The adaptive averaging technique assumes that each ECG segment Seg_i can be estimated from N preceding segments. Due to variability in the ECG, it is possible that the segments from successive complexes are not properly aligned, resulting in a less accurate estimate. To overcome this problem, each of the N preceding segments is cross-correlated with Seg_i:

$$R_{Seg_i,Seg_k}(\tau_k) = \sum_n Seg_i(n)\,Seg_k(n+\tau_k), \quad k = i-1,\ldots,i-N. \tag{4.6}$$

The value for τ_k where the correlation R is maximal depends on the alignment between the segments Seg_i and Seg_k. Therefore shifting Seg_k with τ_k creates the proper alignment between the segments. After the segments have been aligned, the segment Seg_i is estimated:

$$\overline{Seg_i}(n) = \frac{\sum_{k=1}^{N} \alpha_k Seg_{i-k}(n)}{\sum_{k=1}^{N} \alpha_k}. \tag{4.7}$$

$\overline{Seg_i}$ is the estimation for segment Seg_i and α_k are the weights used in the averaging process. The weights are determined by the inverse of the sum of squared errors:

$$\frac{1}{\alpha_k} = \sum_n \left[Seg_i(n) - Seg_{i-k}(n)\right]^2. \tag{4.8}$$

As mentioned before, the P- and T-wave are included in the segment between the start of the complex and the start of the Q-wave and the segment between the end of the S-wave and the end of the complex, respectively. When the P- and T-wave would be estimated as separate segments using adaptive averaging, possible fetal components would affect these estimates. This can be explained by the fact that the amplitude of the P- and T-wave is not much higher than the amplitude of fetal components. Therefore, the determination of the shift τ and the weigth for averaging α_k are affected by the fetal component resulting in an inaccurate estimation of the segment.

4.3.3 *Scaling the estimated segment and reconstructing the ECG complex*

To improve the agreement between the estimated and original segment, the estimated segment is scaled. Scaling is performed in two steps. First, both the estimated segment and the original segment are shifted vertically in order to set the amplitude of the segment boundaries equal to zero. As a result of the finite sample frequency, amplitudes of both segment boundaries are not completely equal. The vertical shift is therefore performed by subtracting the average of both boundary amplitudes, causing the amplitudes of both segment boundaries to be approximately zero. The second step implies the scaling of the estimated segment. Scaling is performed by multiplying the estimated segment with the ratio between the maximum amplitude of the original segment and the maximum amplitude of the estimated segment. After scaling both the estimated segment and the original segment are shifted back. The effect of the scaling is shown in figure 4.4.

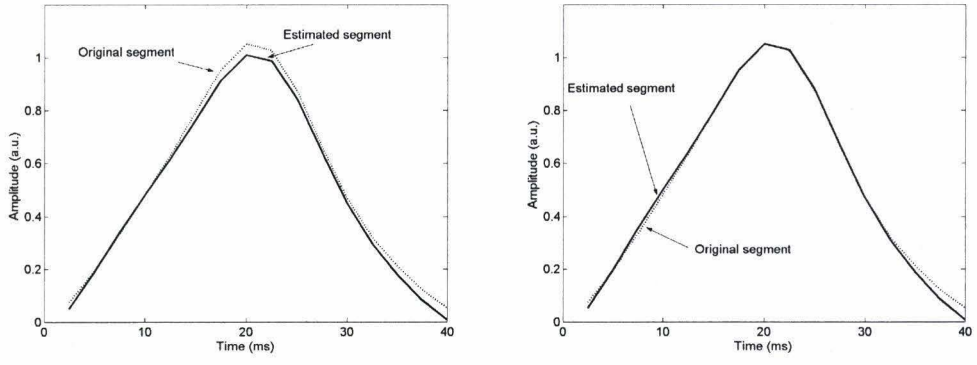

(a) (b)

Figure 4.4: Illustration of the scaling of an estimated R-wave: (a) the estimated R-wave (solid line) and the original R-wave (dashed line) before scaling and (b) the estimated R-wave and original R-wave after scaling. For both figures the waves have already been shiftedback.

As mentioned before, the P- and T-wave are scaled as separate segments. However, definition and scaling of these segments is performed using a different approach than for the other segments. The start and end of the

segment are defined as the first local extrema before and after the peak, respectively. Due to the relatively low signal-to-noise ratio (SNR) of these segments, determination of the positions of these extrema is inaccurate. Therefore, these positions are determined in the estimated segment, which has higher SNR. Since scaling of segments with relatively low amplitude is affected by fetal components, scaling is only performed when the amplitudes of the P- and T-peak are at least 40 percent of the amplitude of the R-peak.

Last step of segmentational adaptive averaging implies the reconstruction of the estimated ECG complex from the estimated segments. In order to obtain smooth transitions between the segments, the segment boundaries, i.e. the outermost sample on either side of the segment, are excluded and the transitions are created by linearly interpolating between the segments.

4.3.4 Brief discussion about segmentational adaptive averaging

In contrast with common averaging techniques, segmentational adaptive averaging (SAA) considers the variability of the ECG and is therefore capable of estimating the morphology of the maternal ECG complex more accurately. Figure 4.5 shows a characteristic maternal ECG complex and the same complex as estimated by SAA and common adaptive averaging (CAA) (i.e. adaptive averaging applied on the ECG complex as a whole).

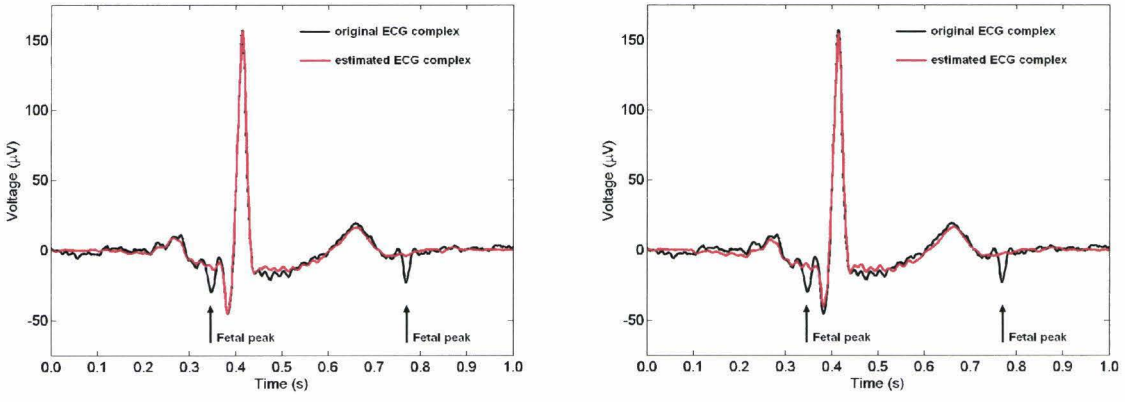

(a) (b)

Figure 4.5: Characteristic maternal ECG complex with (a) the same complex estimated by segmentational adaptive averaging (SAA) and (b) the same complex estimated by common adaptive averaging (CAA). In particular for the Q-wave, estimation performed by SAA is more accurate than the estimation performed by CAA.

The correspondence between the original ECG complex and the complex estimated by SAA is more than 30 percent higher than the correspondence between the original ECG complex and the complex estimated by CAA. The main drawback of using SAA is the fact that the possibility of fetal components affecting the estimated complex is increased with respect to using CAA. When the maximum amplitude of a segment is affected by a fetal component, the scaling factor depends on the fetal component. If this is the case, subtraction of the estimated complex from the original complex affects the fetal ECG. Using separate scaling factors for each segment therefore increases the possibility of affecting the fetal ECG. Additional benefits and drawbacks of SAA are discussed in more detail in chapter 6.1.

4.4 Independent Component Analysis

A central problem in signal processing is finding a suitable representation of the data, by means of a linear transformation. A particular method of finding the linear transformation is called independent component analysis (ICA). As the name implies, the basic goal of ICA is to determine a transformation in which the components are statistically as independent from each other as possible. ICA can be applied, for instance, for blind source separation. Usually, electrophysiological and noisy signals are statistically independent from each other and thus these signals can be recovered from linear mixtures by finding a transformation in which the transformed signals are as independent as possible.

4.4.1 The principle of ICA

The Central Limit Theorem, a classical result in probability theory, states that the distribution of a sum of independent random variables tends towards a gaussian distribution [Hyvärinen, 2000]. Therefore, a sum of two independent random variables usually has a distribution that is closer to gaussian than any of the two original variables. Assume an observation of n linear mixtures $\mathbf{x} = x_1, \ldots, x_n$ of n independent components $\mathbf{s} = s_1, \ldots, s_n$

$$x_j = a_{j1}s_1 + a_{j2}s_2 + \ldots + a_{jn}s_n . \tag{4.9}$$

In order to estimate one of the independent components, consider a linear combination of x_i denoted by $y = \mathbf{w}^T\mathbf{x}$, where $\mathbf{w}$ is a vector to be determined. Denote by $\mathbf{A}$ the mixing matrix containing the matrix elements a_{ij} and define the variables $\mathbf{z} = \mathbf{A}^T\mathbf{w}$. This way, $y = \mathbf{w}^T\mathbf{x} = \mathbf{w}^T\mathbf{A}\mathbf{s} = \mathbf{z}^T\mathbf{s}$ is a linear combination of the independent components s_i with weights given by z_i. Since a sum of two independent random variables is more gaussian than the original variables, $\mathbf{z}^T\mathbf{s}$ is more gaussian than any of the s_i and becomes least gaussian when it in fact equals one of the s_i. In this case, obviously only one of the elements z_i of $\mathbf{z}$ is nonzero. Therefore, $\mathbf{w}$ could be taken as a vector that maximizes the nongaussianity of $\mathbf{w}^T\mathbf{x}$. Such a vector necessarily corresponds to a $\mathbf{z}$ which has only one nonzero component, meaning that $\mathbf{w}^T\mathbf{x} = \mathbf{z}^T\mathbf{s}$ equals one of the independent components. Typically, nongaussianity of a random variable is measured by the absolute value of kurtosis:

$$\text{kurt}(y) = E\{y^4\} - 3\left(E\{y^2\}\right)^2, \tag{4.10}$$

with $E(y)$ defined as the expectated value of y. Kurtosis is zero for a gaussian, zero-mean, random variable, positive for probability distributions peaked at zero and negative for rather flat distributions. Therefore, maximizing the absolute value of the kurtosis of $y = \mathbf{w}^T\mathbf{x}$ results in the retrieval of the independent component s_i.

4.4.2 Drawbacks of ICA

Main drawback of indepent component analyis is the fact that the energy of the independent components can not be determined. The reason for this is the fact that both the mixing matrix $\mathbf{A}$ and the independent components $\mathbf{s}$ are unknown and therefore any scalar multiplier in one of the independent components s_i can be cancelled by dividing the corresponding column $\mathbf{a}_i$ of $\mathbf{A}$ by the same scaler.

Another significant drawback of ICA is the fact that the order of the independent components can not be determined. Since both $\mathbf{A}$ and $\mathbf{s}$ are unknown, the order of the columns in $\mathbf{A}$ can freely be changed, resulting in a corresponding change in the order of the independent components $\mathbf{s}$.

4.4.3 The FastICA algorithm

The FastICA algorithm [Hyvärinen, 1999] has been developed for performing the computations needed for ICA. The algorithm uses an iterative process for finding the local extrema of the kurtosis of a linear combination of the recorded signals $\mathbf{x}$. Basically, the algorithm operates by defining an initial, unit vector $\mathbf{w}_0$ and determining a new vector $\mathbf{w}_i = f(\mathbf{w}_{i-1})$. The function f is obtained from the gradient of the kurtosis. The iterative process stops when the inproduct of the normalized vectors $\mathbf{w}_i$ and $\mathbf{w}_{i-1}$ is close enough to 1, meaning that the kurtosis has reached a local extremum. The final vector $\mathbf{w}_i$ separates one of the independent components from the non-gaussian linear mixture $\mathbf{x}$ in the sense that $\mathbf{w}^T\mathbf{x}$ equals one of the independent components. This is discussed in more detail in appendix B.

4.5 Post processing the fetal electrocardiogram

In some cases, the original recordings have fetal ECG complexes with the same order of magnitude as the background noise. Consequently, the retrieved fetal ECG is affected by a low signal-to-noise ratio (SNR). These ECG complexes can be enhanced by using a smoothing procedure based on a filter working with a moving window [Comani, 2004].

Since the P- and T-wave are relatively slow cardiac events and characterized by a relatively low signal amplitude, these waves are more affected by noise than the R-wave. For this reason, the smoothing factor for the

P- and T-wave has to be larger than the smoothing factor for the R-wave to obtain equal SNR. Basically, the post processing of the ECG complexes operates in two steps. First, for each sample the smoothing factor is determined. This smoothing factor is set inversely proportional to the square root of the maximum signal amplitude in a window centered around the sample. The size of this window equals 20 samples, corresponding to a time interval of 50 ms. The second step of the post processing consists of the determination of a running average with variable window size. This variable window size is proportional to the smoothing factor and normalized with respect to the smoothing factor of the R-peak. This results in a window size of 5 samples for the R-peak, corresponding to a time interval of 12.5 ms and remaining it essentially unmodified, and for the P- and T-wave a typical window size of about 15 samples, corresponding to time interval of 37.5 ms.

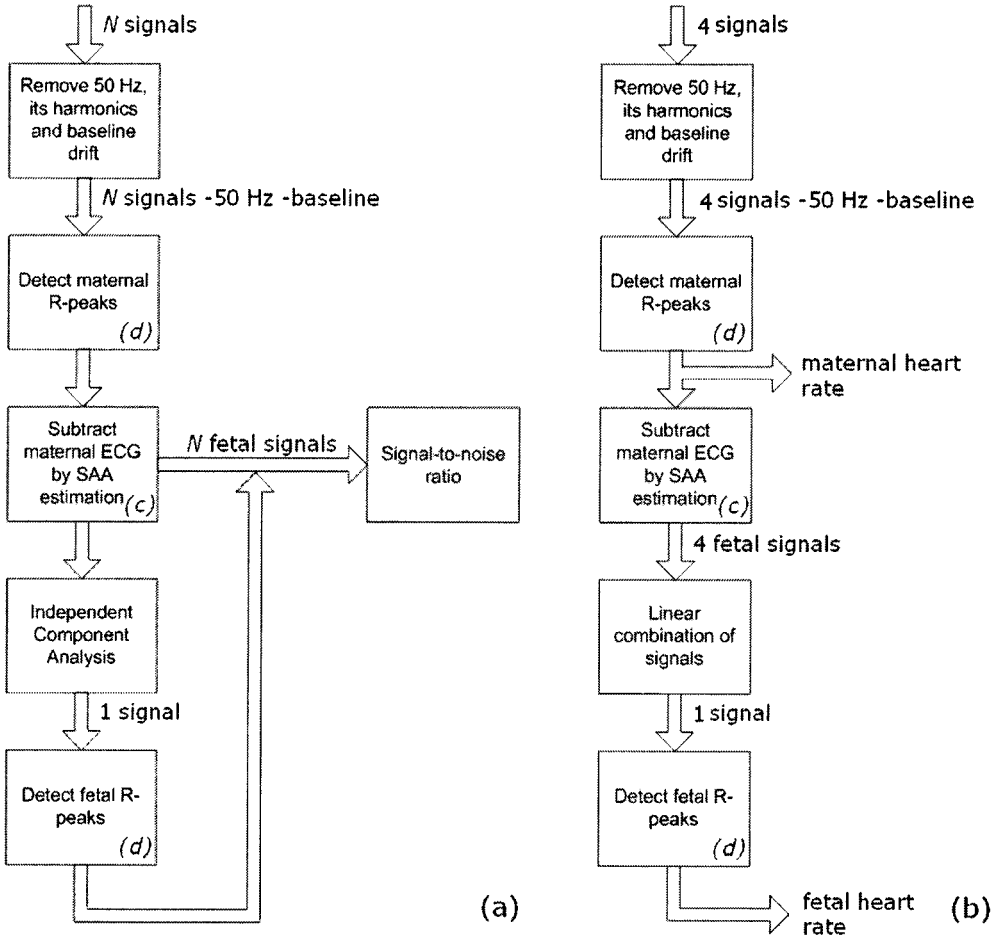
N signals
Remove 50 Hz, its harmonics and baseline drift
N signals -50 Hz -baseline
Detect maternal R-peaks (d)
Subtract maternal ECG by SAA estimation (c)
N fetal signals
Signal-to-noise ratio
Independent Component Analysis
1 signal
Detect fetal R-peaks (d)
(a)
4 signals
Remove 50 Hz, its harmonics and baseline drift
4 signals -50 Hz -baseline
Detect maternal R-peaks (d)
maternal heart rate
Subtract maternal ECG by SAA estimation (c)
4 fetal signals
Linear combination of signals
1 signal
Detect fetal R-peaks (d)
fetal heart rate
(b)

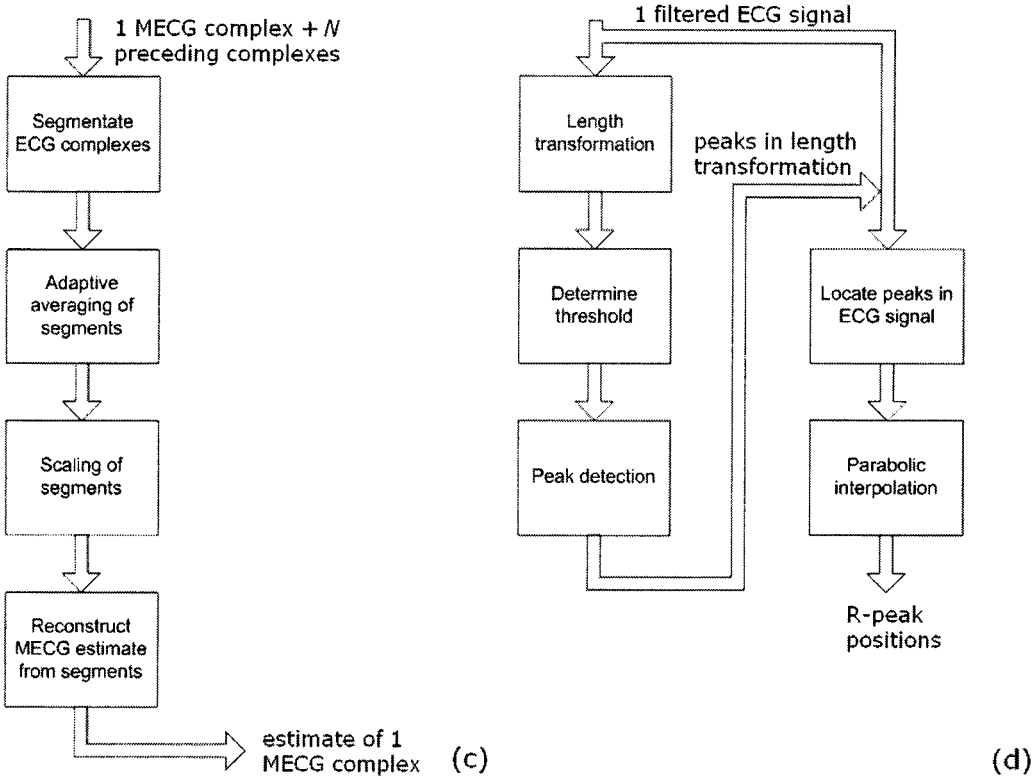
1 MECG complex + N preceding complexes
Segmentate ECG complexes
Adaptive averaging of segments
Scaling of segments
Reconstruct MECG estimate from segments
estimate of 1 MECG complex
(c)
1 filtered ECG signal
Length transformation
peaks in length transformation
Determine threshold
Peak detection
Locate peaks in ECG signal
Parabolic interpolation
R-peak positions
(d)

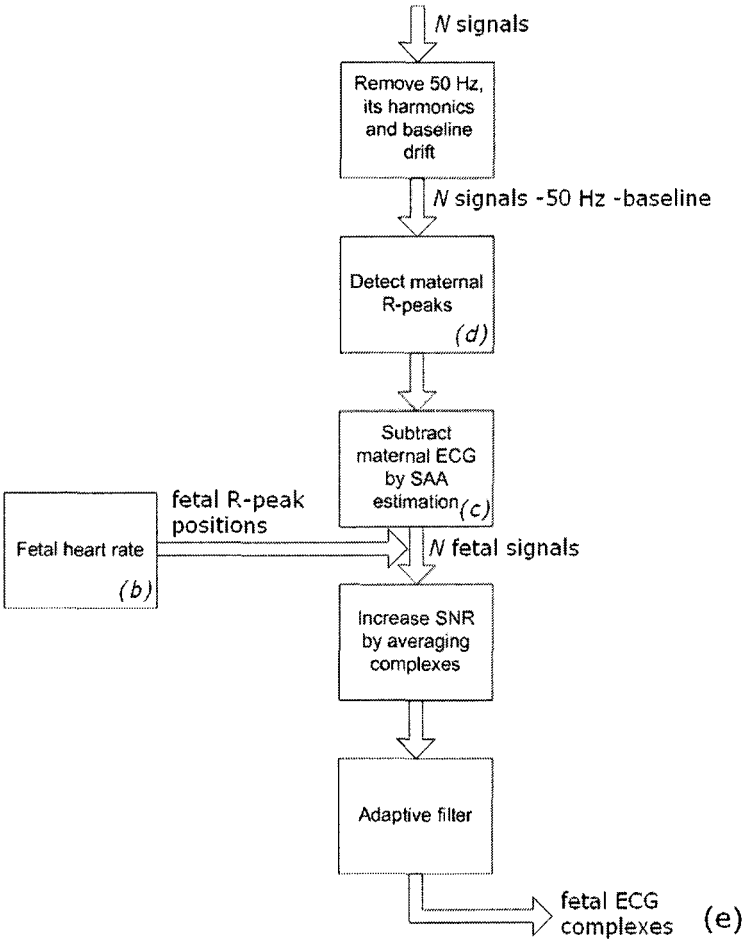

Figure 4.5: Flowcharts of the main components of the algorithm. In (a) the initialization process is shown, in which the four signals with the highest SNR of the fetal ECG are determined. (b) shows the flowchart of the algorithm, used to determine the fetal and maternal heart rate from these 4 signals. In (c) the flowchart of segmentation adaptive averaging is shown, while (d) shows the flowchart of the peak detection algorithm. Finally, (e) shows the algorithm used to determine the fetal ECG complexes. The flowchart for common adaptive averaging is not shown since this is analogous to segmentational adaptive averaging, however without segmentating the ECG complexes.

5 Signal processing: maternal signals

Uterine activity can be calculated from abdominal signals by two distinct methods. The first method exploits the fact that the abdominal surface is deformed by uterine contractions. As a result of these deformations, the abdominal electrodes move with respect to the abdomen, causing the occurrence of motion artifacts. These motion artifacts are reflected in the measured signals by variations in the offset of the signal, the so-called baseline drift.

The second method to calculate uterine activity from abdominal recordings is the determination of the uterine electromyogram (EMG). Naturally, the determination of the uterine EMG provides more information about the actual uterine contraction. Since the frequency of action potential firing and propagation is related to the strength of the contraction, spectral analysis of the EMG provides information about the strength of the contraction. In contrast, due to external sources and elastic properties of the skin, the deformation of the abdomen does not provide as much reliable information about contractile strength. This difference in information on uterine activity provided by motion artifacts and by uterine EMG is analogous to the difference in information between toco transducer and intra-uterine pressure catheter, respectively. A flowchart of both methods is shown in figure 5.3 at the end of the chapter.

5.1 Uterine activity from abdominal deformations

As mentioned in chapter 3, motion artifacts are represented in the signals by low frequencies only. Therefore, uterine activity could basically be determined by applying a low-pass filter on the signals. However, since the frequency of motion artifacts depends on both the patient and the used electrode material, the cut-off frequency for this low-pass filter has to be adjusted continuously between measurements. For this reason the algorithm, used to determine motion artifacts is slightly more complicated than merely the use of a low-pass filter.

The data obtained from abdominal recordings are a mixture of several electrophysiological signals and noisy interferences. To remove 50 Hz powerline interference, the maternal ECG and the skeletal muscle EMG from these data a fourth order Butterworth low-pass filter with cut-off frequency of 0.1 Hz is applied. In order to increase the signal-to-noise ratio of motion artifacts, the absolute signals of all abdominal electrodes are summed. This summation is justified since, due to the elastic properties of the skin, deformations spread all over the abdominal surface and are therefore observed by all electrodes.

To remove low frequent interferences, such as parts of the maternal ECG that are not completely filtered away, from the summed data a running average is determined. The window size for this running average is defined as the ratio between the sample frequency and the frequency at which the spectrum has a global maximum. Since the amplitude of motion artifacts caused by uterine contractions is high with respect to the amplitude of other low frequent signals, this dominant frequency corresponds to the main frequency of contraction induced motion artifacts. Therefore, determination of the running average results in an increase in the signal-to-noise ratio of uterine activity.

5.2 Uterine activity from the electromyogram

5.2.1 Determination of the uterine EMG

Uterine contractions are represented in abdominal recordings as bursts in which main frequencies range from 0.1 Hz to 3 Hz. For this reason the abdominal signals are filtered using a fourth order Butterworth bandpass filter with cut-off frequencies of 0.1 Hz and 3 Hz. Since all abdominal electrodes are positioned on the uterine surface area, the uterine EMG is detected by all electrodes. However, since the distance between uterus and electrode is different for each position, the EMG amplitude differs from electrode to electrode as well. Combining and linearly transforming the electrode signals therefore can result in an EMG signal with higher signal-to-noise ratio. Combination and transformation of the signals is performed using FastICA, an algorithm based on independent component analysis (ICA). The FastICA algorithm is discussed in chapter 4.4.

The uterine EMG is uncorrelated and statistically independent of other electrophysiological signals and noisy interferences in the selected frequency range, with exception of the contraction induced motion artifacts. Therefore, one of the independent components resulting from application of ICA is assumed to represent the uterine EMG. To distinguish between independent components representing the uterine EMG and independent

components representing noise, all independent components are compared to uterine activity as determined from motion artifacts in the signals. The uterine EMG is now defined as the independent component for which the absolute values have the smallest sum of squared errors with respect to this uterine activity. Reason for comparing absolute values of the EMG with uterine activity, instead of the original values, is the fact that activity determined from motion artifacts is basically merely the envelope of low-frequency signals.

After determination of the independent component representing the uterine EMG, the spectrogram of this EMG signal is calculated. This spectrogram is determined by calculating the power spectrum of the Short Time Fourier Transform (STFT), one of the most basic joint time-frequency distributions.

5.2.2 Spectrogram of the uterine EMG

As mentioned in the previous section, uterine activity is represented in the EMG signals as bursts in which the frequencies range from 0.1 Hz to 3 Hz. Distinction, however, can be made between activity in the spectral band between 0.1 Hz and 0.6 Hz and the spectral band between 0.6 Hz and 3 Hz, the low-frequency band and the high-frequency band respectively [Devedeux, 1993]. Activity in the low-frequency band is present in any uterine electrical recording, whereas activity in the high-frequency band is related to efficient labor contractions. Changes in time in the high-frequency spectral band are therefore representative for uterine activity.

In order to determine the spectral contents of a signal in time, the Short Time Fourier Transform (STFT) is used. Basically, this STFT is equivalent to the regular Fourier transform, however with the additional use of a localized window function. For the purpose of providing insight into the principal of STFT, the regular Discrete Fourier Transform is considered at first, before discussing the STFT.

5.2.2.1 Discrete Fourier Transform

One of the most common ways to study the spectral content of a signal is by using the Fourier transform. Let $s(t)$ be a continuous infinite signal, then the Fourier transform $S(f)$ of $s(t)$ is defined as

$$S(f) = \int_{-\infty}^{\infty} s(t) e^{-2\pi i f t} dt . \tag{5.1}$$

When, instead of having infinite length, $s(t)$ has finite length T equation (5.1) converts into

$$S(f) = \int_{0}^{T} s(t) e^{-2\pi i f t} dt . \tag{5.2}$$

In the most common situations signal $s(t)$ is not measured continuously but sampled at evenly spaced intervals in time at sample frequency f_s. For this reason a discrete version of equation (5.2) has to be used, the Discrete Fourier Transform:

$$S(f_n) = S_n \Delta t = \frac{T}{N} \sum_{k=0}^{N-1} s_k e^{\frac{-2\pi i k n}{N}}, \qquad n = -\frac{N}{2}+1, \ldots, \frac{N}{2}, \qquad k = 0, 1, \ldots, N-1 . \tag{5.3}$$

Here N is the total number of samples, s_k the signal at time $k\Delta t$, with $\Delta t = 1/f_s$ and $S(f_n)$ the complex amplitude for a frequency interval $f_n = n\Delta f$ with $\Delta f = 1/T$. These frequency intervals, which are also called frequency bins, range from

$$-\frac{f_s}{2} < f_n \leq \frac{f_s}{2} \tag{5.4}$$

of which only the positive frequencies have physical significance. To prevent aliasing when performing the Discrete Fourier Transform the Nyquist criterion has to be met. The Nyquist criterion requires a signal to be sampled at least twice as often as the highest frequency it contains.

5.2.2.2 Spectral leakage

The Discrete Fourier Transform of a finite signal is a complex quantity and is therefore periodically expanded with period $N\Delta f$. When a signal is truncated, for example by the use of a rectangular window function as shown in figure 5.1, spectral energy is spread across several frequency bins for any frequency component of the signal that does not exactly coincide with a frequency bin, i.e. $f \neq n\Delta f$. This phenomenon is called spectral leakage.

Figure 5.1 shows the truncation of signal $s(t)$. The truncation can be interpreted as the multiplication of $s(t)$ with a rectangular window function $h(t)$. The Fourier transform expands this truncated signal periodically with period $T = n\Delta f$. Since $s(t)$ does not match the criterion of being periodical with period T, discontinuities are present at the edge of adjacent sections, causing the occurrence of spectral leakage.

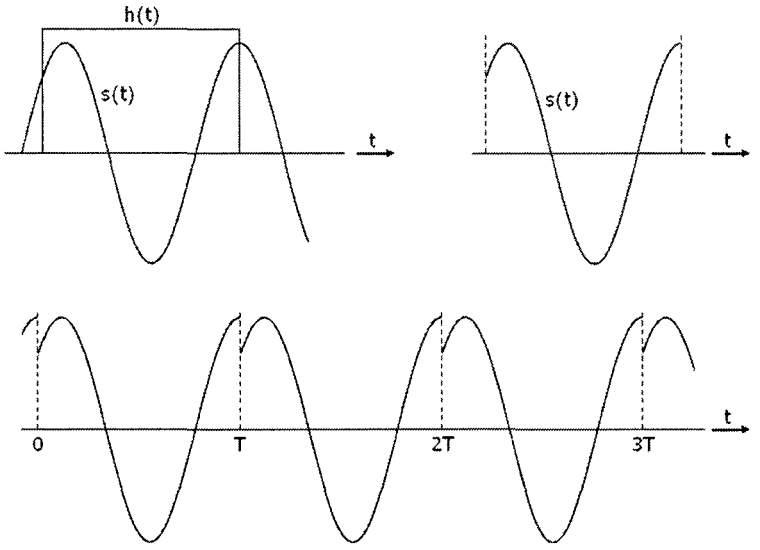

Figure 5.1: Illustration of discontinuities at the edges of the periodic expansion of a truncated signal. Truncation is obtained by multiplying signal $s(t)$ with the window function $h(t)$. These discontinuities will introduce spectral leakage in the spectrum $S(f)$ of the signal.

While in general spectral leakage cannot be eliminated completely, its effects can be reduced by the application of a tapered window function instead of a rectangular window function. Rather than starting and stopping abruptly, the signal now fades in and out towards zero at either sides of the window. As a result, the effect of discontinuities is reduced since mismatched sections of the signal merge. Consequently also the amount of spectral leakage reduces. A disadvantage of using a tapered window is the fact that lines in the spectrum are broadened, causing a reduction in spectral resolution. Figure 5.2 shows the used tapered window function, a so-called Hanning window, and the effect of this window on the periodically expanded signal of figure 5.1.

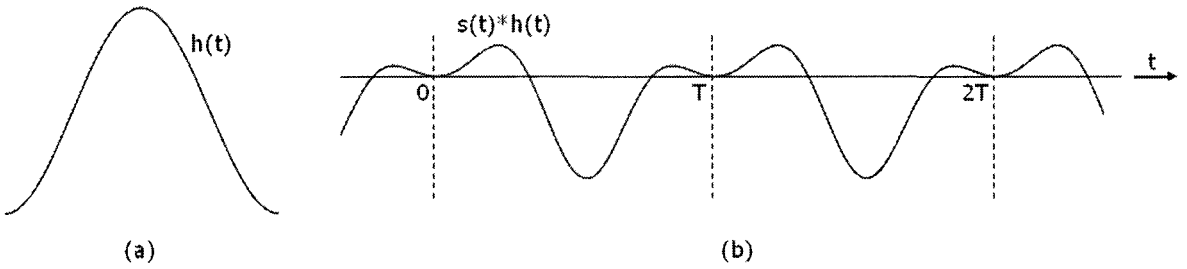

Figure 5.2: (a) The Hanning window, which is used as tapered window function in order to reduce the effect of spectral leakage and (b) the effect of applying the Hanning window on the truncated signal $s(t)$ of figure 5.1.

The theorem of Parseval states that energy is conserved in the Fourier transform

$$\sum_{k=0}^{N-1} |s_k|^2 = \frac{1}{N} \sum_{n=0}^{N-1} |S_n|^2 . \tag{5.5}$$

This implies that in order to obtain the energy of the signal, the square of the Fourier transform $|S(f)|^2$, which is called the power spectrum, has to be determined. Only the positive frequencies in the spectrum have physical significance. Therefore the single sided power spectrum is used, neglecting negative frequency components. As a

result, the amplitude of the single sided power spectrum has to be doubled in order to meet the theorem of Parseval.

As can be seen in figure 5.2, application of the Hanning window $h(t)$ decreases the spectral power of the original signal $s(t)$. To obtain the correct power spectrum from the Fourier transform, the signal has to be corrected for this operation by dividing the power spectrum of the Fourier transform by the average power of the Hanning window. This average power equals:

$$\overline{P}_{Hanning} = \frac{3}{8}\frac{N-1}{N} \tag{5.6}$$

with N the length of the window.

5.2.2.3 Short Time Fourier Transform

The Fourier transform provides information about the spectral contents of a signal $s(t)$. However, it does not reflect the time varying nature of the signal since the basic functions used in the Fourier analysis do not associate with any particular time instant. Information about how the frequency contents of a signal evolve over time can be obtained by the use of a localized window function $h(t)$:

$$STFT(t,f) = \int s(\tau)h(\tau - t)e^{-2\pi i f\tau}d\tau\,. \tag{5.7}$$

If the time duration of $h(t)$ is given by Δ_t and the frequency bandwidth is Δ_f then equation (5.7) expresses the behavior of the signal in the region $[t - \Delta_t, t + \Delta_t] \times [f - \Delta_f, f + \Delta_f]$. Δ_t and Δ_f cannot be chosen as narrow as possible, since the uncertainty principle states that a given distribution cannot provide an unlimited good time and frequency resolution simultaneously

$$\Delta_t\Delta_f \geq \frac{1}{4\pi} \tag{5.8}$$

where the equality only holds for Gaussian window functions.

The main disadvantage of the STFT is the time resolution. In spite of using a window function, it is still necessary to acquire relatively long data sets for analyzing low frequencies. Since the lowest frequency of interest for uterine activity is 0.1 Hz and at least two periods are required for accurate frequency analysis, at least 20 seconds of data should be used. For efficient calculation of the Fast Fourier Transform the data set should contain 2^n, n = 0, 1, 2,... samples and since data are sampled at 400 Hz this means that not until after 20.5 seconds it is possible to obtain spectral information. In order to smoothen the STFT spectrum, overlapping windows are used.

As mentioned before, the power spectrum can be determined from the STFT spectrum by the theorem of Parseval. The resulting distribution is called the spectrogram.

5.2.3 Determination of uterine activity from the EMG spectrogram

The EMG spectrogram contains information about the time-dependent behavior of the EMG power spectrum. In order to determine the time-dependent activity in a specific spectral band, it is therefore required to sum the contributions within that band. Since efficient labor contractions are associated with activity in the spectral band between 0.6 Hz and 3 Hz, uterine activity is determined by summing the contents of the frequency bins within this band.

Strength of contractions increases with the rate of action potential firing and propagation through the uterine muscular tissue. Consequently, spectral analysis of the bursts in the EMG signal provides information about contractile strength. However, due to the relatively low signal-to-noise ratio and low frequency resolution, determination of the dominant frequency for each burst is inaccurate. For this reason, and the fact that EMG amplitudes are heavily influenced by various recording-dependent factors, the mean dominant frequency of the bursts is determined in order to distinguish strength of contractions between patients. Examples of recording-dependent factors affecting the EMG amplitude are electrode arrangement, electrode distance with respect to the recorded muscle fibers, differences in impedance of the tissue-electrode contact and skin filtering, which differs

from one woman to another. Since for each individual recording these recording-dependent factors are assumed to be rather constant, it is possible for a single recording to determine the strength of a particular contraction with respect to the other contractions as the ratio between burst amplitudes in the uterine activity signal, i.e. the summed contributions to the EMG power spectrum within the spectral band between 0.6 Hz and 3 Hz.

In order to determine the mean dominant frequency of the bursts in the EMG signal, these bursts are detected by means of a threshold. Because of the higher signal-to-noise ratio, bursts are detected in the signal resulting from the summation of power spectrum contributions in the high-frequency spectral band, i.e. the band between 0.6 Hz and 3 Hz. When this signal exceeds the threshold for at least 10 seconds, a burst is recorded. An exceeding lasting less than 10 seconds is assumed to be caused by noisy artifacts and is therefore excluded from spectral analysis. The threshold for detection of bursts in the signal $u(t)$ is defined as:

$$Threshold = A\left\{\max\left(u(t)\right) - \overline{u(t)}\right\} + \overline{u(t)}. \tag{5.9}$$

The reason for defining the threshold dependent on the maximal signal amplitude and mean signal amplitude is the fact that for noisy signals the mean signal amplitude, and consequently the threshold value, is rather high, reducing the possibility of noise exceeding the threshold. Furthermore, for signals with relatively low amplitude bursts the threshold value is reduced, assuring the detection of these bursts. The scaling parameter A has empirically been determined to equal 0.2.

The dominant frequency of a burst is defined as the frequency for which the spectrum of the EMG signal has a global maximum. This spectrum is defined as the contents of each frequency bin in the STFT spectrum, summed over a period of time corresponding to the period from the start of the burst till the end of the burst.

5.3 The maternal heart rate

The determination of the maternal heart rate is very similar to determination of the fetal heart rate. For the purpose of completeness however, this subject is treated separately here with the consequence that much overlap exists with the description of the determination of the fetal heart rate.

The most ideal way to determine the heart rate from an ECG signal is by measuring the time between the start of the depolarization at the SA-node of two successive heartbeats. In a standard ECG, this is expressed by the start of the P-wave. Due to noise, it is however not always possible to detect the start of this wave accurately. For this reason, the time between successive R-peaks is used to determine the instantaneous heart rate. The use of the R-wave simplifies the determination of the heart rate but, due to variations in P-R interval length, causes the occurrence of additional jitter. Determining the maternal heart rate based on the time between successive R-peaks results in the need for positioning the electrodes in such way that the R-waves have maximal signal-to-noise ratio.

For both electrode configurations shown in figure 3.1 electrodes have been positioned on the shoulders of the mother. In combination with the reference electrode on the ankle these electrodes approximately constitute the so-called Einthoven triangle. Difference with respect to the actual Einthoven triangle is that electrodes are positioned on the shoulders instead of the hands in order to reduce motion induced artifacts. Since standard lead II of the Einthoven triangle, which is defined as the direction from the right hand to the left ankle, provides the highest R-peak amplitude, the maternal heart rate is determined from the difference between the right shoulder and left ankle electrodes.

The electrical activity of the maternal heart as obtained by the electrodes is contaminated with several kinds of noise, such as 50 Hz powerline interference and motion artifacts. In order to remove the powerline interference a fourth order Butterworth bandstop filter, filtering between 48 Hz and 52 Hz, is applied. Harmonics of the powerline signal are cancelled out by applying a fourth order Butterworth low-pass filter with cut-off frequency of 90 Hz. Finally, the baseline drift is removed by the application of a fourth order Butterworth high-pass filter with cut-off frequency of 1.5 Hz.

Detection of R-peaks in the remaining signal is performed by means of the length transformation and parabolic interpolation, which are both discussed in chapter 4.2. The instantaneous maternal heart rate HR is calculated from the points in time $t_{R\text{-}peak}$ on which these R-peaks are detected by

$$HR(i) = \frac{60}{t_{R-peak}(i+1) - t_{R-peak}(i)}. \tag{5.10}$$

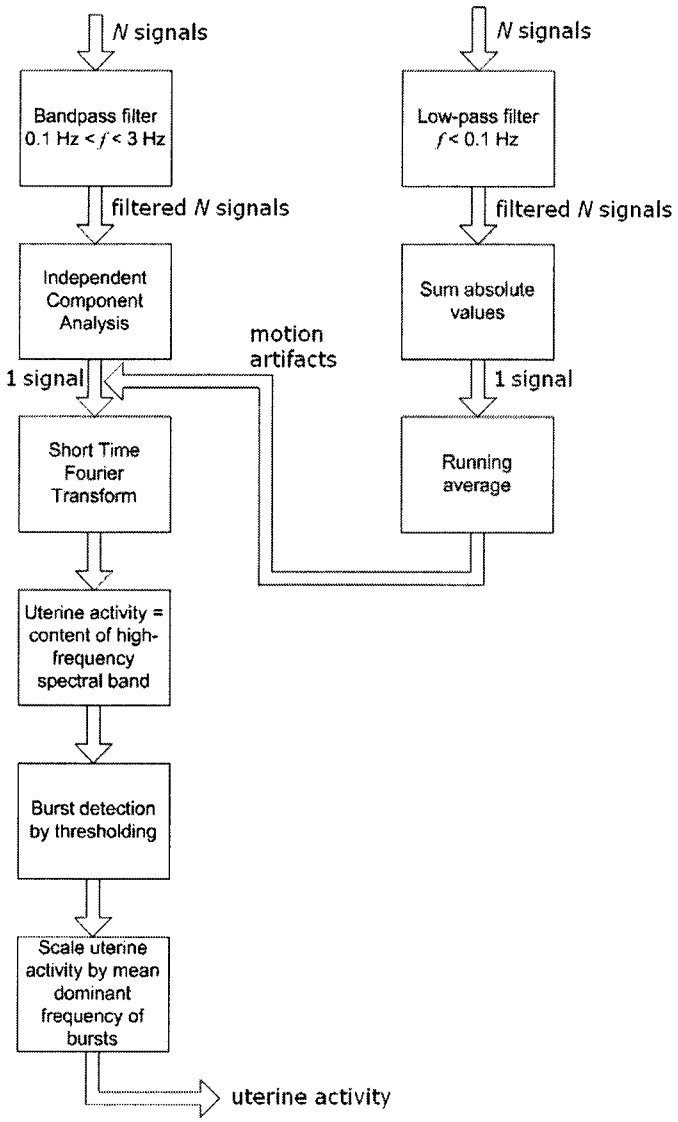

Figure 5.3: Flowchart of the algorithms used to determine uterine activity. On the right the method based on the determination of motion artefacts is shown, while the left shows the method using the EMG signal to determine uterine activity.

6 Results and discussion

In this chapter the main results of the project are presented and discussed. The main focus of the project was on determining the fetal heart rate from abdominal recordings and validate this heart rate by comparison to the heart rate determined from a directly recorded fetal electrocardiogram (ECG). Basically, the algorithm used to determine the fetal heart rate non-invasively can be divided into two parts, as discussed in chapter 4. The first part consists of the estimation and subtraction of the maternal ECG by segmentational adaptive averaging and the second part consists of the detection of fetal R-peaks and calculation of the fetal heart rate. Consequently, the first part of this chapter focuses on the results of the subtraction of the maternal ECG. In the next part of the chapter abdominally determined fetal heart rates are compared to the directly determined fetal heart rate.

Furthermore, algorithms to determine the fetal ECG complex and maternal uterine activity have been developed, discussed in chapter 4 and chapter 5 respectively. Results of the calculation of the fetal ECG complex are presented and discussed in the third part of this chapter, while the fourth part of the chapter compares results of the calculation of uterine activity to intra-uterine pressure registrations. The determination of the maternal heart rate and some general comments are discussed in the last two parts of this chapter.

6.1 Subtraction of the maternal ECG

To illustrate the results of segmentational adaptive averaging (SAA) figure 6.1 shows a few seconds of an abdominal recording and the estimate of the maternal ECG by SAA. The shown recording is performed with the electrode configuration of figure 3.1b – the shown signal is recorded by electrode 11 – which means that the recording is referenced against the average signal of all electrodes. The recording has been processed by filtering the 50 Hz powerline and its harmonics and removing the baseline drift.

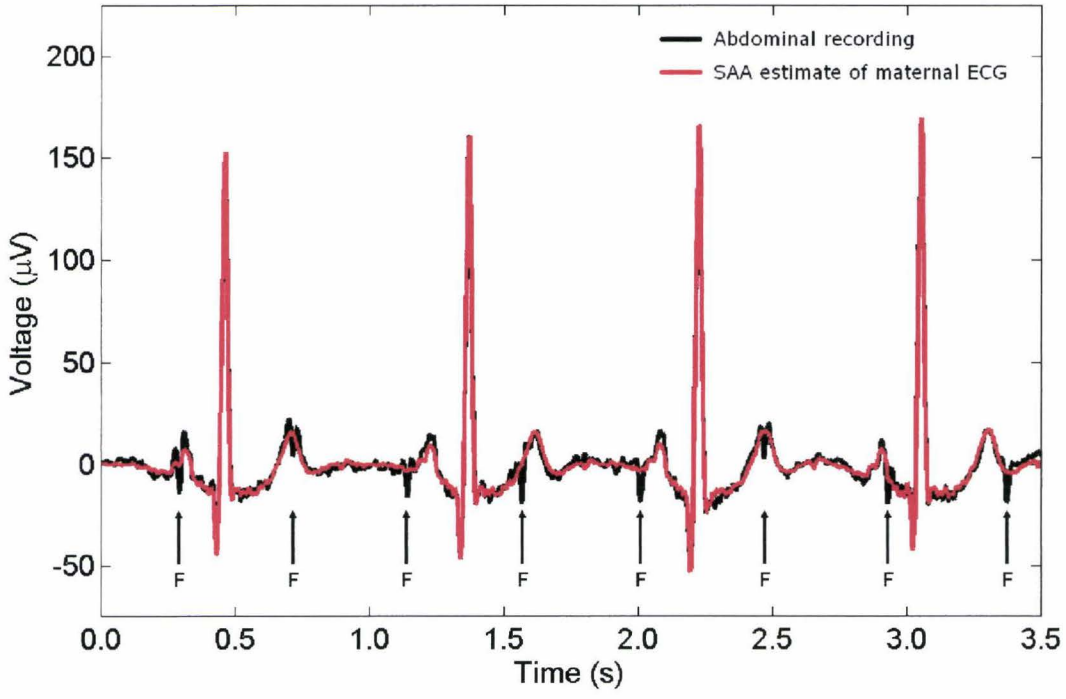

Figure 6.1: Example of an abdominal recording with the electrode configuration of figure 3.1b (black) and the corresponding estimate of the maternal ECG by segmentational adaptive averaging (red). Fetal R-peaks can be distinguished in the abdominal recording and are labeled with F. Note that in most cases the fetal R-peaks cannot be seen as clearly as for this particular recording. The shown abdominal recording has been preprocessed by filtering the 50 Hz powerline interference and its harmonics and by removing the baseline drift.

The amplitude of fetal R-peaks can be in the same order of magnitude as the amplitude of the maternal P- or T-wave, as can be seen in figure 6.1. To prevent the fetal ECG from being affected significantly by the subtraction of the maternal ECG, the amplitude of the fetal R-peak in the maternal ECG estimate has to be reduced to about 5% of its original value. For this purpose 20 preceding ECG complexes are included in the estimation process. Naturally, it is preferred to reduce the amplitude of the fetal R-peaks even further, but averaging more than 20

preceding maternal ECG complexes can result in an insufficient estimation. Changes in the physiological circumstances of the mother are reflected in the ECG and as a result the waveform of the maternal ECG can be changed too much in a time period longer than 20 heartbeats to accurately predict the next ECG complex.

As mentioned in chapter 4.3, the segments representing the P- and T-wave are estimated using a different approach than for the estimation of the waves in the QRS-complex. The main reason for this is that the alignment of segments as calculated in equation (4.6) can cause significant errors when estimating the P- and T-wave as separate segments. Since the amplitude of fetal R-peaks can be in the same order of magnitude as the P- and T-wave, the shift τ_k, required to properly align segment Seg_k with the segment to be estimated, can depend on the position of the fetal R-peaks in both segments. This is illustrated in figure 6.2.

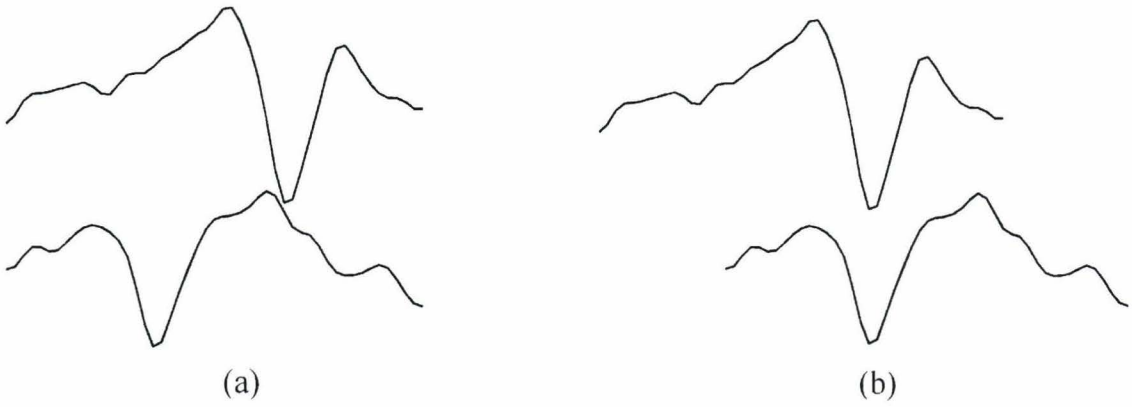

Figure 6.2: Illustration of two maternal P-waves, each containing a fetal ECG complex with the R-peak directed downwards. In (a) the segments are plotted against a simultaneous time-axis while in (b) the segments are aligned by applying equation (4.6). The alignment is clearly affected by the fetal ECG complex.

Figure 6.2 clearly shows the influence of fetal R-peaks on the alignment of two maternal P-waves. Applying adaptive averaging on the aligned P-waves results in an estimated segment containing a relatively large fetal component whereas the amplitude of the average maternal P-wave is reduced, as a result of averaging. Determination of the alignment can be improved by applying equation (4.6) on a longer segment, since increasing the length of the segment results in decreasing the influence of the fetal ECG. For the P-wave, the segment is elongated by defining it as the segment between the start of the ECG complex and the start of the Q-wave, i.e. composite segment 1 in figure 4.3. Figure 6.3 shows the same maternal P-waves as figure 6.2, but with the alignment determined from the elongated segments.

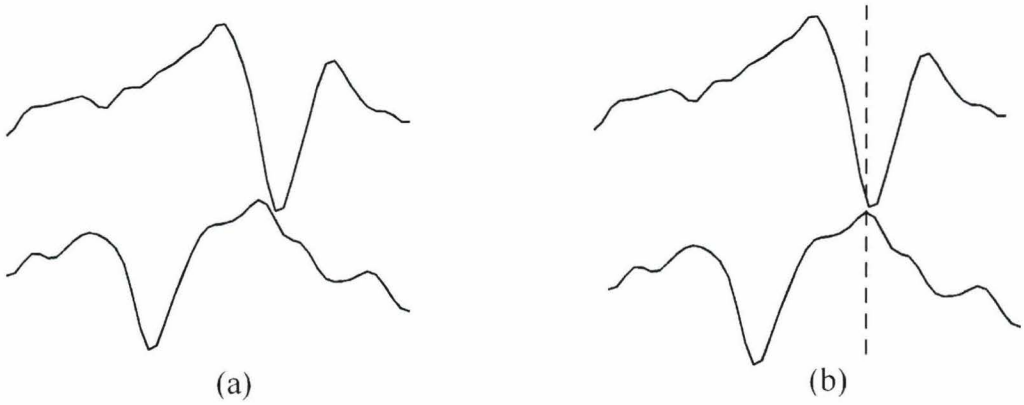

Figure 6.3: Illustration of two maternal P-waves, each containing a fetal ECG complex with the R-peak directed downwards. In (a) the segments are plotted against a simultaneous time-axis while in (b) the segments are aligned by applying equation (4.6) on the elongated segments, i.e. composite segment 1 in figure 4.3. Note that, while the plots only show the part representing the P-wave, the alignment is based on the elongated segments. For (b) the vertical scale is slightly modified in order to prevent crossing of the lines. The dashed line indicates the position of the peak in the P-wave.

As can be seen from figure 6.3, the alignment between the P-waves is much better when applying equation (4.6) on elongated segments instead of the separate P-waves. As a result of the relatively low signal-to-noise ratio (SNR) of the P-waves, determination of the start and end of the P-wave is inaccurate. Therefore, the adaptive

averaging technique described in chapter 4.3.2 is applied on the elongated segments. Scaling, however, is performed on the separate waves.

To improve the agreement between the estimated segments and original segments, the estimated segments are scaled. Since the interval between the start of the complex and the start of the P-wave and the interval between the end of the P-wave and the start of the Q-wave have no net potential but suffer from considerable noise, applying scaling on the elongated segments would result in scaling of merely noise in these intervals. For this reason, scaling is applied on the separate P-waves. Since the SNR of the original segment is low with respect to the SNR of the estimated segment, the start and end of the P-wave are determined in this estimated segment. This is in contrast with determination of the boundaries of other segments, which are determined in the original segment.

Scaling is performed by multiplying the estimated segment with the ratio between the maximum amplitude of the original segment and the maximum amplitude of the estimated segment. This method can cause differences between the estimated segment and the original segment when the maximum amplitude of either one of these segments is affected by the fetal ECG. This can be seen in figure 6.3b in which the dashed line indicates the position of the peak in the P-wave. For the upper graph, the downwards-directed fetal R-peak causes the amplitude of the peak in the P-wave to be degraded. As a result, the maximum amplitude is detected at the local maximum left of the dashed line causing the required degree of scaling to be underestimated and disagreement between the estimated and original segments. This discussion is analogous for adaptive averaging and scaling of the T-wave.

In contrast to common adaptive averaging (CAA), i.e. the adaptive averaging of the ECG complex as a whole, SAA scales all segments separately, increasing the possibility of fetal ECG components affecting the scaling. However, in spite of this drawback, estimation of the maternal ECG complex by SAA is more accurate than estimation of the maternal ECG by other techniques such as CAA. The cause of this is that, in contrast to these other techniques, SAA considers variations in the waveform of the ECG by estimating each wave separately. To illustrate this, the sum of squared errors between the original signal and the estimates by SAA and CAA has been determined for an average recording of 1000 seconds as a measure of agreement between the estimated and original signals. For SAA the agreement between estimated and original signals is more than 30 percent higher than for CAA. This percentage is slightly deceiving since the possibility of parts of the fetal ECG to be present in the estimation by SAA is higher than in the estimation by CAA. The presence of parts of the fetal ECG in the maternal ECG estimate results in an unwanted better agreement between estimated signals and original recordings. This effect is however small compared to the difference in agreement for both methods (smaller than 5 percent).

Figure 6.4a and figure 6.4b show the fetal ECG signals resulting from both the subtraction of the SAA estimate of the maternal ECG from the original abdominal recording, which are both shown in figure 6.1, and the subtraction of the CAA estimate of the maternal ECG from the original recording.

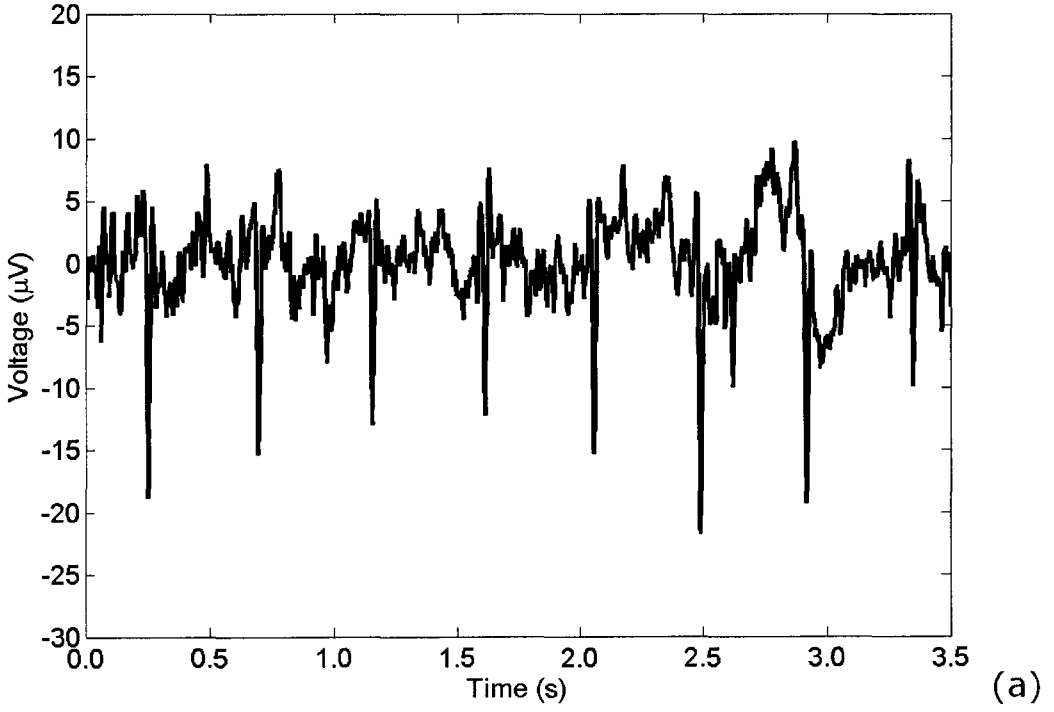

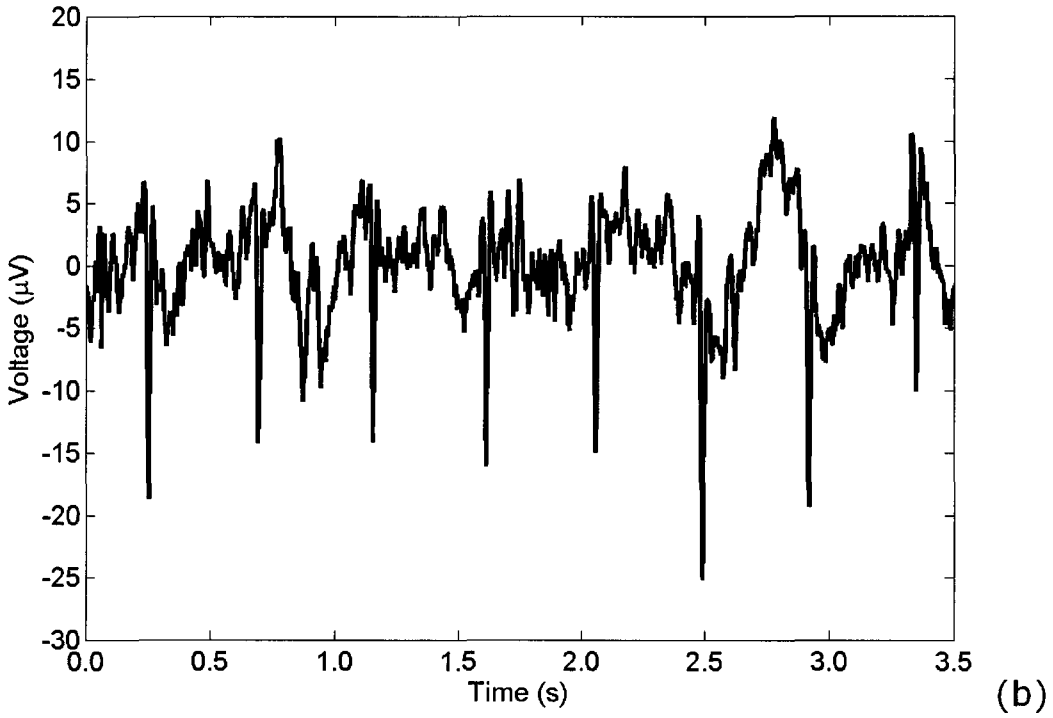

Figure 6.4: (a) The fetal ECG signal resulting from the subtraction of the estimate of the maternal ECG by segmentational adaptive averaging (SAA) from the original abdominal recording shown in figure 6.1 and (b) the fetal ECG signal resulting from the subtraction of the estimate of the maternal ECG by common adaptive averaging (CAA) from the same original abdominal recording.

The signals shown in figure 6.4a and figure 6.4b are composed of the fetal ECG signal, residual parts of the maternal ECG and noise. As can be seen quite clearly – in particular at approximately 0.9 seconds and 2.8 seconds – the SNR of the fetal ECG in figure 6.4a is larger than the SNR of the fetal ECG in figure 6.4b.

The SNR for this particular recording is relatively high but signals with smaller SNR are found more frequently. The SNR is determined by equation (4.1) but instead of the SNR this equation actually determines the ratio between the average amplitude of the fetal R-peaks and the average amplitude of the sum of the fetal ECG and noise. However, for the purpose of determining which signals provide the highest SNR, this equation is satisfactory.

6.2 *The fetal heart rate*

The instantaneous fetal heart rate is calculated from the R-R interval lengths by equation (5.10). The positions of fetal R-peaks are determined after linearly combining the four signals with the highest SNR, as determined in the initialization process. As a consequence of fetal motion, fluctuations in the SNR of each signal are to be expected, possibly resulting in a change of which four signals are to be used for this linear combination. For this reason, it is preferred that the initialization process is performed continuously on the background to update the signals used in the linear combination when necessary. Unfortunately, the software used to develop the algorithm (Matlab, the MathWorks, Inc.) does not support this feature. Therefore the initial linear combination is used for the entire recording.

At labor, the fetus is limited in its mobility and relatively few fluctuations in the SNR of each signal are expected. For stages of pregnancy earlier than labor the fetus is more likely to move, causing a decrease in the SNR of the linear combination. As a result, this SNR can be too low to perform accurate detection of fetal R-peaks during some periods in time. For the purpose of monitoring the fetal heart rate, these periods are left blank, as providing no information is better than providing false information. For performing spectral analysis, continuous signals are required and consequently these periods are filled by applying linear interpolation. Criteria for applying linear interpolation are heart rates outside the range between 100 BPM and 200 BPM and heart rates deviating more than 20% from a set of preceding successive heart rates. To reduce the amount of heart rate data obtained by interpolation, the algorithm checks whether a local maximum in the linear combination of signals can be detected in the close vicinity of the interpolated position. If this is the case, the position of this maximum is taken as the position of the fetal R-peak; otherwise the interpolated position is used.

To validate the algorithm, the fetal heart rate calculated from abdominal recordings is compared to the fetal heart rate calculated from a fetal ECG measured directly with a scalp electrode. The calculation of the fetal heart rate from the directly measured ECG is performed analogously to the calculation of the heart rate from the abdominal recordings, i.e. detection of fetal R-peaks and calculation of the heart rate using equation (5.10). Figure 6.5 shows the beat-to-beat fetal heart rate calculated from both the abdominal recordings and the directly measured ECG for a fetus during labor. As a result of the measurement being performed during labor, fetal mobility was limited and only 1.87% of the calculated heart rate data had to be interpolated.

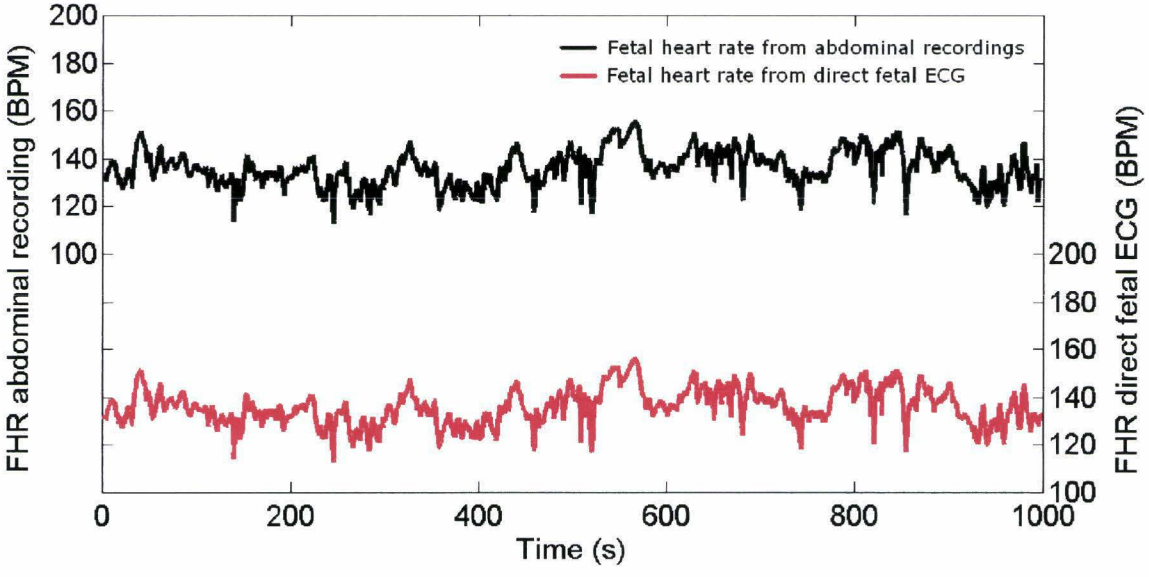

Figure 6.5: Fetal heart rate determined from both the abdominal recordings and the fetal ECG measured directly with a scalp electrode for a fetus during labor. For the heart rate calculated from the abdominal recording 1.87% of the data is obtained by interpolation.

In figure 6.5 can be seen that the beat-to-beat fetal heart rate calculated from abdominal recordings strongly resembles the heart rate calculated from the direct fetal ECG. In order to provide a quantitative measure of this resemblance, in figure 6.6 the heart rates calculated from the abdominal recordings are plotted against the heart rates determined from the directly measured fetal ECG. A linear model of the form $y = ax$ is fitted to the depicted data to describe the relationship between the heart rates calculated by both methods. The best fit can be found for $a = 1.000$ with $R^2 = 99.57\%$ and a correlation coefficient of $R = 0.998$ ($p < 0.001$).

Merely determining the correlation coefficient and the slope a of the linear fit is not enough to assess the degree of agreement between both methods [Bland, 1986]. The occurrence of systematic errors in one of both methods is represented in the linear fit by a change in the slope a. However, systematic errors are made clear more easily by representing the data in a Bland-Altman plot, i.e. the difference between the results of both methods plotted against the mean of them. Figure 6.7 shows this Bland-Altman plot for the data depicted in figure 6.6. Although the Bland-Altman plot is useful for a qualitative determination of the agreement between both methods, it does not provide a sufficient quantitative measure of this agreement.

The mean value of the differences is 0.0 ± 0.7 BPM. These values indicate that there is no systematic bias between the results of both methods and that 95% of the differences are within 1.4 BPM of this mean value. This last remark is based on the fact that the differences have a Gaussian distribution.

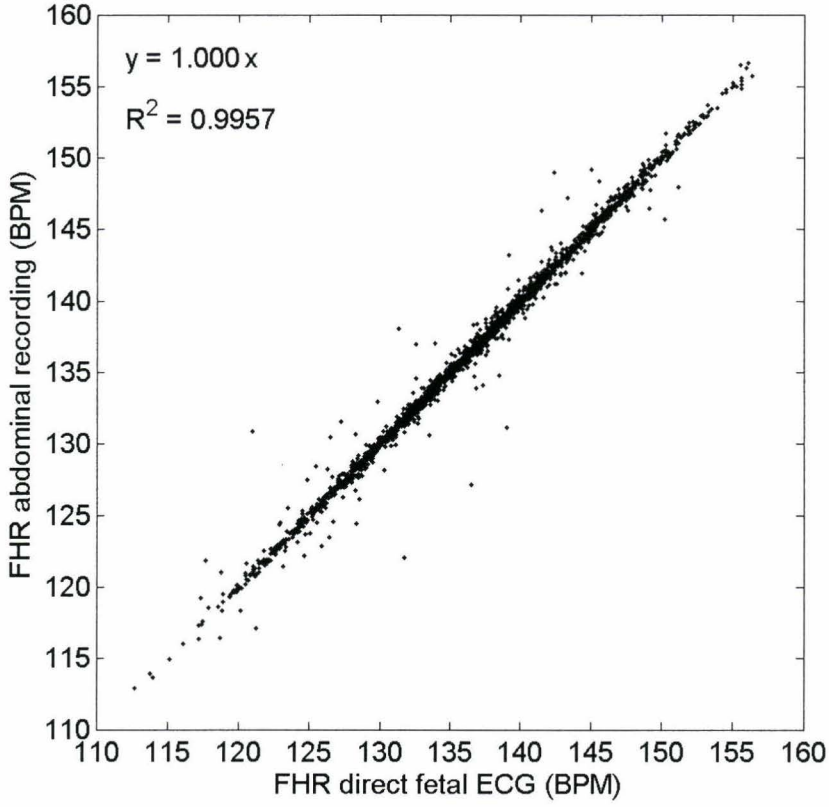

Figure 6.6: Relationship between fetal heart rates calculated from abdominal recordings and the heart rates determined from a fetal ECG that is measured directly with a scalp electrode. The depicted data sets both contain 2256 fetal heart rates determined in a period of 1000 seconds.

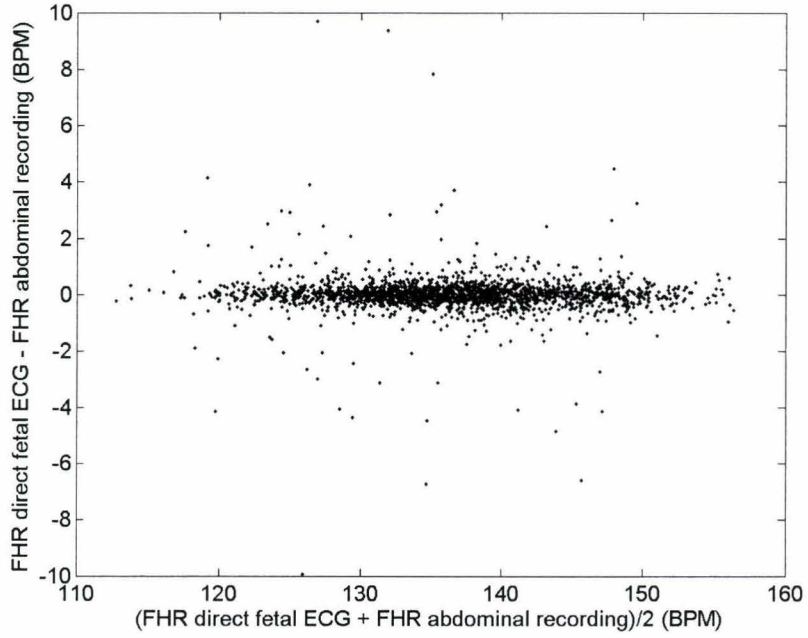

Figure 6.7: Bland-Altman plot of the heart rates calculated from the abdominal recordings and the heart rates determined from the directly measured fetal ECG. The difference between both methods is plotted against the mean of them.

In total, measurements have been performed on 20 different patients, but for only one of these patients the fetal ECG has been measured continuously with the scalp electrode. Therefore, at this moment, conclusions about the validation of the algorithm have to be based on a single measurement. For recordings that show relatively large fetal R-peaks, such as the recording shown in figure 6.1, the capability of the algorithm to calculate the fetal ECG signal from the abdominal recordings can be determined visually.

As a result of high amplitude motion artifacts, electromyogram (EMG) signals from skeletal muscles and the limited input range of the amplifier ADC, the ADC has been saturated for some periods in time for some measurements. During these periods it is impossible to determine a fetal heart rate from the recordings. On the other hand, for stationary periods in time, i.e. periods for which the amplitude of the signal is within the range of the ADC, the algorithm is capable of determining the fetal heart rate for all measurements. Results, however, become less reliable with decreasing gestational age as the degree of interpolation, needed to obtain a continuous fetal heart rate, increases. This is shown in table 6.1 that gives the percentage of interpolation and the percentage of time in which the ADC has been saturated for several gestational ages. Reason for the decrease in the required degree of interpolation with increasing gestational age is not only – as mentioned earlier – the fact that fetal mobility is limited more as pregnancy progresses, but also the fact that the fetal heart grows during pregnancy causing an increase in the amplitude – and therefore in the SNR – of the fetal ECG signal. Furthermore, for gestational ages between 28 and 32 weeks the fetus is covered by the so-called vernix caseosa [Oostendorp, 1989], a waxy white substance coating the skin of the fetus and protecting it from bacteria. This vernix has conductive properties causing electrical shielding and therefore a decrease in the amplitude of the fetal ECG signal.

Table 6.1: Percentages of interpolation needed to obtain continuous fetal heart rates and percentages of the time in which the ADC has been saturated, for several gestational ages. The percentages are calculated from a typical time period of 100 seconds. For gestational ages between 34 and 36 weeks no measurement has been performed yet.

Gestational age (weeks)	Number of measurements	% of interpolation needed	% of time in which the ADC is saturated
< 28	2	9.9 ± 5.0	1.7 ± 1.2
28-30	2	46.2 ± 2.5	10.1 ± 8.1
30-32	2	9.5 ± 4.2	0.9 ± 1.2
32-34	4	9.3 ± 1.7	4.1 ± 1.3
36-38	3	6.5 ± 4.8	2.7 ± 1.8
> 38	7	6.2 ± 4.3	1.3 ± 0.8

As can be seen in table 6.1, the percentage of heart rates that can be determined by the algorithm is considerably smaller for the period between 28 and 30 weeks of gestation than for other periods. Reason for this is the electrical shielding of the fetus from its environment by the vernix caseosa. To a smaller extent, this large percentage of interpolation can be explained by the fact that for these particular measurements the input range of the ADC was exceeded for a longer period of time, requiring additional interpolation. Strikingly, for gestational ages between 30 and 32 weeks the degree of interpolation needed is less than 10 percent, while the fetus is expected to be covered by the vernix caseosa at these ages. A possible reason for this low percentage is that for both patients at this gestational age, the mother was medicated possibly affecting the development or breaking of the vernix.

The percentage of time in which the signals exceed the input range of the ADC is not related to gestational age. This is to be expected since the main reason for the input range to be exceeded is movement of the mother.

Based on table 6.1 and the results of figure 6.5, figure 6.6 and figure 6.7 it can be concluded that the developed algorithm is capable of non-invasive and accurate monitoring of the beat-to-beat fetal heart rate during labor. For stages of pregnancy earlier than labor the algorithm has to interpolate heart rates during some periods in time. As a result, not all provided heart rates are on a beat-to-beat basis. However, for all gestational ages, except for ages between 28 and 30 weeks, the degree of interpolation needed to obtain a continuous heart rate from the measurements is less than 10 percent. Moreover, the measurements that needed more interpolation (over 40 percent) were performed while the fetus was electrically shielded from the environment by the vernix caseosa.

For the purpose of online monitoring the fetal heart rate computation times have to be small. As mentioned in chapter 4.1.2, each time 6 seconds of data is processed by the algorithm and an average fetal heart rate for this interval is calculated. The average computation time t_{comp} for this operation on a standard issue desktop computer equals $t_{comp} = 3.1 \pm 0.6$ s. Based on this average computation time, it can be stated that the algorithm is capable of online monitoring the fetal heart rate, after each 3.1 seconds returning a heart rate averaged over an interval of 6 seconds.

Calculating the average heart rate in an interval of 6 seconds after approximately every 3 seconds results in the use of half-overlapping windows. At the moment, the complete interval of 6 seconds is processed while in fact the estimate of the maternal ECG and the positions of fetal R-peaks in the first half of this interval are already known as a result of the preceding calculation. Using the information in the second half of an interval for

the first half of the next interval therefore results in a significant reduction of computation times. Furthermore, since the embedded data structure of Matlab prevents any significant speed improvement, computation times can be reduced more by rewriting the algorithm in another computer language, such as C++.

6.3 The fetal ECG complex

6.3.1 Increasing the signal-to-noise ratio of the fetal ECG complex

The signal-to-noise ratio of the fetal ECG signal is too low to calculate features such as the length of ECG intervals, as can be seen in figure 6.4. Therefore, each complex is normalized against its maximum amplitude and is cross-correlated with N-1 preceding complexes. Since the maximum value of the cross-correlation supplies information on the similarity between complexes, averaging N complexes while excluding complexes with a relatively low correlation, results in an increase of the SNR of the fetal ECG. Figure 6.8 shows the effect of averaging on a fetal ECG complex.

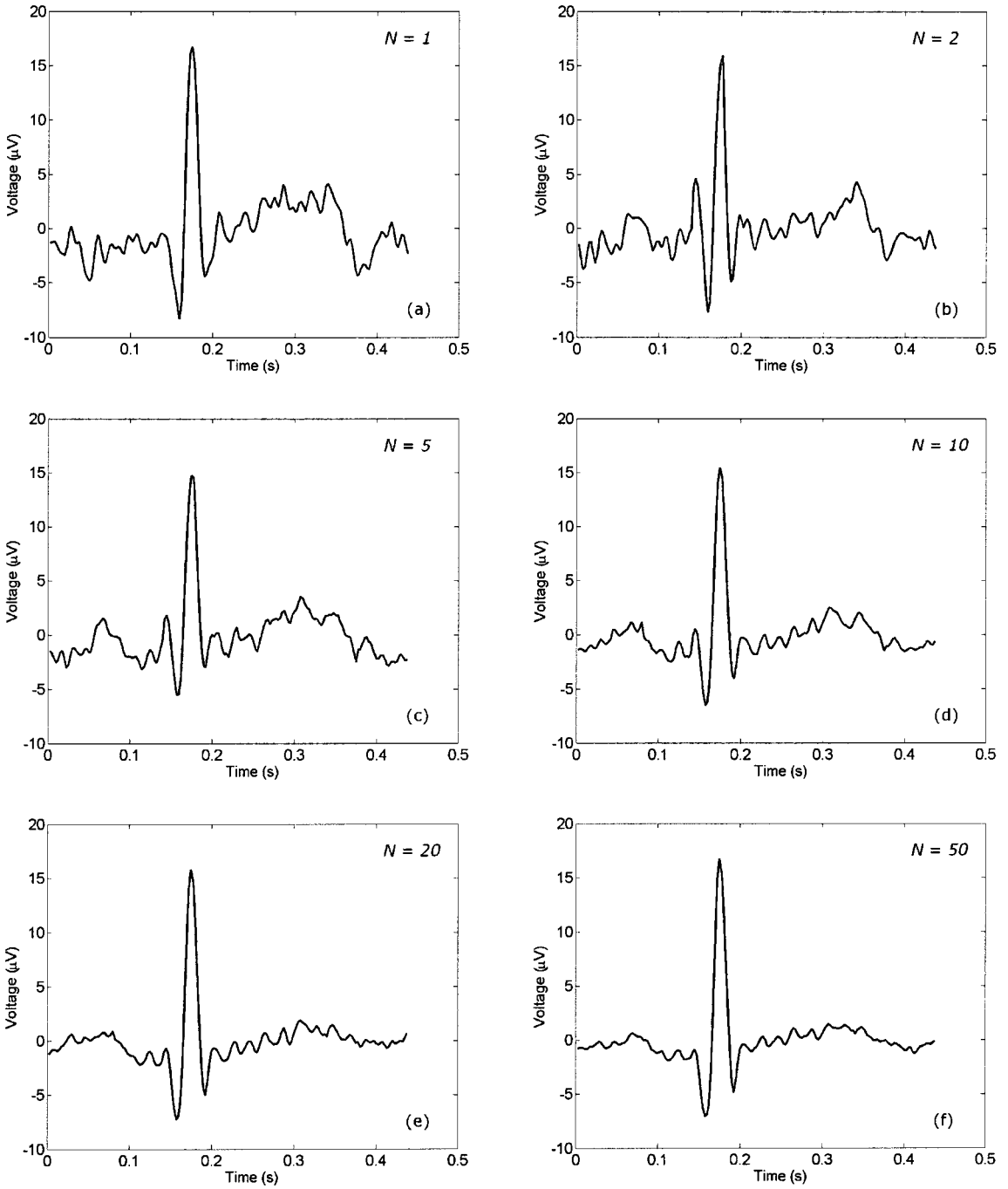

Figure 6.8: The effect of averaging on the signal-to-noise ratio of fetal ECG complexes. (a) shows a fetal ECG complex without averaging. In (b) the ECG complex of (a) is averaged with one other ECG complex. (c) shows the average of 5 while (d) shows the average of 10 fetal ECG complexes. In (e) the average of 20 successive complexes is shown and (f) is the average of 50 ECG complexesThe shown complexes are all lead 6-11 determined from the electrode configuration of figure 3.1b.

The fetal ECG complexes included in the average are aligned based on the position of the R-peak. Since the length of the Q-R interval and the R-S interval is rather constant while the lengths of the P-Q interval and the S-T interval vary between heart beats, averaging the ECG complexes results in a decrease of the amplitude of the P- and T-wave. This can be seen in figure 6.8f in which the amplitudes of the P- and T-wave are reduced significantly with respect to the amplitudes of these waves in figure 6.8c. Therefore, when selecting the number of complexes N included in the average, both the increase in the SNR and the decrease in the amplitude of the P- and T-wave have to be considered. Figure 6.8d, in which $N = 10$, shows a good balance between both effects.

Furthermore, from figure 6.8d-f it can be seen that for $N > 10$ the increase in SNR is small with respect to the increase in N. Reason for this is the fact that the 'noisy tail' on both sides of the QRS-complex is not the result of measurement noise, but is caused by the Butterworth filters, used to eliminate powerline interference and baseline drift. As a result, this additional noise is not randomly distributed and cannot be eliminated by averaging several ECG complexes. However, by applying a filter working with a moving window, as described in chapter 4.5, it is possible to reduce this noise and enhance the SNR. The principle of this filter is analogous to an adaptive low-pass filter and its effect on a fetal ECG complex is illustrated in figure 6.9.

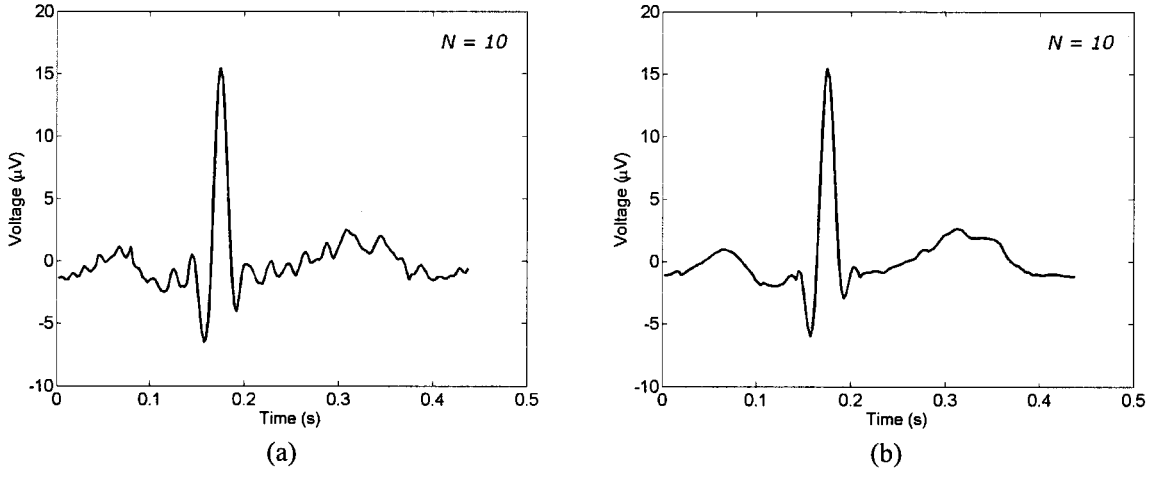

Figure 6.9: Example of the effect of the adaptive filter used to enhance the SNR of the fetal ECG complex. In (a) the fetal ECG complex before application of the filter can be seen while (b) shows the same complex after applying the filter. The shown complexes are both lead 6-11 from the electrode configuration of figure 3.1b.

Figure 6.9b shows an increase in the SNR with respect to figure 6.9a. However, the use of an additional low-pass filter increases the possibility of the occurrence of artifacts. Signal fragments with a sudden change in amplitude are composed of a wide range of frequencies. Applying a low-pass filter on such fragments can cause the effect of additional noise in the signal since the amplitudes of high-frequency components are reduced while the amplitudes of low-frequency components remain unchanged. As a result, the Fourier transform of the fragment shows unwanted, low-frequent waves which are no longer cancelled by high-frequent waves. This effect is discussed in more detail in appendix A and can be seen in figure 6.9b just before the start of the Q-wave and just after the end of the S-wave.

6.3.2 Determination of the standard and extremity leads of the fetal ECG

The recorded ECG leads are difficult to interpret clinically since these leads are not the standard leads that are usually recorded from a patient. For interpreting the fetal ECG complex and obtaining additional information on the condition of the fetus, the ECG is therefore preferred to be determined in a similar way as it is determined outside the uterus. Examples of these usual ECG leads are the standard leads (I, II and III) in the Einthoven triangle and the extremity leads (aVR, aVL and aVF), all shown in figure 6.10.

The ECG complex is composed of electrical potentials that are generated by the heart and recorded at the skin surface. As differences between electrical potentials of several areas of the heart can be represented by an electrical field vector, the ECG can be described as the projection of this so-called cardiac vector on a particular lead. Figure 6.10 shows, in green, the projection of the course of the cardiac vector, known as the vectorcardiogram (VCG), on the plane of measurement and, in yellow, the projection of a momentary vector. A particular lead of the ECG is now defined as the length of the projection of the cardiac vector on this lead. This is illustrated in figure 6.10 for standard leads I, II and III.

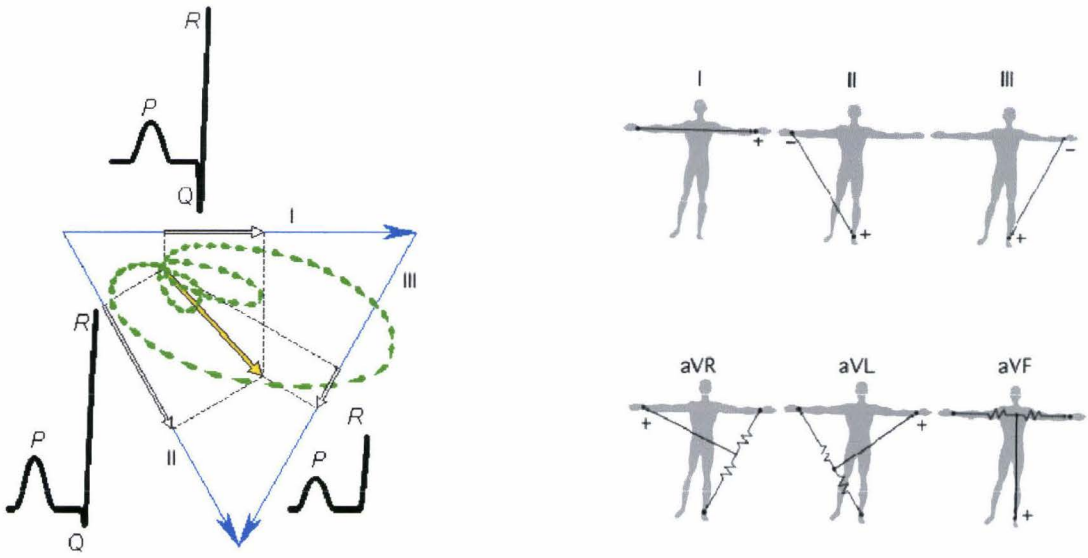

Figure 6.10: Illustration of the Einthoven leads I, II and III and the extremity leads aVR, aVL and aVF. Einthoven assumed the human body to constitute an equilateral triangle with the heart in the center of this triangle. ECG leads are obtained by the projection of the cardiac vector (in yellow) on these leads. In green, the course of the cardiac vector, known as the vectorcardiogram, is projected on the two-dimensional plane of measurement.

As the orientation of the fetus in the uterus is unknown, it is not possible to position the electrodes in such way that the standard and extremity leads of the fetal ECG can be obtained directly. However, by reconstructing the VCG from the leads that are obtained by the electrode configuration of figure 3.1, it is possible to derive the standard and extremity leads.

Reconstructing the cardiac vector is performed by linearly combining the projections of the cardiac vector on the recorded leads. For each point in time all the lead vectors are multiplied by the amplitude in the corresponding ECG complex and summed to obtain the resultant vector. This resultant vector however has to be normalized for the used lead vectors, as is discussed in appendix C. The course of the normalized resultant vector, the VCG, is shown in figure 6.11. It has to be noted that this vector is not the actual cardiac vector but the projection of this vector on the plane of measurement. In spite of the use of averaging and filtering to enhance the SNR of the fetal ECG complex, the VCG is still significantly affected by noise, in particular for low amplitude intervals in the ECG complex such as the P-Q interval and the S-T interval. To enhance the SNR of these intervals and obtain a rather constant SNR over the complete ECG complex, the amplitude of each sample in a low amplitude interval is averaged with the amplitudes of its adjoining samples.

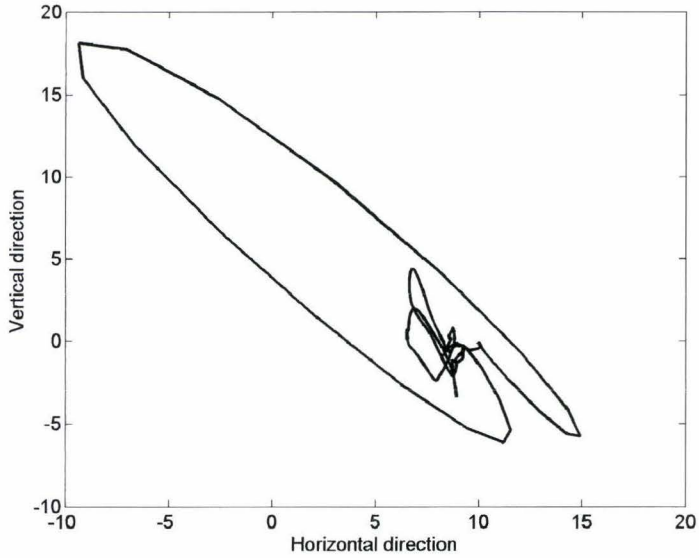

Figure 6.11: The vectorcardiogram resulting from linearly combining the lead vectors of the electrode configuration of figure 3.1b. This vectorcardiogram is the two-dimensional projection on the plane of measurement of the actual course of the cardiac vector. The horizontal direction on the x-axis represents the direction from right to left on the abdomen and the vertical direction on the y-axis represents the direction from feet to head.

In contrast to the VCG, as shown in figure 6.10, the orientation of the VCG of figure 6.11 is directed upwards. Reason for this is the fact that the fetus is positioned upside down in the uterus. Furthermore it can be seen that the VCG of figure 6.11 is compressed with respect to the VCG of figure 6.10. This is caused by the angle between the actual cardiac vector and the plane of measurement, resulting in a more compressed projection.

Figure 6.12 shows the standard and extremity leads of the fetal ECG, determined by the projection of the VCG of figure 6.11 on the corresponding lead vectors. In order to obtain the correct projections, the VCG has been rotated around its origin, that corresponds to the isoelectrical intervals of the ECG that have zero net potential and therefore no cardiac vector, to align with a VCG that is measured outside the uterus, like the VCG of figure 6.10.

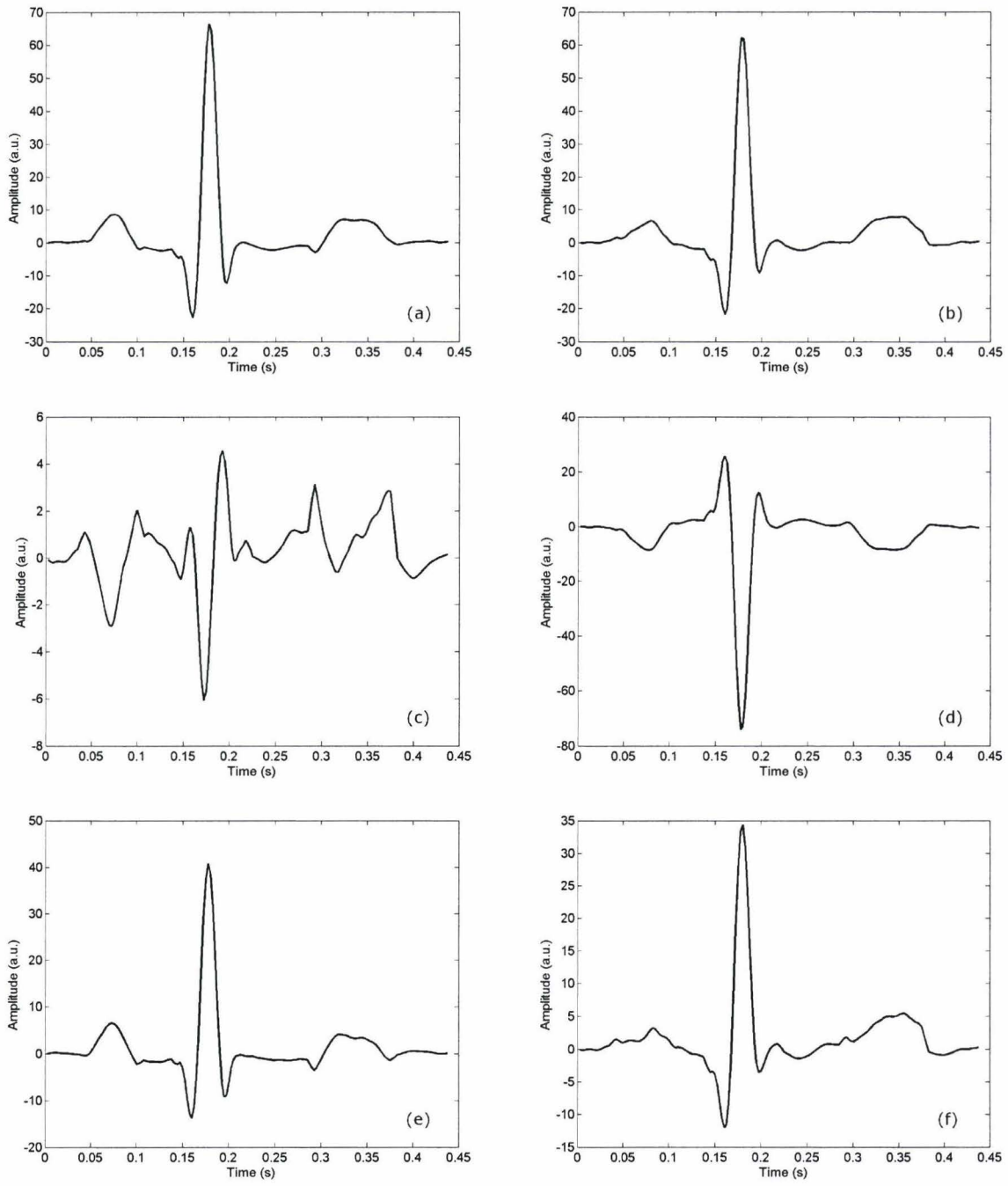

Figure 6.12: Examples of fetal ECG leads determined from the rotated vectorcardiogram of figure 6.11. Figure (a), (b) and (c) show the standard Einthoven leads I, II and III respectively. Figure (d), (e) and (f) show the extremity leads aVR, aVL and aVF respectively.

The vertical scaling of the fetal ECG complexes of figure 6.12 is set to arbitrary units since these complexes are estimated – instead of being actually recorded or accurately calculated – and therefore do not provide a quantitative result. Reason for this is that the reconstruction of the VCG does not consider differences in the

attenuation of potentials at different recording positions. As a result of tissue inhomogeneities and differences in the distance between the fetal heart and the electrode positions, signal attenuation is expected to be different for all electrodes positions. Not considering these differences in attenuation when reconstructing the VCG causes small errors in the shape of the VCG and the shape of the calculated standard and extremity leads.

Nevertheless, the fetal ECG complexes of figure 6.12 show similar waveforms for standard leads I and II and extremity leads aVR, aVL and aVF as for the same leads recorded on a healthy human being outside the uterus [Winsor, 1986]. On the other hand, standard lead III has opposite polarity for the fetal ECG as for the same lead recorded outside the uterus, which is probably caused by inaccurate alignment of the VCG, resulting in a different projection for this lead. This argumentation is validated by the fact that the amplitude of this lead is relatively small, indicating an almost perpendicular projection. Therefore, small deviations in the alignment of the VCG can result in a change in the polarity of the ECG complex.

6.3.3 Electrocardiogram intervals

As mentioned in chapter 2.1.4, the fetal ECG contains information on several features associated with fetal growth and well-being. Fetal hypoxia is reflected in the ECG by the elevation or depression of the ST-segment as well as by changes in the ratio between the P-R and R-R interval lengths. The length of the P-wave and the length of the QRS-complex are related to gestational age and birth weight. The determination of these intervals and segments from abdominal recordings is validated by comparing them to the same intervals and segments as determined from the directly measured fetal ECG. However, since the SNR of the ST-segment is low with respect to the SNR of the peaks in the P-wave and R-wave and since the ratio between the P-R and R-R interval lengths is equivalent to the elevation or depression of the ST-segment, information on fetal hypoxia is obtained from the ratio between the P-R and R-R interval lengths. This argumentation holds for obtaining information on gestational age and birth weight as well; this information is obtained from the length of the QRS-complex.

Ideally, the length of an interval is defined as the difference between the points in time on which both waves start. Due to noise it is however not always possible to determine the start of a wave accurately. Therefore, interval lengths are defined as the difference between the points in time on which both waves have maximum amplitude. The ratio between P-R and R-R interval lengths is shown in figure 6.13 for both the abdominal recordings and the directly measured ECG. Figure 6.14 shows the corresponding Bland-Altman plot.

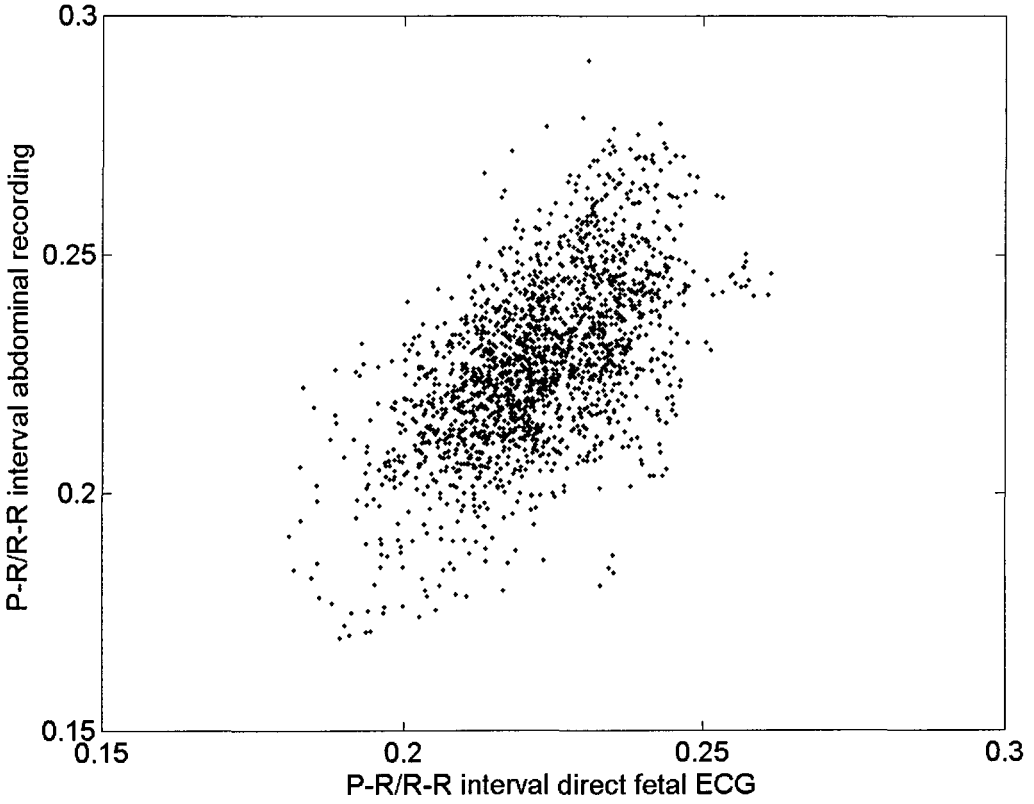

Figure 6.13: Relationship between the P-R and R-R interval length ratio calculated from the abdominal recordings and the P-R and R-R interval length ratio determined from the directly measured fetal ECG.

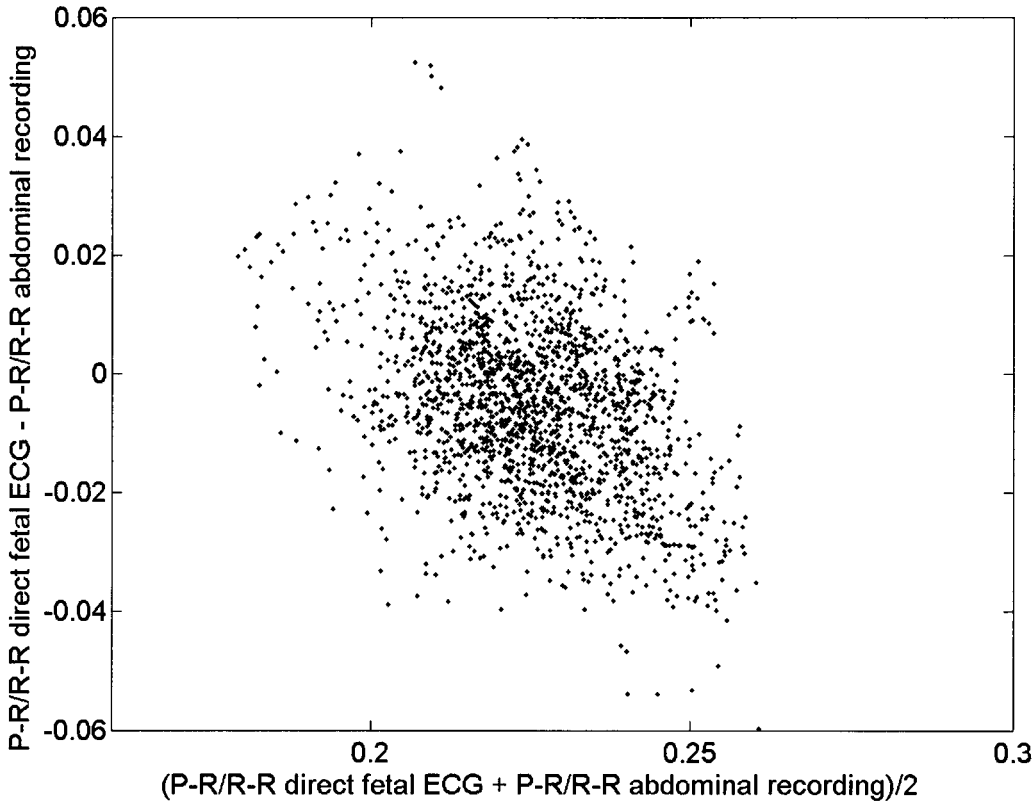

Figure 6.14: Bland-Altman plot of the ratio between the P-R and R-R interval length calculated from the abdominal recordings and the directly measured fetal ECG. The difference between the ratios for both methods is plotted against the mean.

To obtain a quantitative measure of the relation between the P-R and R-R interval length ratios for both methods, a linear model of the form $y = ax$ is fitted to the data depicted in figure 6.13. The best fit can be found for $a = 1.023$ with $R^2 = 34.0\%$ and a correlation coefficient of $R = 0.583$ ($p < 0.001$). The mean value of the differences in figure 6.14 equals -0.01 ± 0.01, which means that there is no significant systematic bias between both methods and that 95% of the results is within 0.03 of this mean.

Based on these results it can be concluded that abdominal recordings can be used to determine the P-R interval length, averaged over a certain period of time, but since correlation with the directly measured fetal ECG signal – the so-called golden standard – is too low, it is not possible to determine instantaneous P-R interval lengths from them. Reason for this too low correlation is the lower SNR of the abdominal recordings with respect to the directly measured ECG. This lower SNR is reflected in the abdominally determined P-R values by a larger spreading in the values, which can be seen quite easily from the trend in the Bland-Altman plot. The Bland-Altman plot shows a significant trend from the upper left corner to the lower right corner of the graph. A large positive deflection of the abdominally determined P-R and R-R ratio results in an increase in the mean value and a decrease in the difference. Conversely, a large negative deflection results in a decrease of the mean value and an increase in the difference.

Figure 6.15 shows the relation between the QRS interval lengths calculated from the abdominal recordings and from the directly measured ECG. The corresponding Bland-Altman plot can be seen in figure 6.16. In contrast to the relation between both methods for the P-R and R-R ratios, determination of the correlation between both methods for the QRS-interval length has no significance. The length of this interval is rather constant since it depends on the size of the heart and the propagation speed of action potentials through the ventricular tissue, both of which are hardly affected by the physiological circumstances of the fetus. Therefore, spreading in the determined QRS interval lengths is mainly caused by noise.

As can be seen in figure 6.16, using the same argumentation as for figure 6.14, is the spreading in QRS interval lengths for the abdominally determined ECG complexes larger than the spreading in the directly measured ECG complexes. Reason for this difference is the difference in sampling frequencies. While the abdominal recordings are performed with a sampling frequency of 400 Hz, is the directly measured fetal ECG sampled at 1 kHz frequency. The detection of peaks in the directly measured ECG signal is therefore more than twice as accurate as the detection of peaks in the abdominal recordings.

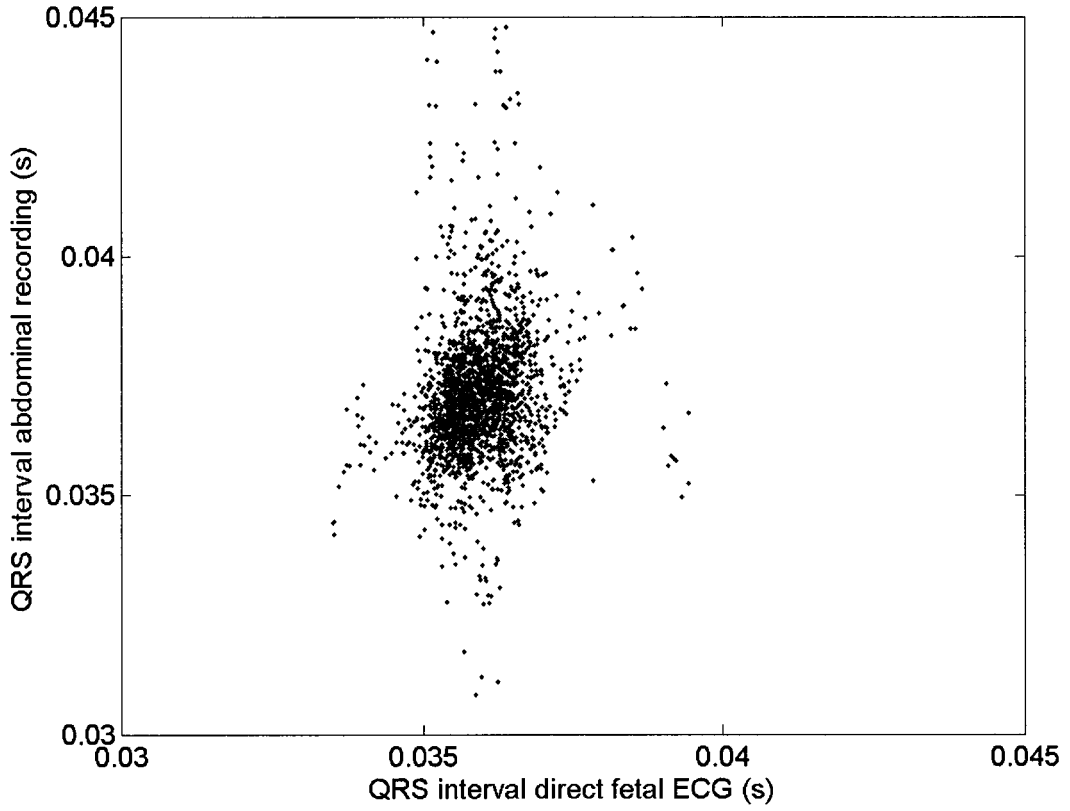

Figure 6.15: Relationship between the QRS interval length calculated from the abdominal recordings and the QRS interval length determined from the directly measured fetal ECG.

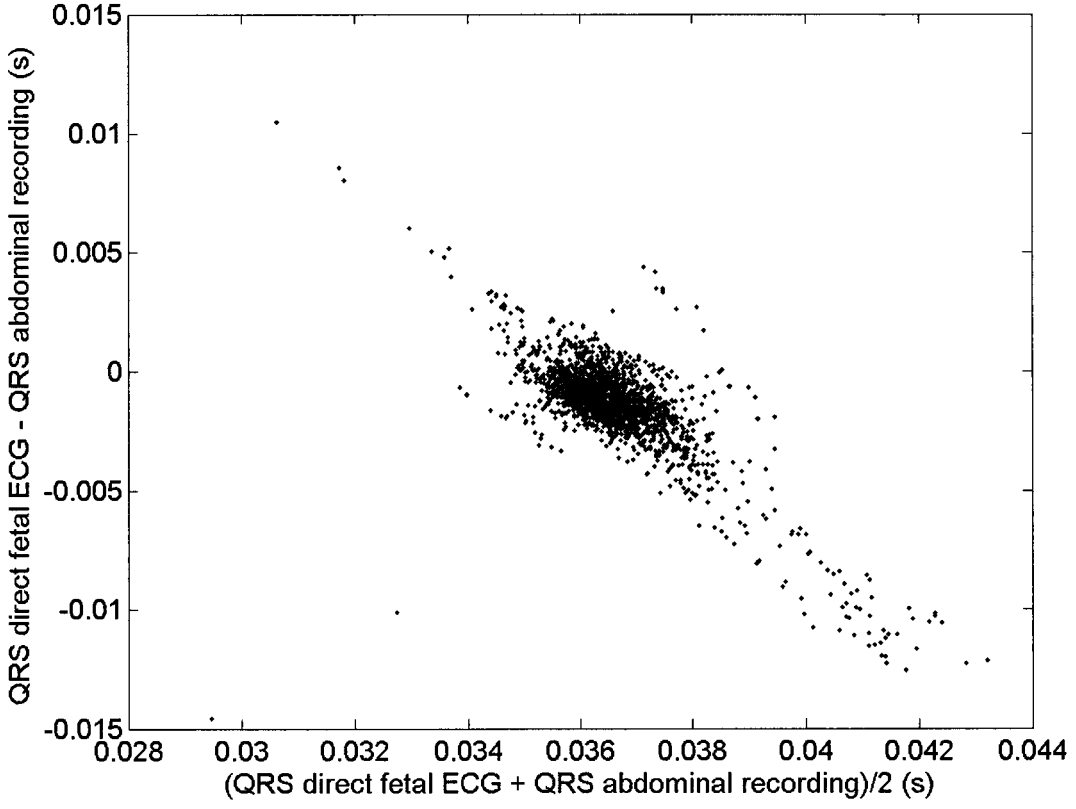

Figure 6.16: Bland-Altman plot of the QRS interval lengths calculated from the abdominal recordings and the directly measured fetal ECG. The difference between the interval lengths for both methods is plotted against the mean.

The mean value of the differences in figure 6.16 equals -0.001 ± 0.002 s, which means that the fetal ECG complexes calculated from abdominal recordings can be used to determine average QRS interval lengths.

In conclusion, results of the determination of the average ratios between P-R and R-R interval length and the average QRS interval lengths are consistent with the corresponding values determined from the directly measured fetal ECG and are in agreement with physiologically expected values [Stinstra, 2002].

6.4 Uterine activity

As mentioned in chapter 5, uterine activity is reflected in the abdominal recordings by two distinctive principles. Uterine contractions cause deformations of the abdominal surface, resulting in motion artifacts in the recordings. Furthermore, the propagation of action potentials through the uterine muscular tissues can be detected on the abdomen, the so-called uterine electromyogram (EMG).

6.4.1 Uterine activity from abdominal deformations

Motion artifacts caused by uterine contractions are represented by drifting of the baseline in the abdominal recordings and are shown in figure 6.17.

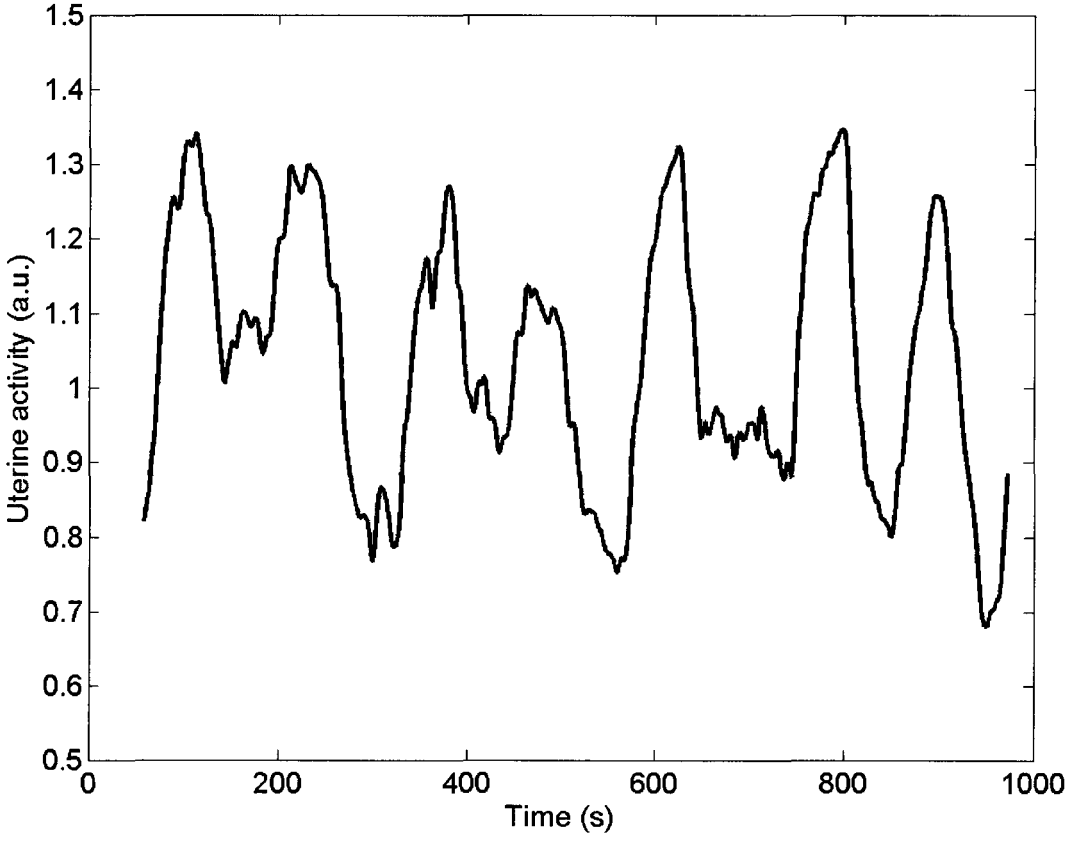

Figure 6.17: Uterine activity determined from deformations on the surface of the abdomen. The depicted data is obtained from the same patient on whom the fetal heart rate and ECG complexes, depicted in the previous paragraphs, have been determined.

Simultaneously to the abdominal recordings, intra-uterine pressure has been measured with a pressure catheter in order to validate uterine activity calculated from abdominal recordings. Unfortunately, the system used to measure this intra-uterine pressure – the cardiotocograph (CTG) – is a closed system. Therefore data can only be exported visually by means of a cardiotocogram. Consequently, only a qualitative measure for validation of the calculated uterine activity can be provided. Figure 6.18 shows the part of the cardiotocogram, which represents the intra-uterine pressure and which corresponds to the data depicted in figure 6.17. The horizontal axis represents the time, for which each square box corresponds to a time period of 30 seconds. Differences in the SNR between uterine activities of figure 6.17 and figure 6.18 can be explained by the fact that the intra-uterine

pressure is processed in the CTG by an unknown algorithm, that causes the smooth appearance of the intra-uterine pressure.

Figure 6.18: Part of the cardiotocogram representing the intra-uterine pressure. This pressure is obtained by a pressure catheter positioned inside the uterus. The vertical axis has been normalized by the system against an unknown value, whereas the horizontal axis represents the time, for which one square box corresponds to a time interval of 30 seconds.

Figure 6.17 and figure 6.18 show simultaneous bursts in uterine activity. Periods between bursts, however, show disagreement in amplitude. While for the intra-uterine measurement the pressure is rather constant for all inter-burst intervals, the amplitudes for the inter-burst intervals in the abdominal recording show variation. Reason for this variability is the fact that the uterine activity is calculated from abdominal recordings by summing absolute values for all electrodes. Randomly distributed noise is therefore summed as well, causing the variation in the amplitude of inter-burst intervals.

6.4.2 Uterine activity from the electromyogram

Uterine activity is determined by summing the power of the uterine EMG spectrum within the spectral band between 0.6 Hz and 3 Hz. The distribution of this EMG power spectrum over time is called the spectrogram and is shown in figure 6.19.

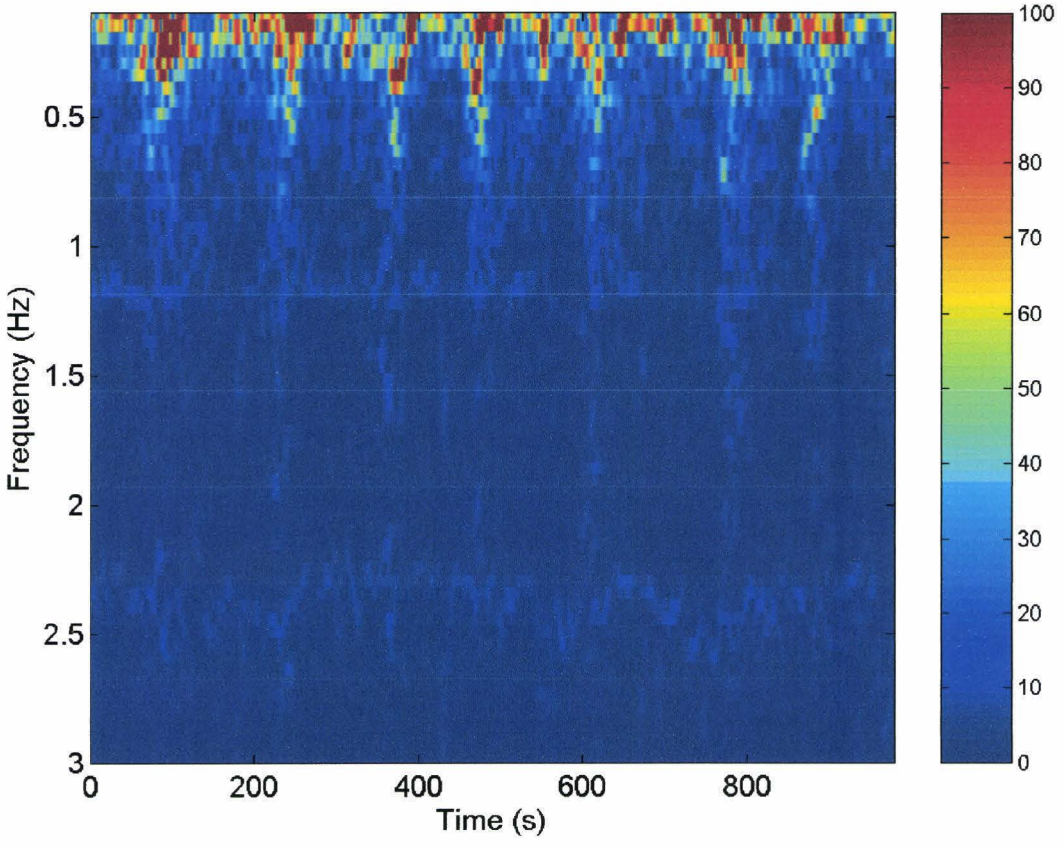

Figure 6.19: Spectrogram calculated from the Short Time Fourier Transform (STFT) of the uterine EMG signal. To reduce the effect of spectral leakage the STFT has been performed with a Hanning window. To smoothen the spectrogram, overlapping windows, each containing 2^{13} samples, are used.

The spectrogram of figure 6.19 not only shows the relatively broad banded uterine activity, but also activity at approximately 1.2 Hz and 2.4 Hz. This activity is caused by portions of the maternal ECG that have not been filtered sufficiently and therefore represents the maternal heart rate and its harmonics. As a result of the low frequency resolution ($\Delta f = 0.05$ Hz) of the spectrogram, the dominant frequency of bursts cannot be determined accurately enough to be used as a measure of contractile strength. The uterine activity calculated from the spectrogram of figure 6.19 is shown in figure 6.20.

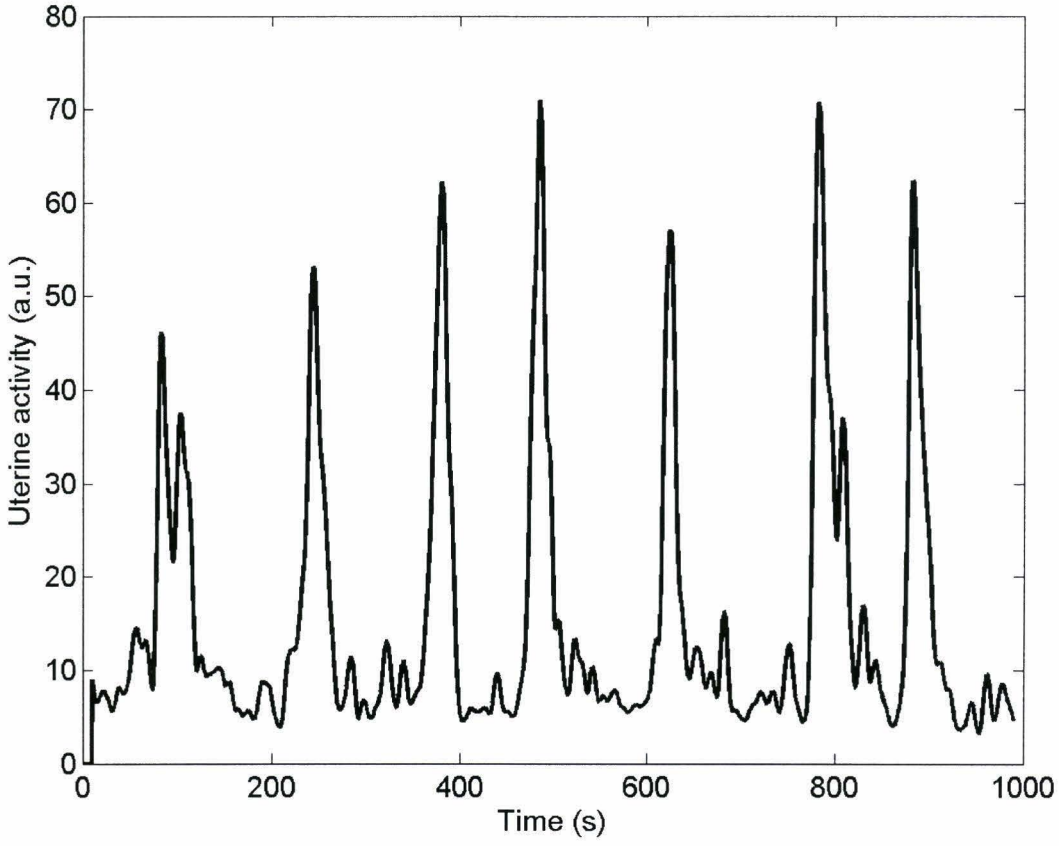

Figure 6.20: Uterine activity determined from the EMG signals detected at the abdomen. The uterine activity is calculated by summing the contributions to the spectrogram within the spectral band between 0.6 Hz and 3 Hz.

The uterine activity depicted in figure 6.20 shows simultaneous bursts with the intra-uterine pressure in figure 6.18. However, uterine activity in figure 6.20 shows a low SNR with respect to the SNR of figure 6.18, in particular for the inter-burst intervals and for the first burst. Reason for this is the fact that the intra-uterine pressure in figure 6.18 has been processed by the CTG after acquisition, resulting in an increase in the SNR.

Relative amplitudes of the bursts in figure 6.20 are inconsistent with amplitudes of the bursts in the intra-uterine pressure. In figure 6.18 the third, fourth and last bursts have lower amplitudes than the other bursts, whereas in figure 6.20 these bursts have relatively high amplitudes. Reason for this inconsistency is the fact that contractile strength – and therefore intra-uterine pressure – is related to the dominant frequency in the EMG spectrum rather than to EMG amplitudes. In contrast to this, amplitudes of bursts in uterine activity determined from abdominal deformations are related to the contractile strength, which can be seen when comparing burst amplitudes in figure 6.17 to amplitudes in figure 6.18.

In conclusion, the abdominally determined uterine activity can be used to determine the occurrence of bursts in the intra-uterine pressure. The amplitude of these bursts and the amplitude of the inter-burst intervals, however, cannot be determined accurately due to the low SNR for the abdominal deformations and the low frequency resolution for the uterine EMG signal.

6.5 The maternal heart rate

After the maternal R-peaks have been detected, the instantaneous maternal heart rate is calculated by equation (5.10). Figure 6.21 shows the maternal heart rate for the same patient on whom the fetal heart rate, fetal electrocardiogram and uterine activity, depicted in the previous paragraphs, have been determined.

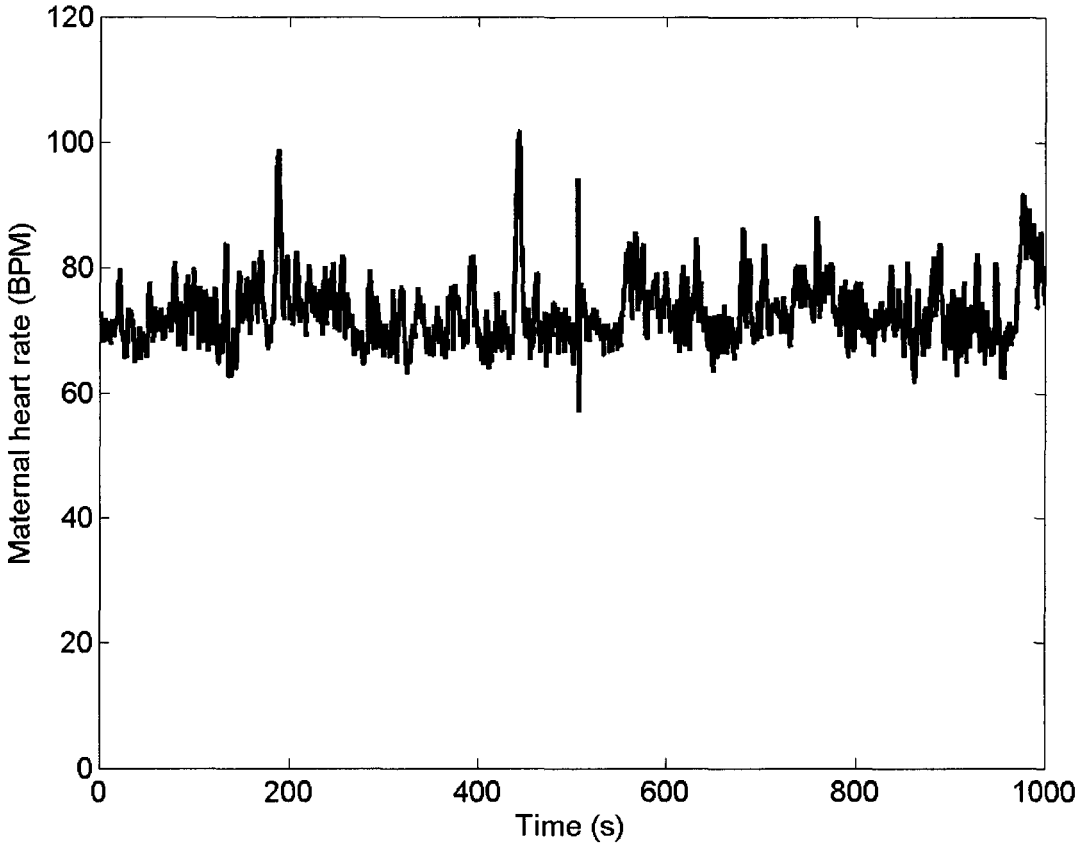

Figure 6.21: Maternal heart rate determined from one of the shoulder electrodes (electrode 2) depicted in the electron configurations of figure 3.1.

Since heart rates are usually determined from an ECG signal measured at the shoulder, there is no other method that can be used to validate the algorithm. However, performance of the peak detection algorithm can be validated visually by verifying whether all peaks have been detected accurately. For the maternal heart rate depicted in figure 6.21, all maternal R-peaks are detected accurately – even for the presumed artifacts at 187, 443 and 505 seconds.

6.6 General discussion

As mentioned in chapter 4.1.1, the calculation of the fetal heart rate is performed on a linear combination of the four signals that provide the largest fetal SNR. This selection criterion – the mean amplitude of the fetal R-peaks with respect to the root mean square of the signal, as described in equation (4.1) – is however far from ideal. Systematic noise in the abdominal signals can be summed in the resulting linear combination, causing a minimal increase in the SNR of this linear combination with respect to the SNR of the individual signals. Considering the vectorcardiogram, as shown in figure 6.11, in combination with the SNR by equation (4.1) is beneficial for the SNR of the linear combination. From the orientation of the vectorcardiogram, the position of the fetus in the uterus and therefore the bipolar electrode lead providing maximal deflection of the fetal R-peak can be determined. Using bipolar abdominal leads instead of unipolar – or actually, unipolar with the average of all electrodes as reference – leads reduces the amount of noise in the resulting linear combination, since most of the systematic noise is eliminated by the subtraction of two unipolar leads. Combining the bipolar abdominal leads while considering the SNR of these leads, results in an increase of the SNR of the linear combination and therefore a more accurate determination of the fetal heart rate.

As a result of using bipolar leads, the amplitude and SNR of the maternal ECG in the recordings is reduced significantly. Consequently, estimating the maternal ECG with segmentational adaptive averaging is less accurate. To overcome this problem, the maternal ECG has to be subtracted first before calculating the bipolar leads from the recorded unipolar leads.

Reconstruction of the vectorcardiogram also serves for reducing the number of electrodes positioned on the maternal abdomen. As mentioned previously, the bipolar lead providing the maximal deflection of the fetal R-peak can be determined quite easily from the vectorcardiogram. Combining the vectorcardiograms for many patients will therefore probably result in a reduced set of electrode positions, providing fetal ECG signals with a SNR high enough to calculate the fetal heart rate from. At the moment, not enough measurements are performed to draw such conclusions from.

The development of the vernix caseosa at gestational ages of about 28 weeks does not only affect the amplitude of the fetal signal and therefore the determination of the fetal heart rate, but also has significant effect on the calculation of fetal ECG complexes. As gaps in the vernix appear from gestational ages of about 32 weeks, attenuation of the fetal ECG signal is not constant for all electrodes, causing erroneous reconstruction of the vectorcardiogram. The gaps in the vernix are presumably formed around the fetal mouth and umbilicus [Oostendorp, 1989] causing the amplitudes of the leads resembling extremity lead aVF to be high with respect to the amplitudes of other leads. Conclusions about the physiological circumstances of the fetus from gestational ages of 28 weeks that are based on the fetal ECG complex should therefore be made with extreme caution.

Chapter 2.3 described the relation between the fetal heart rate and maternal uterine activity. To examine this relation visually, the fetal heart rate depicted in figure 6.5 and the maternal uterine activity depicted in figure 6.20 are plotted together in figure 6.22 in the form of a cardiotocogram. The response of the fetal heart rate to uterine contractions however does not match the description. Reason for this is the fact that the measurement is performed in an early stage of labor and as a result contractions are not strong enough to impose serious stress on the fetus.

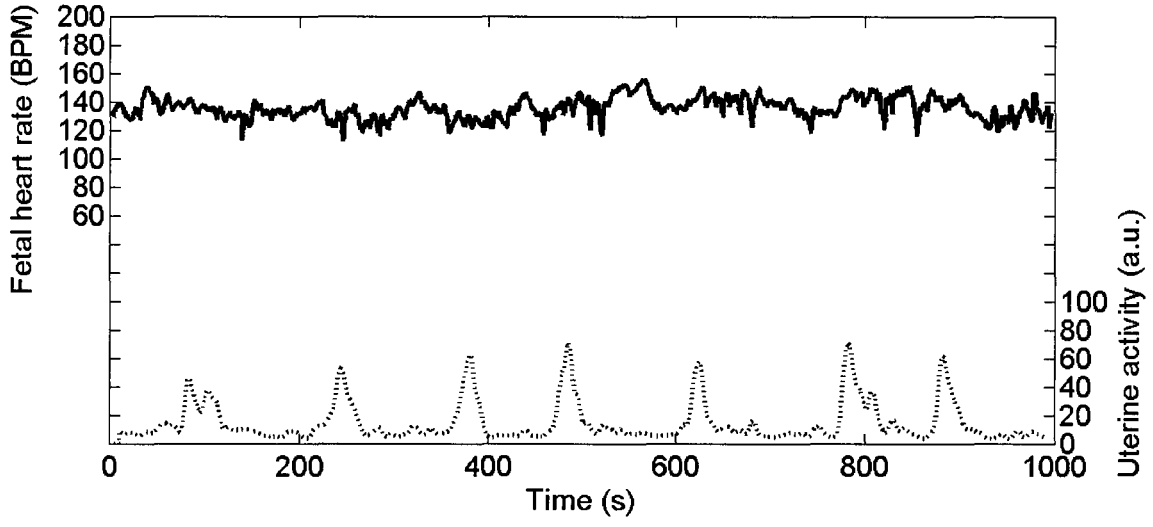

Figure 6.21: Cardiotocogram composed of the abdominally determined fetal heart rate and maternal uterine activity. The solid line represents the fetal heart rate whereas the dotted line represents uterine activity. Uterine activity is determined from the electromyogram signals detected at the abdomen.

7 Conclusions

In this study an algorithm to calculate the fetal heart rate and fetal electrocardiogram (ECG) from abdominal recordings on the mother has been developed. One of the main parts of the algorithm is the subtraction of the maternal ECG by segmentational adaptive averaging (SAA). SAA estimates the maternal ECG complex by applying adaptive averaging and scaling techniques on segments of the ECG complex. With respect to common adaptive averaging (CAA), i.e. adaptive averaging of the ECG complex as a whole, SAA estimates have about 30 percent better agreement with the corresponding maternal ECG complexes. Drawback of SAA is that some fetal ECG complexes are affected by the subtraction of the maternal ECG estimate. The signal-to-noise ratio (SNR) of the resultant fetal ECG signal is however high with respect to the resultant signal from CAA. In conclusion, it can be stated that SAA provides a valuable tool for estimating and subtracting the maternal ECG complex from abdominal recordings.

For one patient, fetal heart rates calculated from the abdominal recordings are compared to heart rates calculated from a direct fetal ECG, measured with a scalp electrode. The agreement between the abdominally determined fetal heart rates and this "golden standard" is good: the correlation coefficient is 0.998 ($p < 0.001$). For other measurements, the capability of the algorithm to determine the fetal heart rate is estimated visually. For all gestational ages, except between 28 and 30 weeks – the period in which the fetus is electrically shielded from its environment by the development of the vernix caseosa – the algorithm is capable to determine the fetal heart rate, needing less than 10 percent interpolation.

For the purpose of online monitoring the fetal heart rate, the algorithm is capable of returning a heart rate, averaged over a period of 6 seconds, after approximately 3 seconds computation time on a standard issue desktop computer. When processing the data offline, the algorithm can determine the fetal heart rate on a beat-to-beat basis, enabling the accurate spectral analysis of the heart rate to obtain additional information on the condition of the fetus.

To increase the SNR of the fetal ECG complexes, ten successive ECG complexes are averaged and after averaging the resultant average is filtered with an adaptive filter. Using less than ten ECG complexes in the averaging results in an average signal with a too low SNR, while using more then ten complexes causes a loss of detail in the averaged complex. Due to variations in interval lengths – in particular for the P-R interval and the S-T interval – and the fact that complexes are aligned by coinciding the R-peaks, P-waves and T-waves suffer a reduction in amplitude and an increase in width as a result of averaging.

Since changes in the ratio between the P-R interval length and the R-R interval length can be used as a measure to diagnose fetal hypoxia, instantaneous P-R/R-R values from the abdominal recordings are compared to the P-R/R-R values from the directly measured ECG. As a result of noise the agreement between instantaneous values is low – the correlation coefficient is 0.583 ($p < 0.001$) – and therefore the abdominally determined ECG cannot be used to determine instantaneous P-R/R-R values. However, the averaged values of the P-R and R-R intervals ratios agree well – the mean difference is -0.01 ± 0.01. Averaging is here performed with more than 2000 P-R/R-R values in a time period of 1000 seconds. Slow trends in the ratio between P-R and R-R interval lengths can therefore be determined reliably and accurately from abdominal recordings and can serve as a measure to diagnose hypoxia.

The length of the QRS-complex is associated with gestational age and the expected birth weight and is determined by the size and propagation properties of the fetal heart. Since the size of the heart is constant over relatively large periods of time, spreading in the calculated QRS-lengths is mainly caused by noise. Determining the agreement between instantaneous QRS-lengths from abdominal recordings and from the directly measured fetal ECG therefore has no significant value. The agreement between averaged values however has significance and this agreement is good – the mean difference is -0.001 ± 0.002 s. Based on these results it can be concluded that the averaged interval lengths in the abdominally determined fetal ECG provide a measure to diagnose fetal hypoxia and determine the gestational age and expected birth weight.

The reconstruction of the fetal vectorcardiogram from the abdominal recordings provides a tool to calculate the standard ECG leads and the extremity leads, but at present is associated with many inaccuracies. Differences in attenuation of the fetal ECG signal as a result of different distances between the fetal heart and the electrodes are not considered. Furthermore, the influence of the vernix caseosa, causing additional differences in attenuation by electrically shielding some parts of the fetal body, is ignored. Nevertheless, the obtained standard ECG leads and extremity leads show good resemblance to the corresponding ECG leads of a healthy human being outside the uterus, except for standard lead III.

Next to providing a tool to calculate the standard ECG leads and the extremity leads, the vectorcardiogram serves another purpose. The direction for which the vectorcardiogram has maximum amplitude

is equal to the direction of the electrical axis of the fetal heart. So for a fetus with a normal electrical axis, the vectorcardiogram provides a tool to determine the orientation of the fetus inside the uterus.

Uterine activity of the mother is determined based on two different phenomena. Not only is the uterine activity calculated from the electromyogram (EMG) signals originating from the uterus, but also is uterine activity calculated from motion artifacts, caused by deformations of the abdominal surface. Results of both methods are consistent with an intra-uterine pressure measurement conducted simultaneously with abdominal recordings, i.e. bursts in uterine activity determined from both methods coincide with bursts in intra-uterine pressure.

Difference between both methods is that for the uterine activity determined from the uterine EMG the SNR is relatively high, but the amplitude of a particular burst with respect to other bursts cannot be determined. Burst amplitudes in the EMG signal are related to the dominant frequency in the spectrum, but as a result of the low frequency resolution ($\Delta f = 0.05$ Hz) this dominant frequency cannot be determined accurately. The uterine activity calculated from abdominal deformations has a relatively low SNR but the amplitude of a particular burst with respect to other bursts can be determined. Stronger uterine contractions cause greater deformations of the abdominal surface and consequently motion artifacts with higher amplitudes.

8 Technology assessment and recommendations

At present, the most widely used device to obtain information on the condition of the fetus is the fetal cardiotocograph (CTG) monitor. In stages of pregnancy earlier than labor this CTG uses Doppler ultrasound to determine the fetal heart rate and a toco-transducer to measure uterine contractions. During labor, when the fetal membranes have ruptured, the CTG can determine the fetal heart rate from an electrocardiogram (ECG), measured directly with a scalp electrode, and the intra-uterine pressure from a pressure catheter positioned inside the uterus.

The use of Doppler ultrasound is associated with many inaccuracies, as the ultrasound probe has to be repositioned with each movement of the fetal thorax. As a result it is difficult to obtain continuous beat-to-beat fetal heart rates for long periods of time. The use of the fetal ECG signal, determined from the maternal abdomen, cannot only overcome this problem, but can also provide additional information on the fetal condition by means of the fetal ECG complex. For this reason an algorithm is developed that can be used for several purposes in clinical practice. Not only can it be used to monitor the fetal heart rate online and to determine the beat-to-beat fetal heart rate for relatively long periods in time for performing spectral analysis on, but also the algorithm can be used to reconstruct the fetal vectorcardiogram (VCG). From this VCG all fetal ECG leads can be calculated and used for interpretation by a physician. Furthermore, the algorithm is capable of calculating maternal uterine contractions and the maternal heart rate. In conclusion, the developed algorithm should be able to replace the fetal ECG monitor, as it is capable of providing the same information as the CTG more reliably and accurately and is also capable of providing additional information, by means of the fetal VCG.

Before the developed algorithm – in combination with electrodes, an amplifier and a computer – can actually replace the fetal CTG monitor several steps have to be taken. The main steps are summed below.

- The algorithm has to be validated by performing more measurements, simultaneously recording the abdominal signals and the signals from the scalp electrode and the intra-uterine pressure catheter. These measurements can only be performed during labor when the fetal membranes have ruptured. For stages of pregnancy earlier than labor, fetal heart rates and maternal uterine contractions determined from the electrophysiological signals on the maternal abdomen can only be compared to the fetal heart rate calculated from Doppler ultrasound recordings and uterine contractions determined by the toco-transducer. Since these results do not serve as "golden standard", comparisons in stages of pregnancy earlier than labor have less significant contribution to the validation of the algorithm.
- To monitor the fetal heart rate online, computation times have to be reduced significantly. At the moment the online monitoring algorithm uses half-overlapping windows of 6 seconds of data. As a result, the data in the last 3 seconds of a particular window is equal to the data of the first 3 seconds of the next window. Using the processed data of the last half of a particular window in the first part of the next window therefore reduces computation times approximately by a factor 2. Furthermore, computation times can be reduced more by writing the algorithm in another computer language such as C++.
- To increase the accuracy of the calculated fetal heart rates, the degree of interpolation needed to obtain a continuous heart rate has to be reduced. For this reason the selection of the four signals that are used for calculating the fetal heart rate has to be adjusted. Not only should the selection be based on both the shape of the VCG and the signal-to-noise ratio of the ECG leads resulting from this VCG, as described in chapter 6.6, but the selection should also be updated continuously by running the initialization process in the background.
- For minimizing patient discomfort the number of electrodes positioned on the patient has to be reduced. The fetal VCG and the signal-to-noise ratios of the bipolar ECG leads resulting from this VCG can be used to determine which electrode positions provide signals with high enough fetal ECG amplitudes to calculate fetal heart rates, fetal ECG complexes and maternal uterine contractions from. Consequently, evaluating the fetal VCG and corresponding bipolar ECG leads for several measurements can result in a smaller selection of electrode positions providing signals that are good enough to perform the required calculations on.
- Determination of the uterine EMG cannot be performed online at the moment. So for the purpose of registering an online cardiotocogram, i.e. simultaneously recorded fetal heart rates and maternal uterine contractions, the algorithm has to be adjusted. Uterine activity determined from abdominal deformations can be determined online, but due to the relatively low signal-to-noise ratio of this signal, it is not preferred to serve as measure of uterine contractions. However, since the uterine activity from abdominal deformations is used for the determination of which independent component represents the uterine EMG signal, the ICA (independent component analysis) transformation matrix can be updated

continuously. This enables the algorithm to online monitor uterine contractions by means of the online calculation of uterine EMG amplitudes.

Furthermore, the determination of relative contraction strengths is not possible from the uterine EMG signal because the frequency resolution of the Short Time Fourier Transform is too low for accurately determining the dominant frequency of each burst. This frequency resolution is improved by using wavelet transformations instead of the Short Time Fourier Transform.

- At the moment, the calculation of the fetal vectorcardiogram from the ECG leads on the abdominal surface is inaccurate. Differences in signal attenuation resulting from differences in the distance between electrode positions and the fetal heart are ignored, as is the influence of the vernix caseosa. By considering the attenuation of each signal it should be possible to improve the calculation of the vectorcardiogram significantly.
- At the moment the algorithm operates by means of laboratory software. To facilitate the use of the algorithm it has to be incorporated in a more user-friendly device.

Appendix A: The Butterworth filter

A.1 Low-pass filter

A data signal normally consists of a mixture of frequency components. The frequency contents of a signal and their powers can be obtained through operations such as the Fast Fourier Transform (FFT). A low-pass filter passes relatively low frequency components in the signals and stops the high frequency components. The pass band and the stop band are divided in by the so-called cut-off frequency. In other words, frequency components higher than the cut-off frequency are stopped by the application of a low-pass filter. The behaviour of a filter can be summarized by the frequency response function H_c. The frequency response of the Butterworth low-pass filter is given by:

$$|H_c(\omega)|^2 = \frac{1}{1+(\omega/\omega_c)^{2N}}, \tag{A.1}$$

in which ω is the frequency, ω_c is the cut-off frequency and N is the order of the filter. For $\omega = 0$ the frequency response is 1 and the signal is passed unattenuated. For $\omega = \infty$, H_c becomes 0 and the frequency component is stopped completely. When $\omega = \omega_c$ the frequency response is $2^{-½}$, regardless of the order of the filter. The frequency band between the pass band ($|H_c(\omega)|^2 \approx 1$) and the stop band ($|H_c(\omega)|^2 \approx 0$) is named the transition band and in this band the frequency components are passed attenuated by the filter.

Since ω is complex, the frequency response H_c does not only attenuate the frequency components but also imposes a phase shift on them. To correct for this shift the filter is applied twice on the data signal, one time in forwards direction and one time in backwards direction. Figure A.1 shows the attenuation of the data signal as a function of the normalized frequency for a fourth order Butterworth low-pass filter with a cut-off frequency of 0.45π rad/sample, corresponding to a frequency of 90 Hz for filtering harmonics of the 50 Hz powerline signal, when sampling at f_s = 400 Hz.

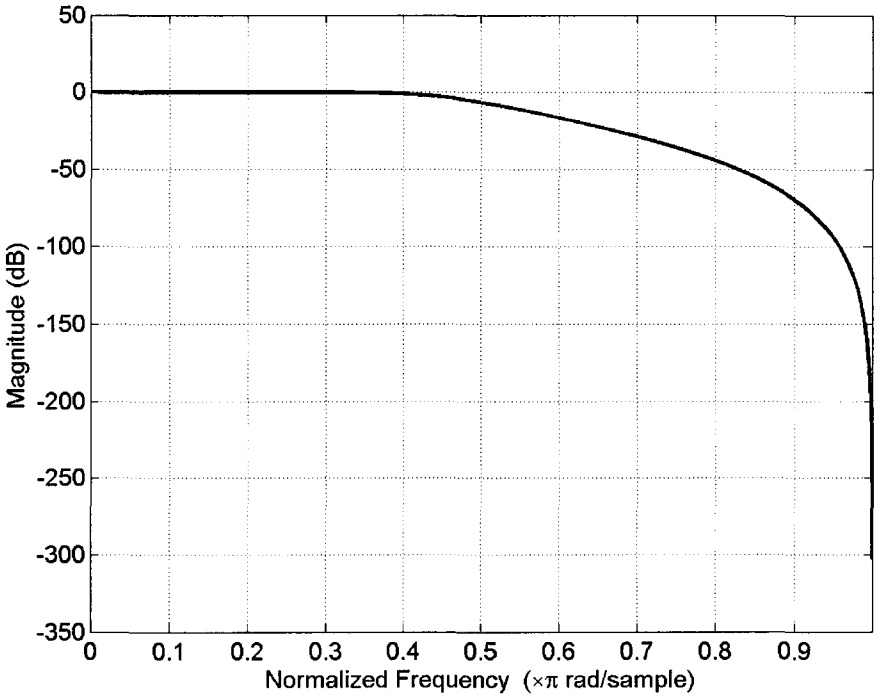

Figure A.1: Attenuation of data signal plotted against the normalized frequency for a fourth order Butterworth low-pass filter with cut-off frequency of 0.45π rad/sample.

As discussed in chapter 6.3.1, the application of a low-pass filter can cause additional noise in the signal when sudden changes in the amplitude are present. This is illustrated in figure A.2 for a step function.

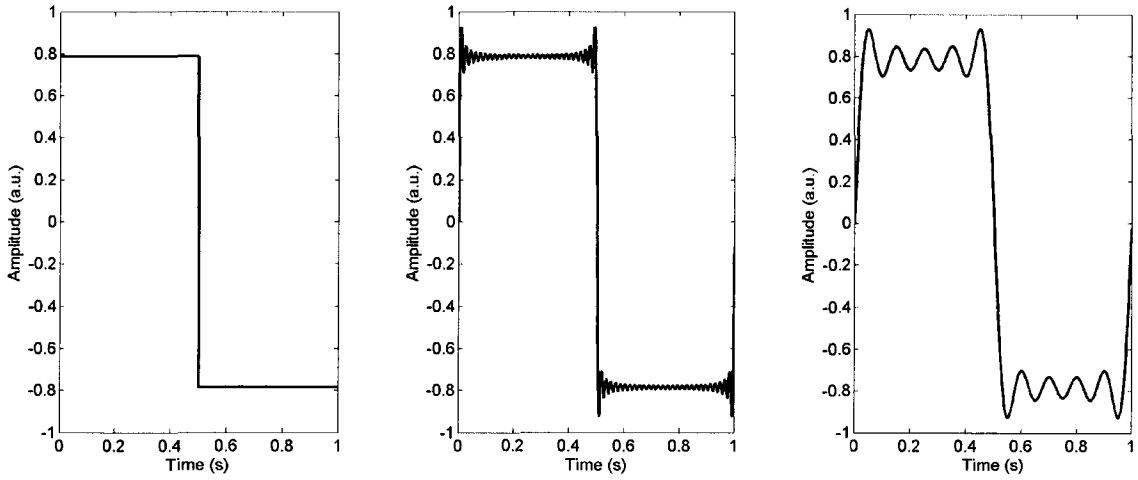

Figure A.2: Illustration of the effect of a low-pass filter on a step function. In (a) the step function is shown, (b) shows the Fourier transform of this step function for odd integer frequencies up to 57 Hz and (c) shows the low-pass filtered Fourier transform with a cut-off frequency of 9 Hz.

Figure A.2b is composed of the summation of odd integer frequencies from f = 1 Hz to f = 57 Hz with amplitudes equal to $1/f$. Figure A.2c is composed of odd integer frequencies from f = 1 Hz to f = 9 Hz with the same amplitudes as in figure A.2b. The difference between figure A.2b and figure A.2c is associated with the application of an ideal low-pass filter and can therefore serve as an illustration of the application of a low-pass filter on a step function. Because the low-pass filter stops the high frequency components in the step function, these components can no longer compensate for the low frequency components in the plateaus next to the step. As a result, these uncompensated low frequency components cause additional noise in the filtered step function.

A.2 High-pass filter

Figure A.3 shows the frequency response of the fourth order Butterworth high-pass filter with a cut-off frequency of 1.5 Hz.

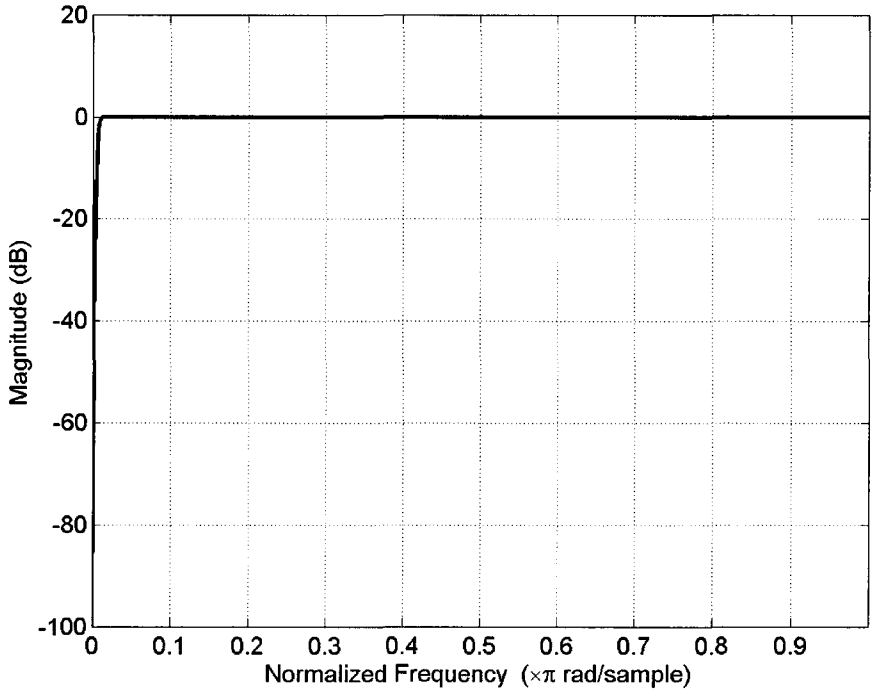

Figure A.3: Attenuation of data signal plotted against the normalized frequency for a fourth order Butterworth high-pass filter with cut-off frequency of $7.5\pi \cdot 10^{-3}$ rad/sample, corresponding to a frequency of 1.5 Hz when sampling at f_s = 400 Hz.

A.3 Bandstop filter

Figure A.4 shows the frequency response of the fourth order Butterworth bandstop filter, filtering between 48 Hz and 52 Hz.

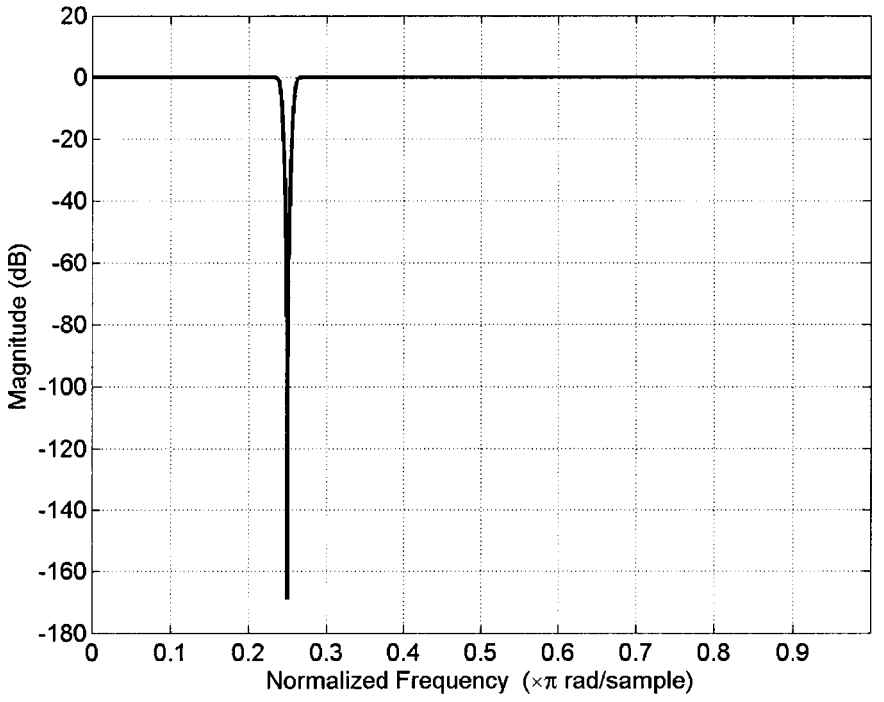

Figure A.4: Attenuation of data signal plotted against the normalized frequency for a fourth order Butterworth bandstop filter, filtering between 0.24π rad/sample and 0.26π rad/sample, corresponding to frequencies of 48 Hz and 52 Hz when sampling at $f_s = 400$ Hz.

Appendix B: The FastICA algorithm

Independent component analysis (ICA) is a statistical signal processing technique for separating a combined set of data into independent components. Assume a set of observations of n random variables $[x_1(t), x_2(t),\ldots, x_n(t)]$, that is generated by a linear instantaneous mixture of m independent components $[s_1(t), s_2(t),\ldots, s_m(t)]$. This can be written as:

$$\begin{pmatrix} x_1(t) \\ x_2(t) \\ \ldots \\ \ldots \\ x_n(t) \end{pmatrix} = A \begin{pmatrix} s_1(t) \\ s_2(t) \\ \ldots \\ s_m(t) \end{pmatrix}, \tag{B.1}$$

in which $A = [a_1,\ldots,a_m]$ is a constant full-rank $[n \times m]$ matrix called the mixing matrix. ICA consists of estimating the matrix A and the sources $s_i(t)$ from the observed $x_j(t)$. This problem can be solved under the condition that the number of observations n is larger than or equal to the number of independent components m. Typically, ICA methods estimate the unmixing matrix W:

$$\begin{pmatrix} s_1(t) \\ s_2(t) \\ \ldots \\ s_3(t) \end{pmatrix} = W \begin{pmatrix} x_1(t) \\ x_2(t) \\ \ldots \\ \ldots \\ x_n(t) \end{pmatrix}, \tag{B.2}$$

in which $s_i(t)$ be as independent as possible for $i = 1,\ldots,m$.

To estimate the independent sources $s_i(t)$ from the linear mixture, ICA uses the principle that statistically independent signal components tend to be characterized by probability distributions that are not Gaussian. In order to solve this problem for fetal ECG signals, the fixed point ICA algorithm FastICA is used because of its efficiency from the point of view of computational effort. Starting from the definition of a single independent component:

$$s_i(t) = w^T x = \sum_{j=1}^{n} w_j x_j \tag{B.3}$$

FastICA uses the kurtosis of the signals as a measure to determine the Gaussianity of the probability distributions [Hyvärinen, 1997]. This kurtosis is defined for a zero-mean random variable v as

$$\text{kurt}(v) = E\{v^4\} - 3\left(E\{v^2\}\right)^2. \tag{B.4}$$

Kurtosis is null for a Gaussian random variable, positive for probability distribution peaked at zero and negative for distribution flatter than Gaussian distributions. This means that kurtosis is suitable to assess the statistical independence of given variables. In order to maximize and/or minimize the kurtosis under the constraint $\|w\| = 1$, the natural gradient method can be used. This method has the following learning rule:

$$w(t+1) = w(t) \pm \mu(t)\left[x(t)\left(w(t)^T x(t)\right)^3 - 3\|w(t)\|^2 w(t) + f\left(\|w(t)\|^2\right) w(t)\right] \tag{B.5}$$

in which $x(t)$ is the sequence of recorded signals, $\mu(t)$ is the learning rule and f is a penalty term due to the constraint $\|w\| = 1$ [Hyvärinen, 1997]. Before applying the learning rule, the recorded signals $x(t)$ are preprocessed by means of centering and whitening. Centering is performed by subtracting the mean value to obtain zero-mean signals. Whitening is a linear transformation of the vector $x(t)$ into another vector $x^*(t)$, whose components are uncorrelated and have variances equal to unity. The learning rule stops at a fixed point for which

$|w^T(t)w(t\text{-}1)|$ is sufficiently close to unity. The linear combination w^Tx is now one of the required independent components, as stated in equation (B.3).

The FastICA algorithm is derived from equation (B.5) [Hyvärinen, 1997, Hyvärinen, 1999] and consists of:

1. randomly choosing an initial vector $w(0)$ with unit norm,
2. applying the fixed point iteration rule $w(t) = E\{x(w(t\text{-}1)^Tx)^3\}\text{-}3w(t\text{-}1)$ to approximate $w(t)$, with $E\{y\}$ the expectated value of y,
3. normalizing $w(t)$ and
4. repeating points 2. and 3. until $|w^T(t)w(t\text{-}1)|$ is sufficiently close to unity.

One ICA basis vector is then estimated. Other ICA basis vectors can be estimated by sequentially projecting a new starting basis vector $w(0)$ onto the subspace, orthogonal to the ones covered by the previous vectors [Comani, 2004].

To provide an illustration of the performance of the FastICA algorithm, three independent signals present in abdominal recordings are simulated. These signals are the 50 Hz powerline interference, random white noise and a fetal ECG signal and are shown in figure B.1. These simulated signals are linearly combined to constitute three simulated abdominal recordings, which are shown in figure B.2. Application of the FastICA algorithm on these abdominal recordings results in the three independent components that are shown in figure B.3.

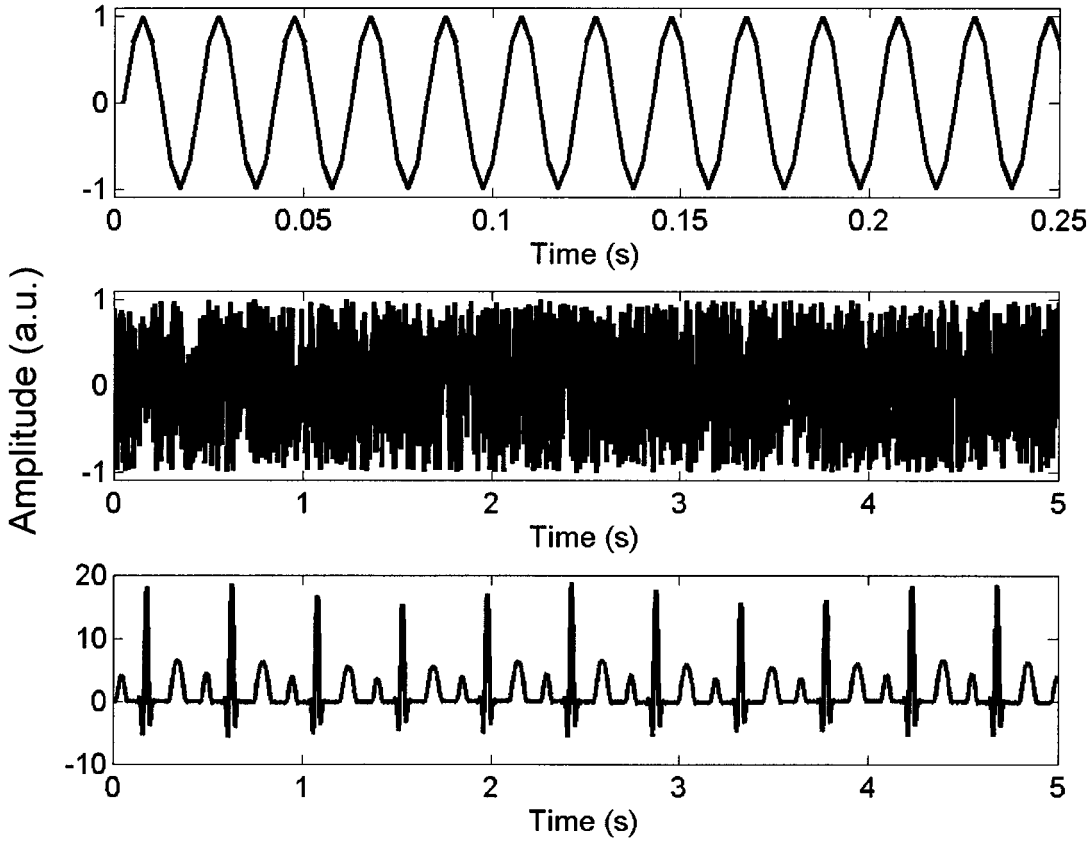

Figure B.1: Illustration of the simulated signals. The upper graph shows the simulated 50 Hz powerline interference. The center graph shows the random white noise while the bottom graph shows a simulated fetal ECG signal. As can be seen in the bottom graph is the fetal ECG signal periodically attenuated as a result of maternal respiration.

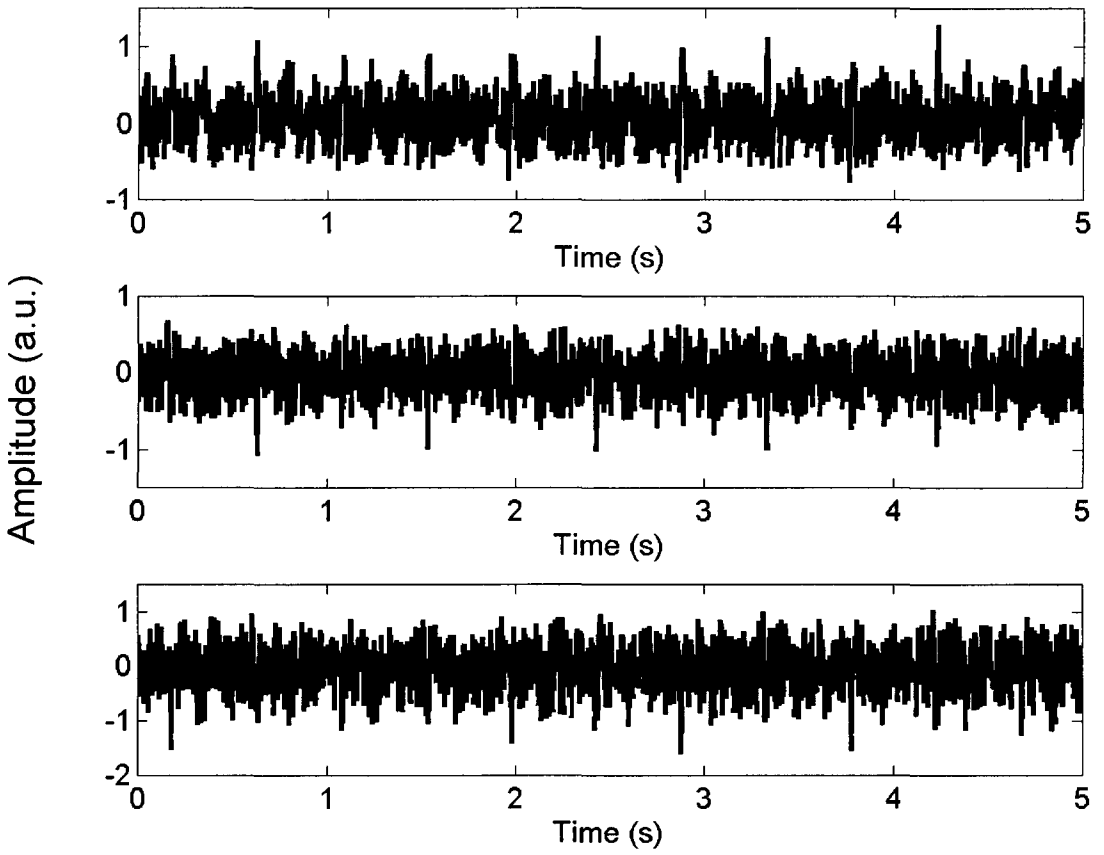

Figure B.2: Linear combinations of the simulated signals of figure B.1. These linear combinations serve as simulations of abdominal recordings, however without maternal ECG signals.

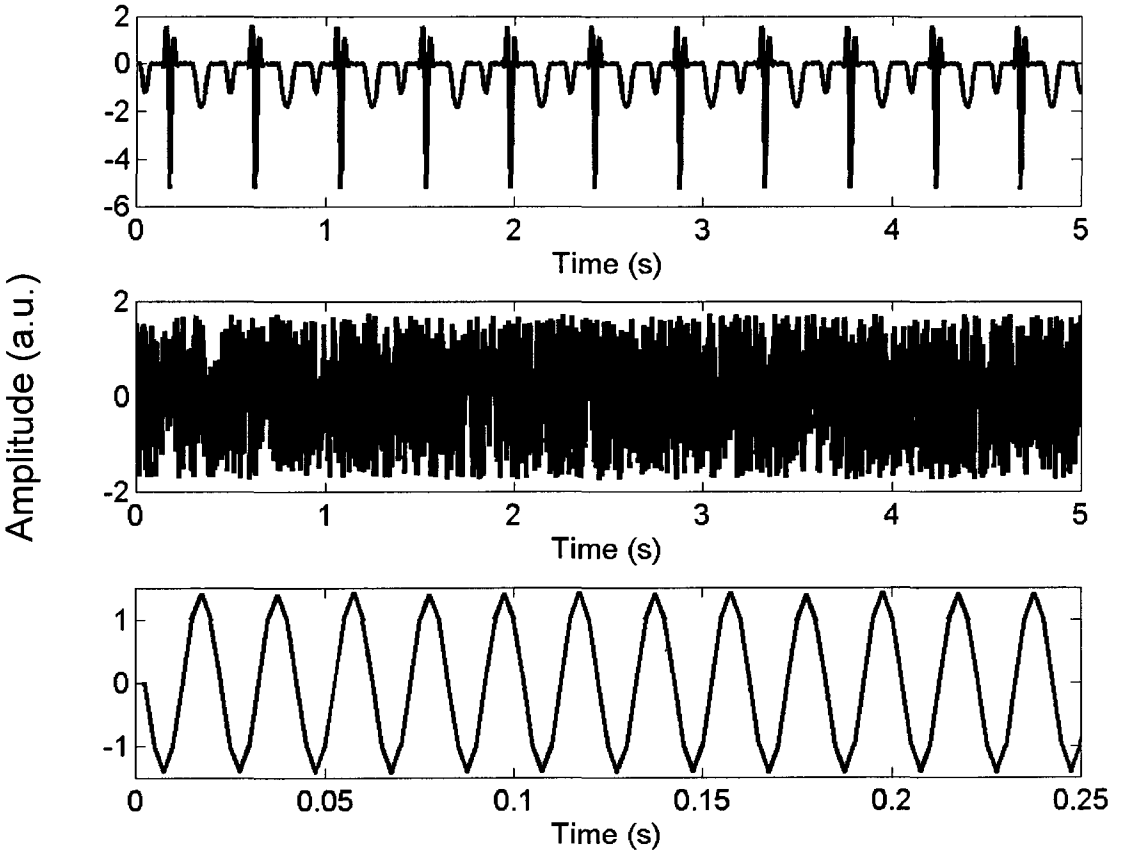

Figure B.3: Independent components determined from the linear combinations of figure B.2 by applying the FastICA algorithm.

When comparing figure B.3 to figure B.1, it can be seen that the energy and polarity of the signals cannot be determined by the FastICA algorithm. Reason for this is that both the mixing matrix A and the independent components $s_i(t)$ are unknown and therefore any scalar multiplier in one of the independent components $s_i(t)$ can be cancelled by dividing the corresponding column a_i of A by the same scalar. Furthermore, the attenuation as a result of maternal respiration as simulated in the original fetal ECG signal cannot be seen in the corresponding independent component. Reason for this is that the maternal respiration is statistically independent of the fetal ECG signal and is therefore expected to be estimated as a separate independent component – or included in one of the other independent components.

Main reasons for not using the FastICA algorithm to determine the fetal heart rate and fetal ECG complexes from abdominal recordings are the large computation times, making online monitoring nearly impossible, and the fact that the FastICA algorithm is not always capable of calculating the fetal ECG signal as a separate independent component for reasons that are yet unknown.

Appendix C: The vectorcardiogram

The reconstruction of the projection of the fetal vectorcardiogram on the maternal abdomen serves as a method to calculate common recorded ECG leads, which can be clinically interpreted by a physician to obtain information on the condition of the fetus. Since the position and orientation of the fetus inside the uterus are unknown, the used electrode positions probably constitute uncommon leads, which nevertheless can be used to reconstruct the vectorcardiogram.

Assume the abdominal surface to be a two-dimensional plane with as the x-axis the direction from left to right and as the z-axis the direction from feet to head. Each ECG lead has a time-dependent amplitude of the corresponding ECG complex: $A(t)$, so the contribution of ECG lead vector $b_m = (b_{mx},b_{mz})$ to the vectorcardiogram $v(t) = (v_x(t),v_z(t))$ can be expressed as:

$$v_{xb_m}(t) = \frac{b_{mx}}{\|b_m\|} A_{b_m}(t) \tag{C.1}$$

$$v_{zb_m}(t) = \frac{b_{mz}}{\|b_m\|} A_{b_m}(t) \tag{C.2}$$

The vectorcardiogram $v(t)$ can be reconstructed by summing the contributions of all ECG lead vectors. However, as a consequence of the limited number of electrodes positioned on the abdomen, there is a finite number of lead vectors available. This has to be corrected for when summing the individual contributions to the vectorcardiogram. Assume n ECG leads are recorded on the maternal abdomen, then the vectorcardiogram $v(t) = (v_x(t),v_z(t))$ is calculated by:

$$v_x(t) = \frac{b_{1x}}{\|b_1\|} \frac{A_{b_1}(t)}{b_{1x}+\ldots+b_{nx}} + \ldots + \frac{b_{nx}}{\|b_n\|} \frac{A_{b_n}(t)}{b_{1x}+\ldots+b_{nx}} \tag{C.3}$$

$$v_z(t) = \frac{b_{1z}}{\|b_1\|} \frac{A_{b_1}(t)}{b_{1z}+\ldots+b_{nz}} + \ldots + \frac{b_{nz}}{\|b_n\|} \frac{A_{b_n}(t)}{b_{1z}+\ldots+b_{nz}} \tag{C.4}$$

Figure C.1 provides an illustration of how the cardiac vector at time t is reconstructed from two ECG lead vectors and their corresponding ECG complexes.

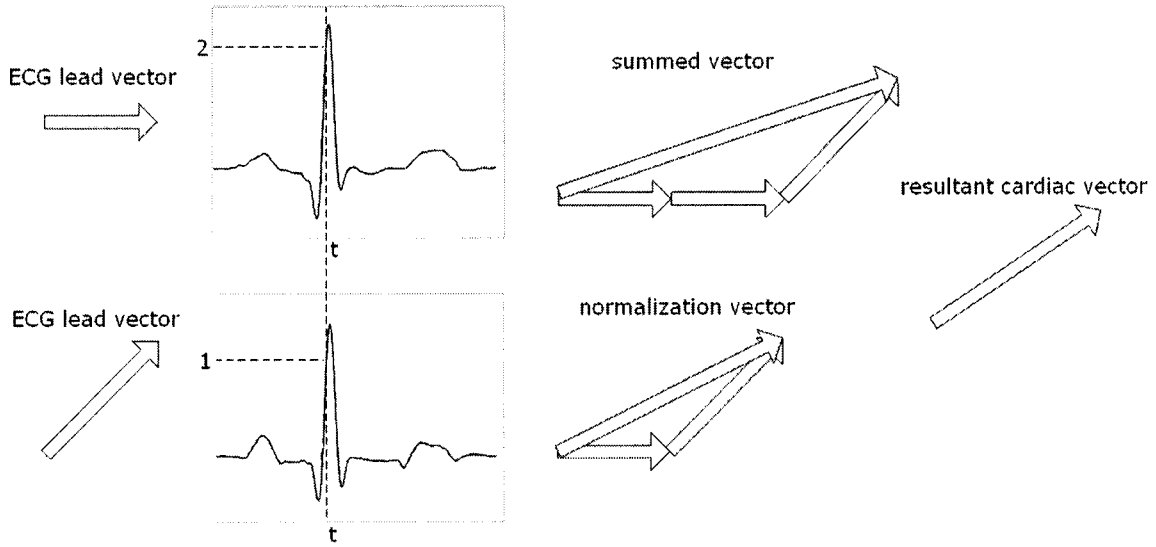

Figure C.1: Reconstruction of the cardiac vector from two ECG lead vectors. The lead vectors are multiplied by the amplitude of the ECG complex at time t and summed. To correct for the used ECG lead vectors the summed vector is normalized by the normalization vector.

Appendix D

Abstract submitted to the 46th annual meeting of the European Society for Paediatric Research

August 31 – September 3, Siena, Italy

Abstract submitted on 30 March 2005 and accepted on 18 May 2005. The abstract has been forwarded to "Pediatric Research" for publication in the August issue.

Monitoring the fetal heart rate and fetal electrocardiogram: abdominal recordings are as good as direct ECG measurements

R Vullings[1,4], CHL Peters[1,4], P Andriessen[2], SG Oei[3,5] and PFF Wijn[1,4]

[1] Department of Medical Physics, Máxima Medical Centre, Veldhoven, The Netherlands
[2] Department of Neonatology, Máxima Medical Centre, Veldhoven, The Netherlands
[3] Department of Obstetrics and Gynaecology, Máxima Medical Centre, The Netherlands
[4] Faculty of Applied Physics, Eindhoven University of Technology, Eindhoven, The Netherlands
[5] Faculty of Biomedical Engineering, Eindhoven University of Technology, Eindhoven, The Netherlands

Aim: The aim of this project is to develop an algorithm to monitor online the fetal heart rate (fHR) and fetal electrocardiogram (fECG) from maternal abdominal recordings.

Methods: Measurements have been performed using 12 electrodes on the abdomen of the mother. In an initialization phase, the algorithm calculates the fetal signal for each electrode after effectively removing the maternal ECG and suppressing the electromyogram (EMG). Next, the algorithm selects the 4 signals in which the fetal component is most present and uses these signals for further calculations. The reduction of the number of electrodes used in the calculation decreases computation times significantly and enables the algorithm to monitor the fHR online. To increase the signal-to-noise ratio of the calculated fECG-complex, 10 consecutive PQRS-complexes are averaged. By means of cross correlating the PQRS complexes, PQRS-complexes containing artifacts are excluded from the averaging process. The algorithm is validated by comparing the calculated fHR from the abdominal recordings to the fHR determined from direct ECG signals measured with a scalp electrode.

Results: A total of 530 paired fECG complexes are analyzed. The fHR obtained from both methods correlates very well (correlation coefficient 0.99, $p < 0.001$). The resulting fECG-complex clearly shows the fetal P-wave, QRS-complex and T-wave.

Conclusions: The proposed algorithm provides a valuable tool for obtaining noninvasively and online information of the fHR and fECG in stages of pregnancy earlier than labor. Future research is aimed at the uterine EMG, morphology of the fetal PQRS complexes and fHR variability analysis in order to obtain more detailed information of the fetal condition.

Appendix E

Abstract submitted to the 7th World Congress of Perinatal Medicine

September 21-24, Zagreb, Croatia

Abstract submitted on 4 May 2005 and accepted on 20 May 2005.

The fetal heart rate and sympathetic activity determined non-invasively from the maternal abdomen

R Vullings[1,3], CHL Peters[1,3], JOEH van Laar[2], PFF Wijn[1,3] and SG Oei[2,4]
[1] Department of Medical Physics, Máxima Medical Centre, Veldhoven, The Netherlands
[2] Department of Obstetrics and Gynaecology, Máxima Medical Centre, Veldhoven, The Netherlands
[3] Facutly of Applied Physics, Eindhoven University of Technology, Eindhoven, The Netherlands
[4] Faculty of Biomedical Engineering, Eindhoven University of Technology, Eindhoven, The Netherlands

Aim: The aim of this project is to perform spectral analysis on the beat-to-beat fetal heart rate, determined non-invasively from the maternal abdomen, in order to assess information on the activity of the fetal sympathetic and parasympathetic systems. Activity of these systems changes under influence of physiological circumstances and therefore spectral analysis is assumed to supply additional information on the fetal condition.

Methods: Measurements were performed using 12 electrodes on the abdomen of the mother. A new algorithm was developed to calculate the fetal heart rate on a beat-to-beat basis from these recordings. (This algorithm was validated by comparing the calculated fetal heart rate from the abdominal recordings to the fetal heart rate determined from direct ECG signals measured with a scalp electrode.) Sympathetic activity and parasympathetic activity were determined by calculating the power in the low frequency spectral band (0.04-0.15 Hz) and the high frequency spectral band (0.4-1.5 Hz) using customized spectral bands.

Results: One patient was measured during delivery. A randomly obtained period of 1000 seconds was analyzed. During uterine contractions the parasympathetic activity increased and the fetal heart rate decreased. At the end of the contractions the fetal heart rate returned to its baseline and an increase of sympathetic activity was measured.

Conclusion: The proposed method provides a valuable tool for obtaining non-invasively the fetal heart rate and fetal sympathetic and parasympathetic activity both during labor and in stages of pregnancy earlier than labor.

Bibliography

[Bland, 1986] Bland J.M., Altman D.G. Statistical methods for assessing agreement between two methods of clinical measurement. *Lancet* **i**: 307-310, 1986.

[Comani, 2004] Comani S., Mantini D., Lagatta A., Esposito F., Di Luzio S. and Romani G. L. Time course reconstruction of fetal cardiac signals from fMCG: independent component analysis versus adaptive maternal beat subtraction. *Physiol. Meas.* **25** 1305-21, 2004.

[Devedeux, 1993] Devedeux D., Marque C., Mansour S., Germain G. and Duchêne J. Uterine electromyography : a critical review. *Am J Obstet Gynecol.* 169(6):1636-53, 1993.

[Guyton, 1996] Guyton A.C. and Hall J.E. Textbook of Medical Physiology. W.B. Saunders Company, Philadelphia PA., 9th edition, 1996.

[Hyvärinen, 1997] Hyvärinen A. and Oja E. A fast fixed point algorithm for independent component analysis. *Neural Comput.* **9** 283-92, 1997.

[Hyvärinen, 1999] Hyvärinen A. Fast and Robust Fixed-Point Algorithms for Independent Component Analysis. *IEEE Transactions on Neural Networks* 10(3): 626-634, 1999.

[Hyvärinen, 2000] Hyvärinen A. and Oja E. Independent component analysis: algorithms and applications. *Neural Netw.* May-Jun;13(4-5):411-30, 2000.

[Oostendorp, 1989] Oostendorp T.F., Van Oosterom A. and Jongsma H.W. The fetal ECG throughout the second half of gestation. *Clin. Phys. Physiol. Meas.* Vol. 10. No. 2: 147-160, 1989.

[Peters, 2001] Peters C.H.L. Time-frequency analysis of the beat-to-beat fetal heart rate measured by Doppler ultrasound. Master's thesis, Eindhoven University of Technology, Dept. of Applied Physics, 2001.

[Peters, 2004] Peters C.H., ten Broeke E.D., Andriessen P., Vermeulen B., Berendsen R.C., Wijn P.F., Oei S.G. Beat-to-beat detection of fetal heart rate: Doppler ultrasound cardiotocography compared to direct ECG cardiotocography in time and frequency domain. *Physiol. Meas.* **25**(2) 585-93, 2004.

[Rosén, 1976] Rosén K.G., Hokegard K.H. and Kjellmer I. A study of the relationship between the electrocardiogram and hemodynamics in the fetal lamb during asphyxia. *Acta Physiol Scand* **98** 265, 1976.

[Stinstra, 2002] Stinstra J., Golbach E., Van Leeuwen P., Lange S., Menendez T., Moshage W., Schleussner E., Kaehler C., Horigome H., Shigemitsu S. and Peters M.J. Multicentre study of fetal cardiac time intervals using magnetocardiography. *Br J Obstet Gynaecol* 109: 1235-1243, 2002.

[Sundström, 2000] Sundström A.K., Rósen D. and Rósen K.G. Fetal surveillance. Neoventa Medical AB, 2000.

[TMS Int. B.V., 2001] TMS International B.V. Installation Guide and User Manual for the portable physiological measurement system Porti5-xx/ASD Version 2.25, 2001.

[Toonen, 1998] Toonen F.A.J. De mogelijkheid tot geautomatiseerde p- en r-top detectie in elektrocardiogrammen van neonaten. Master's thesis, Eindhoven University of Technology, Dept. of Applied Physics, 1998.

[Winsor, 1986] Winsor T. Electrocardiografie voor de medicus practicus. *Clinical Symposia*, 1986.